Journal of THERMOELECTRICITY

Editorial Board

CONTENTS

* – publication of the lectures presented at the XVII International
Forum on Thermoelectricity

Shuchitangshu Chatterjee

MECON Limited, Doranda,
Ranchi, 834002, Jharkhand, India

THERMOELECTRICS IN INDIAN SCENARIO

S.Chatterjee

Controlling simultaneously the electric and thermal properties of materials can lead to very efficient thermoelectric devices. In thermoelectric materials, the application of a temperature gradient generates a voltage, and vice versa. By exploiting this coupling between thermal and electrical properties, devices can be made that carry heat from a cold side to a hot side or that generate electricity from heat flows. Ensuring a sustainable energy supply is one of the grand challenges for science and technology in the 21st century. There is an urgent need for improved ways of generating power, without heavy reliance on fossil fuels. Thermoelectric devices, which exploit the Seebeck effect to provide direct thermal into electrical energy conversion, offer considerable attractions for a more efficient use of existing energy resources. In particular, thermoelectric power generation enables useful electrical power to be extracted from waste heat. However, the performance, cost and availability of thermoelectric materials are significant barriers to the broad implementation of thermoelectric technology. Commercial thermoelectric devices are still largely based on bismuth telluride alloys, and their thermoelectric figure of merit, combined with the scarcity of tellurium, limit these devices to niche applications. For these reasons, research in thermoelectric materials is very active worldwide, with the field rapidly advancing into entirely new classes of materials. This encompasses not only a wide range of inorganic materials, but also organic molecules and polymers. Advances following different routes were highlighted in this study.

Key words: Peltier Effect, Thermoelectric Cooling Helmet, Computational fluid dynamics, heat transfer, heat pipe, volume flow rate, Pressure drop.

Introduction

Thermoelectric Advancement under the aegis of MECON: R&D Division of MECON LTD., Ranchi has done extensive work on thermoelectrics since the last 30 years. The present work is the synopsis of the previous work done and advancement achieved in thermoelectric field [1 – 10].

Solid State Microclimate Conditioning Unit for Defence Personnel

Solid state microclimate conditioning unit was successfully designed, developed and demonstrated for defence personnel working at high ambient temperature or at desert.

The cooling unit was integrated in MBT ARJUN TANK and successfully demonstrated at CVRDE, Avadi. Final demonstration trials of such solid state cooling unit were conducted at Mahajan Field Firing Range at Rajasthan (**Indo-Pak Border) in June 2005 [11].** The project was sponsored by DIPAS, (DRDO), Delhi.

Anti-Tank Missile

A critical problem on anti-tank missile was assigned by DRDL, (DRDO) Hyderabad to MECON. The project was completed successfully and well accepted by DRDL. The project was funded by DRDL, DRDO Hyderabad and completed in the year 2004. Implementing agency was Indian army [12 – 13].
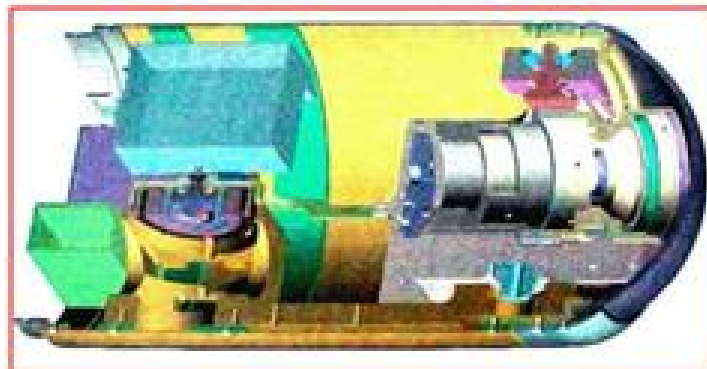
Heating Gloves and Socks for Defence Personnel

MECON has successfully designed and developed battery operated heating gloves and socks for Defence Personnel working at sub-zero environment. The project was funded by DIPAS, (DRDO), Delhi. The project was implemented in Defence (Kargil, Leh) and completed in the year 2006.

Thermoelectric Cold Chain Chest Operated by 12 V DC Vehicular battery

Thermoelectric cold chain chests developed by MECON are suitable for use in medical and health-care programs for storing and / or transporting medicines, drugs, vaccines, serum, semen diagnostic materials for urban as well as rural areas. The project was funded by DST, Delhi. Implementing agency was AIIMS and was completed in the year 2003 [14 – 15].

Thermoelectric Cooling/Heating Helmet

Three types of cooling/heating helmets were developed that are distinct in terms of process of development, usability, and feasibility in industrial premises.
A. Direct cooling/heating helmet.
B. Back pack cooling/heating helmet.
C. Trolley based cooling/heating helmet.

A. Direct Cooling/Heating Helmet

The helmet is fitted with TE module and conventional heat sink. Cooling is by conduction and the heat sink is of convective type. The cold side of the module is in contact with perforated aluminum sheet inside the helmet. Head cooling is by conduction over the cold aluminum sheet towards the head. Rechargeable battery pack and electrical switch is fixed with waist belt. The helmet is constructed based on a fiber-glass shell, provided with a heat distribution surface internally, which is separated from the fiberglass shell surface by a layer of insulation. The external and internal surfaces of the fibre-glass shell are insulated leaving openings for the extraction of heat from the inner surface through the thermoelectric module units thermally bonded to the inner conducting layer. Thermoelectric modules are thermally connected with the inner heat distribution surface. Each

thermoelectric module is thermally connected to an external heat sink and such heat sink has an inbuilt fan, thus enabling the thermoelectric device to extract heat from the inner heat distribution surface, when electrically powered.

The heat distribution surface is cooled at multiple points, as equidistant as possible, thus optimizing the temperature changes in linear directions away from the cold spot. The heat distribution surface envelops the major part of the surface of the head and effectively creates a common air volume which enables the surface of the head to experience the same environment as created by the operation of the thermoelectric modules for the whole surface, uniformly. Thus the external heat sinks are oriented with respect to the helmet surface such that the air-flows are independent and non-interfering [16].

B. Back Pack Cooling/Heating Helmet

It is basically circulating dry & cold air underneath the head to keep the person dry which, in a sense, will keep him cool even on hot environmental condition. The system extracts around 80 Watts of metabolic heat from human head at an ambient of 55ºC. Our cooling system is made of hybrid heat sink (convective and heat pipe both) with thermoelectric modules, small fans, blower and rechargeable

battery to be carried as back pack. Heat sink assembly has components like inlet duct (divergent), cold plate, outlet duct (convergent), TE modules, aluminum block, heat pipe, fins, and fan as shown in figure below. Hot ambient air is forced to flow through cold plate by blower. Blowers are DC radial type designed to generate enough pressure drops to make flow through the cold plate. Divergent and convergent ducts guide the flow through cold plate. Cold

plate has several baffles which retards the flow and helps in heat transfer. Hot side fan is used to facilitate forced convection heat transfer from hot side fins. Volume flow rate for fan was investigated for desired design performance. Heat dissipated from the hot side of TE modules is transferred to heat pipe through aluminum block. It is assumed that there is no heat loss (convection and conduction) from aluminum block and hot side TEM temperature is taken as input to heat pipe. Increasing the length of heat pipe & keeping the number of fins same would not have any impact on heat dissipation quality of hot side assembly. However, with introduction of a greater number of fins on the heat pipe, an improvement in heat dissipation is possible [17].

C. Trolley Based Cooling/Heating Helmet

This unit is a thermo mechanical assembly of a heat pump (the thermoelectric modules), heat sinks, spacer and cold plates that work on thermoelectric Peltier principle in which water is used to accumulate and transfer heat in the cooling system. The cold water through the narrow tube absorbs the metabolic heat of the head and transfers the same to the cold chamber, which is again cooled by the TE module. The cold face of the module is in contact with the cold chamber filled with water. The hot side of the module is in contact with the heat sink through which the heat generated in the hot surface of the module is dissipated. Fans are used for force dissipation of heat. The quicker the hot surface heat will be removed, the quicker the cold face temperature will come down.
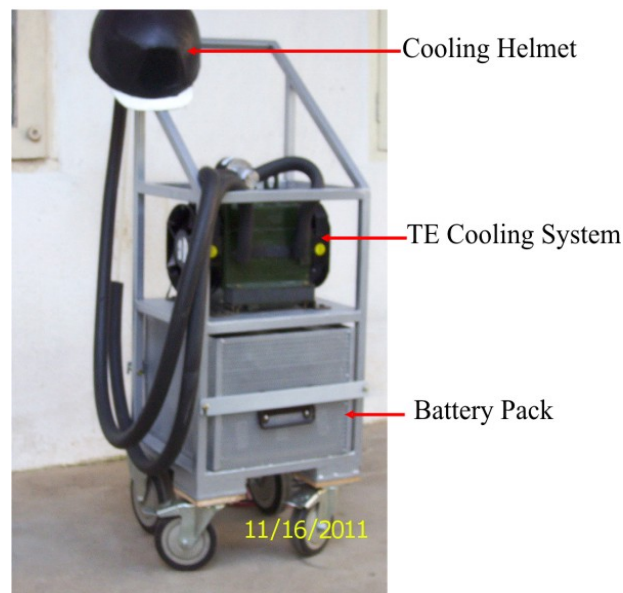
Thermoelectric Filter

MECON's in house Research and Development Division has successfully developed the system and applied for its Indian Patent to overcome cold starting problem in automobiles arising due to extremely low temperature by using thermoelectric in conjunction with a thermal storage device. The thermal storage device acts like a heat reservoir and thermoelectric modules acting as heat pumps extract heat from the thermal storage device and pump it to the filter thereby enabling quick starting of

the automobiles in cold environments. It has been experimentally proved that an automobile can be started within 100 seconds using proposed device. [18]

Air Warrior Body Ventilation Vest for Defence Personnel

Air warrior body ventilation vest is a light weight, comfortable, breathable, tube type undergarment worn against the skin. It provides cooling to circulate a coolant dry air to the torso of body to remove metabolic heat from personnel working in heat stress environments. The system requires extracting around 80 to 90 Watts of metabolic heat from human body at an ambient of 55 $^{\circ}$C, which will be operated by portable blower & rechargeable battery [19].
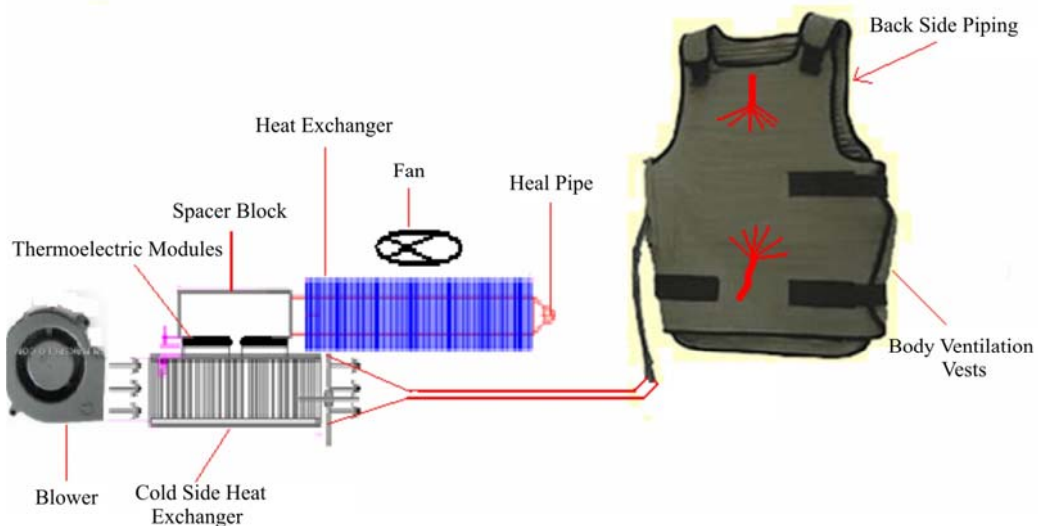
Solid State Cooling Drinking Water Tank for Armoured Vehicles

During the journey to war field; it is an acute problem for the soldier for getting comfortable cold drinking water, especially during summer. Generally after three hours soldiers used to take warm water for drinking purpose and due to this the physiological parameters of human body go from bad to worse. Similarly, for cooking their food, they were unable to get warm or hot water during their war field. Such warm or hot water they may like to use for preparing their meals ready to eat. Hence; keeping this in mind; design of solid state water cooler/heater for Army personnel by considering all the boundary condition given for respective Armoured Vehicles. By using solid state cooling/heating

concept is going to use to cool or heat the water of Armoured Vehicles, which can be operated by DC power supply (mainly by their back-up battery system), Voltage ranging from 20 V DC to 28 V DC during their war field. The power consumption from DC power supply depends on the parameters like ambient temperature, supplied voltage & amount of heat to be extracted or to be thrown [20].
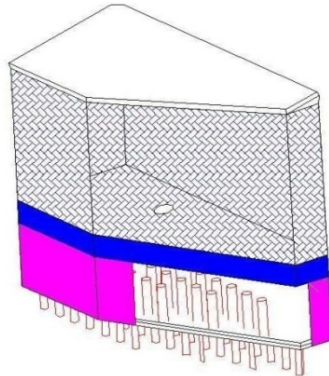
Thermoelectric stretcher

Thermoelectric heated / cooled wheeled stretcher mainly consists of two parts:

Part – 1 Consists of a stretcher made of series & parallel connection of conducting tubes to circulate hot or cold fluids across the stretcher to prevent soldiers from casualty.

Part – 2 Consists of thermoelectrically cooling / heating unit, which is a thermomechanical assembly of heat pump, i.e. thermoelectric modules, heat & cold sinks, one positive displacement pump and one axial fan to dissipate heat from the system. This thermoelectric stretcher will provide adequate heating or cooling to the soldier depending upon their requirements by changing the polarity of thermoelectric array.
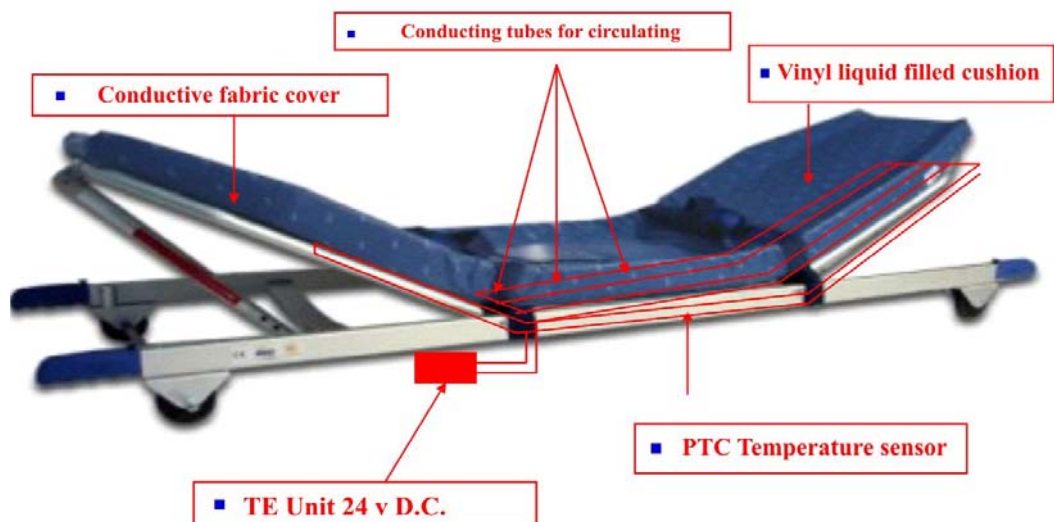
The cooling & heating system, employing this technology are solid state and CFC free devices. They are highly reliable and easily maintainable devices. Performance of the system has been ensured by our innovating design, assembly, made possible by software developed from our mathematical

modelling. Thermal impedance matching of all the components of the unit treated as discrete thermal models with discrete characteristics has been ensured. Liquid cooling stretcher is used to absorb the excess metabolic heat from the body using thermoelectrically chilled fluid, such as water. In this unit cooling is transferred by conduction through PVC tubes carrying cooling medium. The cooling medium absorbs the metabolic heat energy and flows to the thermoelectric cooling unit which transfers the heat energy therefrom. Thus the system operates in a closed loop.

The unit is a thermo mechanical assembly of heat pump (the thermoelectric modules), heat sinks, spacers and cold plates. The thermoelectric modules are sandwiched between the heat sinks on the one side, and the spacers and cold plate on the other side. Each cold plate is in turn sandwiched between two sub assemblies. Each of these subassemblies is made up of a set of thermoelectric modules, heat sinks and spacers. A number of sandwich assemblies can be stacked together to remove the required amount of heat from water flowing through the cold plate. A suitable pump is used to make water flow through the cold plate in tandem, or parallel as required. The cold plate has a spiral hole with obstructions in the flow path, to provide maximum heat transfer area, as well as turbulence in flow. Fans are mounted (if required) at suitable locations to carry the heat away from the heat sinks efficiently. The heat sinks have the optimum design of fins, to provide maximum area of heat transfer.
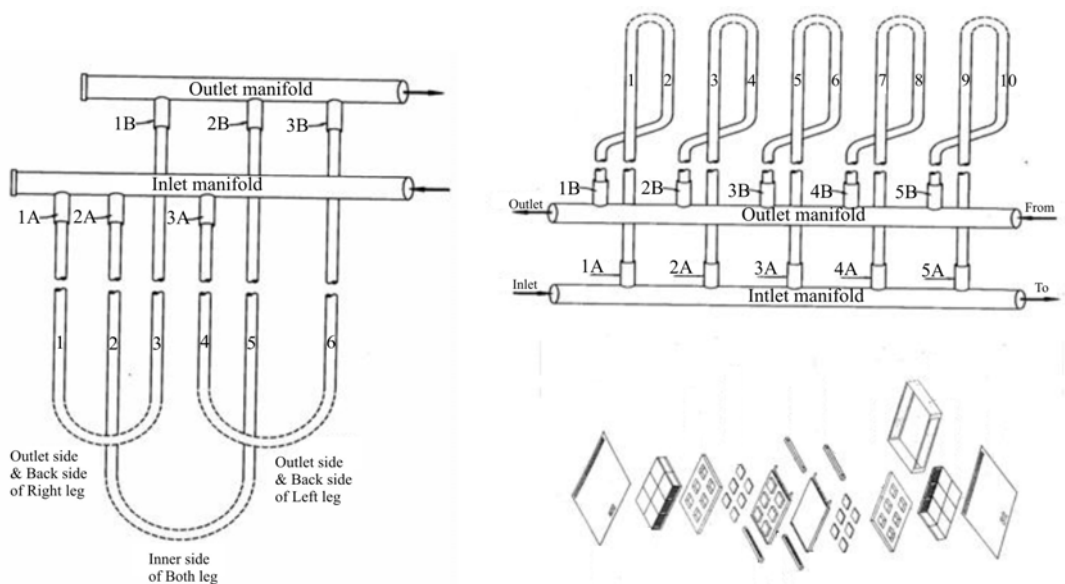
Galena Thermoelectric Generator [21 – 26]

| Beneficiated Ore | Pellets |

Chunk Ore

Thermoelectric Generator

Galena Ore

Chunk Ore

Beneficiated Ore

Properly doped with different dopant in different mole percent at inert atmosphere (Na_2S, Pb, In etc.)

Pellet formation

Inert atmospheric n & p type pellet

Vacuum hot pressed n & p type of pellet

Achieved optimum Thermoelectric properties like α, ρ & k i.e. optimize figure of merit

Resistivity was in $m\Omega cm$ level $\alpha \sim 190 - 200$ $\mu v/°K$, $k(k_L + k_{el}) \sim 6.6 \times 10^{-3}$ cal/s cm°K

Coated with galena adhesive coating for prevention from oxidation/corrosion etc.

Made n & p type of couples by Nickel contact

Contact was not good

Overall resistance of TEG was gone high and hence the output of generator was low

Thermoelectrics in Indian Scenario other than MECON

Dr. Chandra Mohan Bhandari from the University of Allahabad has done the following successful research in the thermoelectric domain:
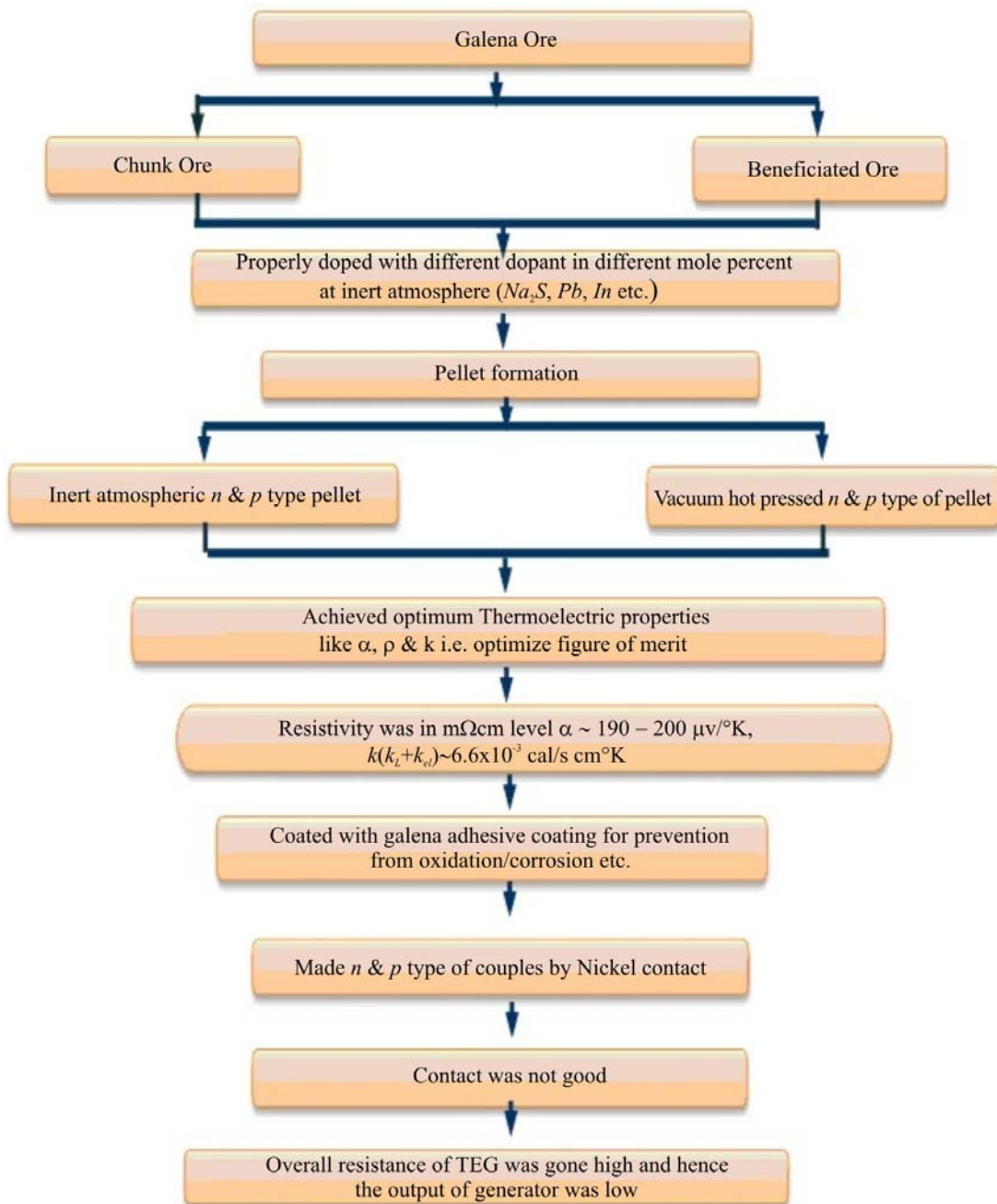
Thermal conductivity of *Ge-Si* alloys at high temperature, Role of longitudinal and transverse phonons in lattice thermal conductivity of *GaAs* and *InSb*, Temperature dependence of density-of-states effective mass and electronic and phonon contributions to thermal resistance of doped *Si-Ge* alloys at high temperatures, influence of point defects on phonon drag thermoelectric power, magnon drag thermoelectric power, thermal conductivity of highly disordered semiconductor alloys, effect of grain size on the thermoelectric conversion efficiency of semiconductor alloys at high temperature, the generalization of Callaway thermal conductivity equation, theoretical analysis of thermoelectric figure of merit, temperature dependence of the figure-of-merit of improved thermoelectric materials based upon lead telluride, lattice thermal conductivity of small-grain-size *Pb-SnTe* and *Pb-GeTe* thermoelectric material, electronic contribution to the thermal conductivity of narrow band gap semiconductors: effect of non-parabolicity of bands. Towards a thermal conductivity minimum: thermoelectric considerations, solid solubility in thermoelectric semiconductors, Seebeck coefficient and electrical conductivity of *Si-Ge* alloys, phonon drag thermoelectric power in copper alloys, fine grained *Si-Ge* alloys as superior thermoelectric materials, electronic thermal transport in
thermoelectric material effect of band nonparabolicity, thermoelectric behaviour of multivalley semiconductors, minority carrier effects on the thermoelectric figure-of-merit, preparation and thermoelectric properties of improved *PbSnTe* alloys [27 – 30].

Dr. Ramesh Chandra Mallik, from IISC Bangalore has done the following successful research in the thermoelectric domain:

Ball Mill Synthesis of bulk quaternary $Cu_2ZnSnSe_4$ and thermoelectric studies, thermoelectric properties of *In-* and *I-* doped *PbTe*, *Sn*-doped *BiCuSeO*, *Bi*-doped tetrahedrite, *Cd*-doped tetrahedrite, *In*-doped $Cu_2CdSnSe_4$, *PbTe* with Indium and Bismuth secondary phase, *Co* substituted synthetic tetrahedrite; synergistic combination of atomic scale structural engineering and panoscopic approach in *p*-type *ZrCoSb*-based half-Heusler thermoelectric materials for high ZT, thermoelectric materials for sensor applications, *In*-doped multifilled *n*-type skutterudites, thermoelectric properties of *Mn* substituted synthetic tetrahedrite, improvement of electrical conductivity in $Pb_{1-y}Sn_yTe$ alloys doped with manganese for high temperature thermoelectric applications, nanostructuring of *p*- and *n*-type skutterudites reaching figures of merit of approximately 1.3 and 1.6, respectively, thermoelectric properties of indium doped $PbTe_{1-y}Se_y$ alloys, Cu_2GeSe_3, *Zn* doped Cu_2SnSe_3, two-phase *PbTe* with Indium inclusions, $Fe_{0.2}Co_{3.8}Sb_{12-x}Te_x$ skutterudites, chalcogenide based $Cu_{2.1}Zn_{0.9}Sn_{1-x}In_xSe_4$ $(0 = x = 0.1)$, thermoelectric properties of *PbTe* with encapsulated bismuth secondary phase, *Bi*-added Co_4Sb_{12} skutterudites, chalcogenide based $Cu_{2+x}ZnSn_{1-x}Se_4$, Indium filled and Germanium doped Co_4Sb_{12} skutterudites and examination of thermoelectric properties of other materials too has been done [31 – 35].

Dr. Ravi Kumarn from IIT Madras has done following successful research in the thermoelectric domain:

Thermodynamic modelling of *Ti-Zr-N* system, thermal conductivity of precursor derived *Si-B-C-N* ceramic foams using Metroxylon sagu as sacrificial template.

Prof. Tapas De from IIT Kharagpur has done the following successful research in the thermoelectric domain:

Thermal conductivity and viscosity of Al_2O_3 nanofluid based on car engine coolant. Investigation of thermal conductivity, viscosity, and electrical conductivity of graphene based

nanofluids. Thermophysical and pool boiling characteristics of *ZnO*-ethylene glycol nanofluids. Investigations on the pool boiling heat transfer and critical heat flux of *ZnO*-ethylene glycol nanofluids. Thermal properties of silicon powder filled high-density polyethylene composites. Role of interfacial layer and clustering on the effective thermal conductivity of *CuO*-gear oil nanofluids. Excess electrical conductivity and thermoelectric power of (YBa_2Cu_3. $05Ox$) Agn pellets. Temperature dependence of the thermoelectric power of $La_{1-x}K_xMnO_3$ compounds in light of a two phase model. Thermoelectric power of undoped and doped *Y-Ba-Cu-O* superconductor between 77 and 300 K. Temperature dependence of electrical conductivity and thermoelectric power of *Bi-Sb* tapes prepared by liquid quenching. Thermoelectric power of deoxygenated Bi_1 $6Pb_0$ $4Sr_2Ca_2Cu_3O_{10+\delta}$ sintered superconducting pellets. Thermoelectric power of samarium substituted $Y_{1-x}Sm_x$ $Ba_2Cu_3O_{7-\delta}$ superconducting pellets. Thermal conductivity of (2223) *Bi-Pb* cuprate superconductors: influence of doping and heat treatment time [36 – 41].

Dr. U.V. Varadaraju from IIT Madras has done the following successful research in the thermoelectric field:

Thermoanalytical investigations on the sol-gel synthesis of $YBa_2Cu_3Ov_7$. Thermodynamic stabilities of ternary oxides in the *Ba-Pb-O* system by the e.m.f. technique. High-temperature resistivity and thermopower studies on substituted *Bi*-2212 and *Bi*-2201 systems. Thermoanalytical investigation of the formation of $YBa_2Cu_{3 \text{ and } 6.5}$, resistivity. Thermopower and single-particle tunneling studies on some zinc-doped yttrium barium copper oxide superconductors. Enhancement of thermopower in the high Tc superconductor yttrium barium copper oxide ($YBa_2Cu_3O_7$) and related compounds [42].

Prof. Umarji Arun M, from IISC Bangalore has done the following successful research in the thermoelectric domain:

Silicides are a potential candidate for high temperature applications such as heating elements, protective coatings, ceramic engines etc. because of its non-toxicity, availability of raw materials, chemical and thermal stability. Despite its advantages, the thermoelectric performance (*ZT*) of the material is low. So, efforts are on in enhancing the thermoelectric performance of the material. Band structure engineering and phonon engineering are some of the methodologies in improving the material properties. This can be done by chemical doping and nanostructurization. This in turn can be carried out by doping the material with *Mn, Co, B*, etc. Nanostructurization can enhance *ZT* value by decreasing the thermal conductivity. Effect of Composition on thermoelectric properties of polycrystalline $CrSi_2$, chromium disilicide, *Mn* and *Al* on thermoelectric properties of chromium disilicide, control oxygen stoichiometry and thermoelectric properties in $(RE)BaCo_2O_{5+\Delta}$, mechanically alloyed chromium silicide, Nanostructuration via solid state transformation [43 – 45].

Dr. R. Gopalan from Centre for Automotive Energy Materials has done successful research in high T_c superconductors, magnetic materials, Li-ion battery, thermoelectrics, structure-property correlation of functional materials, processing of nanopowders of *Fe-Co-Sb* alloy by RF plasma technique [46 – 49].

Prof. Pallab Banerji from IIT Kharagpur has done the following successful research in the thermoelectric domain. His area of interest is low dimensional semiconductors: structures & devices, materials for energy applications, such as thermoelectricity and photovoltaics, photonics, III – V and other compound semiconductors.

Exploration of *Zn* resonance levels and thermoelectric properties in iodine doped *PbTe* with *ZnTe* nanostructures, Carrier transport phenomenon and thermoelectric properties in melt-grown tellurium doped *n*-type $Bi_{0.88}Sb_{0.12}$ alloy, thermoelectric properties of $PbSe_{0.5}Te_{0.5}$: x (PbI_2) with

endotaxial nanostructures: a promising *n*-type thermoelectric material. An alternative approach to optimal carrier concentration towards ideal thermoelectric performance. Enhancement of thermoelectric power factor through modification of electronic structure in *PbTe*: *Cr*. Dramatic enhancement of thermoelectric power factor in *PbTe*: *Cr* co-doped with iodine. Embedded *Ag*-rich nanodots in *PbTe*: enhancement of thermoelectric properties through energy filtering of the carriers. Gain structure induced thermoelectric properties in PbTe nanocomposites [50 – 53].

Prof. Aritra Banerjee from University of Calcutta has done the following successful research in the thermoelectric domain.

Synthesis and characterization (transport, magnetic and optical properties). Defect induced structural and thermoelectric properties. The effect of quenching from different temperatures. Correlation between defect and magnetism of low energy Ar^{+9} implanted and un-implanted $Zn_{0.95}Mn_{0.05}O$. Magnetic properties of *Mn*-doped *ZnO*: the role of synthesis route, *Mg* and *Al* co-doping of *ZnO* thin films: effect on ultraviolet photoconductivity, magnetic, resonance, optical properties [54].

Dr. Kaurav Netram from Govt. Holkar Science College Indore has completed the following research work in the thermoelectric domain.

He has work on thermal properties (including, thermopower) of iron based materials. Our investigation shows that these materials could be used for low temperature refrigeration. Some of the recent results on *FeSe/FeTe/FeS* compounds are under discussion. Enhancement of the thermoelectric performance by *Y* substitution in $SrSi_2$. A room-temperature *ZT* value of approximately 0.4 is thus achieved for $Sr_{0.92}Y_{0.08}Si_2$, about one order of magnitude larger than that of stoichiometric $SrSi_2$. The high value and complicated temperature dependence of thermopower (*S*) in $YMn_{1-x}Ru_xO_3$ compounds. Presently, working on the tailoring of properties in pervoskite type materials, which depends on effective and precise control of the chemical pressure by way of replacing the ionic radii of *A*/*B* atoms. This is not only because specific electronic, magnetic and thermal properties are coupled to specific valence states of the *A*/*B* atoms in these oxides, but also because even a small nonstoichiometry may frustrate the desired properties, such as valence mixing. In other cases, certain presence of nonstoichiometric defects is desirable, such as in ionic and/or electronic conductors in batteries, fuel cells, etc. In fact, this fascinating and promising research field is still widely debated, as the enhancement of thermoelectric performance and fundamental physical mechanisms are yet far from being ultimately clarified and/or achieved. This task implies to probe the changes in the various thermal transport properties, in particular, the thermoelectric performance by changing the chemical pressure in $A_2B'B''O_6$ type double perovskites materials. At present, he is at sample preparation stage.

Dr. Kumar Chattopadhyay Maulindu from Raja Ramanna centre for Advanced Technology has studied temperature dependence of thermoelectric power and thermal conductivity in ferromagnetic shape memory alloy *Ni* 50 *Mn* 34 In 16 in magnetic fields, Thermoelectric Power Studies on $YBa_{2-x}Ca_xCu_3O_{7-\delta}$ System [55].

Dr. D. Siva Prahasham from Centre for Automotive Energy Materials ARCI has done nanomaterial synthesis, characterization, consolidation, structure-properties correlation. XPS, SPS processing, thermoelectric materials and device fabrication, nanocrystalline *Fe-Co-Sb* thermoelectric alloy powder by RF plasma technique.

Dr. Raj Kishora Dash from University of Hyderabad has done research on nanomaterials (metals, metal oxides, carbon nanotubes and graphene) properties, morphology of Bi_2Te_3 nanostructured thermoelectric materials, rational synthesis of morphology controlled Bi_2Te_3 nanostructured thermoelectric materials. Applications of nanomaterials/nanotechnology in sensors, heat transfer, aerospace, NEMS, automotive, solar cell, nano fluids. MEMS, NEMS, sensors, bio-MEMS, microfluidic devices and nano/micro fabrication. Thermodynamic behavior of a model

covalent material described by the environment-dependent inter-atomic potential, effect of chemical synthesis parameters on the structure.

Dr. G. Vaitheeswaran from ACRHEM,University of Hyderabad has done research on solid state theory, material science*,* magnetism, superconductivity, high-pressure studies, elastic and mechanical properties investigated using first principles density functional calculations (DFT). Study of structural, mechanical and high-pressure behavior of high energy materials. Double perovskites (spintronic materials), multiferroics, rare-earth compounds, rare-earth and transition metal oxides, Heusler alloys, study of materials under extreme conditions.

Dr. Manjusha Battabyal from ARCI has done research on powder metallurgy, squeeze casting, SPS and HIPping, thermoelectric materials and device fabrication, high temperature materials, transmission electron microscopy, thermophysical properties, mechanical testing.

Prof Ranjan Kumar from Punjab University has done research on theoretical condensed-matter physics: study of structure, phonons, electronic and mechanical properties, thermodynamic properties of pure and doped (B, N) graphene, effect of pressure on electronic and thermoelectric properties of magnesium silicide. First principle investigation of the electronic and thermoelectric properties of Mg_2C, effect of disorder on electronic, magnetic and optical properties of Co_2CrZ Heusler alloys. [56 – 57]

Dr. D.K. Mishra from CSIR-NPL has conducted his research on developing the materials with promising low and high temperature semiconducting thermoelectric property, exploratory synthesis and characterization of new inorganic compounds skutterudites, Mg_3Sb_2-based Zintl phase compound, half-Heusler-based bulk nanocomposite in order to improve in thermoelectric performance, high temperature materials for thermoelectric conversion (e.g. skutterudites, Mg_3Sb_2 Zintl phase compounds, Half-Heusler/Full-Heusler nanocomposites and other novel materials), simulation of crystal structures, analysis of electron diffraction pattern.

Dr. Debanand Sa from Banaras Hindu University has conducted his research on correlated electron systems, low and high temperature superconductivity, Fermi and non-Fermi liquids in low dimensional systems, Kondo and quantum impurity problems, nested and spin-Peierls systems, ferroic and multiferroic materials, emergent gauge theories, topological insulators and superconductors.

Raman scattering in orthorhombic multiferroic $RMnO_3$, superconductivity in $Na_xC_oO_{2-y}H_2O$, hidden quantum critical point in a ferromagnetic superconductor, superconductivity from a non-Fermi liquid: A Ginzburg-Landau approach, a generalized Ginzburg-Landau approach to second harmonic generation.

Ms Monika Mudgel from National Physical Laboratory has studied the negative thermoelectric power of over-doped $Bi_2Sr_2CaCu_2O_8$ superconductor, anomalous thermoelectric power of $Mg_{1-x}Al_xB_2$ system with x = 0.0 to 1.0.

References

1. S. Chatterjee & et. al. Effect of Sintering Temperature and Time on the Electrical Properties of Pellets Made from Beneficiated Galena Ore, *J. Mater. Sci* 22, 2793 (1987).
2. S. Chatterjee & et. al. Grain Size Effect on the Polarity of Seebeck Coefficient of Natural Galena, *J. Energy Convers. Mgmt.* 31(2), 175 (1991).
3. S. Chatterjee & et. al. Low Cost Solar Selective Absorbers from Indian Galena, *J. Optical Engineering* 32(11), 2923 (1993).

4. S. Chatterjee & et. al. Stress Developed on Typical Galena Thermocouples, *J. Thermoelectricity* 1(1997).

5. S. Chatterjee & et. al. An Improved Setup for the Simultaneous Measurement of Thermoelectric Coefficient and Electrical Conductivity in Vacuum/Inert Atmosphere at Different Ambient Temperatures, *J. Inst. Soc. India* 17, 87 (1987).

6. S. Chatterjee & et. al. Feasibility Study on Dross Galena for Thermoelectric Generator, *J. MECON, India* 14(2), 67 (1995).

7. S. Chatterjee & et. al. On the Electrical and Thermoelectric Properties of Sintered PbS Pellets, *Proc. 5th International Conference on Thermoelectric Energy Conversion* (USA, Arlington, University of Texas, March,1984), p. 145.

8. S. Chatterjee & et. al. On Low Cost Approach for Fabrication Lead Sulphide Based TEG for Terrestrial Applications*, Proc. 7th Miami International Conference on Alternative Energy Source* (USA, Florida, University of Miami, December,1985), p. 425.

9. S. Chatterjee & et. al. On the Properties of Thermoelements Made by Hot Pressing Galena and Beneficiated Galena Ore, *Proc. 6th International Conference on Thermoelectric Energy Conversion* (USA, Arlington, University of Texas, March, 1986), p. 59.

10. S. Chatterjee & et. al. Thermoelectric Generator Using Natural Galena Aggregate and Galena Concentrate, *Proc.7th International Conference on Thermoelectric Energy Conversion* (USA, Arlington, University of Texas, March, 1988), p. 14.

11. S. Chatterjee & et. al. Solid State Cooling / Heating Micro Climate Conditioning Device & a Garment Connected Therewith, *Patent Sealing.*

12. S. Chatterjee & et. al. Athermalization of Infra-Red Camera of Projectile Weapons, *J. Applied Thermal Engineering* 29(10), 2106 (2009).

13. S. Chatterjee & et. al. A Novel Mechanism for Athermalization of Themographic Camera Using Thermoelectrics, *Proc. 19th National & 8th ISHMT – ASME Heat and Mass Transfer Conference* (India, JNTU Hyderabad, January, 2008).

14. S. Chatterjee & et. al. Solid State Cooling / Heating Box, *Patent Sealing*.

15. S. Chatterjee & et. al. Thermoelectric Cold Chain Chests for Storing/Transporting Vaccines at Remote regions, *J. Applied Energy* **76**(4), 415 (2003).

16. S. Chatterjee & et. al. Thermoelectric – Direct Cooling/Heating Helmet, *Patent filing*.

17. S. Chatterjee & et. al. Hybrid Thermoelectrically Cooled/Heated Back Pack Air Circulating Helmet System, *Patent filing*.

18. S. Chatterjee & et. al. Solid State/Thermoelectrically Heated Oil/Diesel Filter for Automobiles in Cold Regions, *Patent filing*.

19. S. Chatterjee & et. al. Solid State Air Warrior Body Ventilation Vests for Defence Personnel, *J. Inst. Soc. India* 46(1), 40 (2016).

20. S. Chatterjee & et. al. Conceptual Design & Simulation on Peltier Cooling Drinking Water System for Armoured Vehicles, *J. Inst. Soc. India* 44 (4), 227 (2014).

21. S. Chatterjee & et. al. Process for Preparing p-type Thermoelements for Thermoelectric Device from Galena Concentrate, *Patent Sealing*.

22. S. Chatterjee & et. al. Process for Preparing n-type Thermoelements for Thermoelectric Devices from Galena Concentrate, *Patent Sealing*.

23. S. Chatterjee & et. al. Process for Preparing *p*-type Thermoelements for Thermoelectric Devices from Galena Aggregate, *Patent Sealing* No.

24. S. Chatterjee & et. al. Process for Preparing *n*-type Thermoelements for Thermoelectric Devices from Galena Aggregate, *Patent Sealing*.

25. S. Chatterjee & et. al. Process for Preparing High Temperature Sustaining Adhesive for Thermoelectric Modules, *Patent Sealing*.

26. S. Chatterjee & et. al. A Divisional Patent on Process for Preparing Thermoelectric Modules Using High Temperature Sustaining Adhesive and Their Process for Preparing Thermoelectric Modules Using High Temperature Sustaining Adhesive, *Patent Sealing*.

27. M. P. Singh and C.M. Bhandari. Thermoelectric Properties of Bismuth Telluride Quantum Wires, *Solid State Communications* 127, 649 (2003).

28. M. N. Tripathi and C. M. Bhandari. High-Temperature Thermoelectric Performance of *Si-Ge* Alloys, *J. Phys.: Condens. Matter* 15, 5359 (2003).

29. M. P. Singh and C. M. Bhandari. High-Temperature Thermoelectric Behavior of Lead Telluride, *Pramana-Journal of Physics* (Accepted).

30. C. M. Bhandari. Germanium-Silicon Alloys as High Temperature Thermoelectric Materials, *Contemporary Physics* 21, 219 (1960).

31. Prem Kumar D. S, R. Chetty, O.E. Femi, K. Chattopadhyay, P. Malar, and R. C. Mallik. Thermoelectric Properties of *Bi*-Doped Tetrahedrite, *J. Electronic Materials* $1 - 7$ (2016).

32. A. Bali, R. Chetty, and R. C. Mallik. Thermoelectric Properties of PbTe with Indium and Bismuth Secondary Phase*, Indian J. Physics* 90, 665 (2016).

33. Raju Chetty, Ashoka Bali, and Ramesh Chandra Mallik. Tetrahedrites as Thermoelectric Materials: An overview, *J. Materials Chemistry C* 3, 2364 (2015).

34. Ashoka Bali, H. Wang, G. J. Snyder, and Ramesh Chandra Mallik. Thermoelectric Properties of Indium Doped $PbTe_{1-y}Se_y$ Alloys, *J. Applied Physics* 116, 033707 (2014).

35. Ashoka Bali, Il-Ho Kim, Peter Rogl, and Ramesh Chandra Mallik. Thermoelectric Properties of Two-Phase *PbTe* with Indium Inclusions, *J. Electronic Materials* 43, 1630 (2014).

36. M. Kole, T. K. Dey. Effect of Aggregation on the Viscosity of Copper Oxide-Gear Oil Nanofluids, *International Journal of Thermal Sciences* 50(9), 174 (2011).

37. M Kole, T. K. Dey. Thermal Conductivity and Viscosity of Al_2O_3 Nanofluid Based on Car Engine Coolant, *J. Physics D: Applied Physics* 43(31), 315501 (2010).

38. S Das, TK Dey. Electrical Conductivity and Low Field Magnetoresistance in Polycrystalline $La_{1-x}K_xMnO_3$ Pellets Prepared by Pyrophoric Method, *Solid State Communications* 134(12), 237 (2005).

39. M.Kole, T.K. Dey, Investigation of Thermal Conductivity, Viscosity, and Electrical Conductivity of Graphene Based Nanofluids, *J. Applied Physics* 113(8), 084307 (2013).

40. Manjusha Battabyal and T. K. Dey, Seebeck Coefficient in Polycrystalline $La_{0.7}Sr_{0.3-x}Ag_xMnO_3$ Pellets: Analysis in Terms of a Phase Separation Model, *J. Phys: Condensed Matter* 18, $493 - 505$ (2006).

41. Manjusha Battabyal and T. K. Dey, Seebeck Coefficient in Polycrystalline $La_{0.7}Sr_{0.3-x}Ag_xMnO_3$ Pellets: Analysis in Terms of a Phase Separation Model, *J. Phys: Condensed Matter* 18, 493 (2006).

42. V.Ponnambalam, U.V.Varadaraju, High-Temperature Resistivity and Thermopower Studies on Substituted *Bi*-2212 and *Bi*-2201 Systems, *Physica C: Superconductivity and Its Applications* 227(1 − 2), 102 (1994).

43. S.Perumal, S.Gorsse, U.Ail, B.Chevalier, R.Decourt, and A.M. Umarji, Effect of Co-substitution of *Mn* and *Al* on Thermoelectric Properties of Chromium Disilicide, *J.Materials Science* 22748 (2013).

44. S.Perumal, S.Gorsse, U.Ail, B.Chevalier, R.Decourt, and A.M. Umarji, Effect of Composition on Thermoelectric Properties of Polycrystalline CrSi, *J.Electronic Materials* 1042, 42 (2013).

45. S.Perumal, S.Gorsse, U.Ail, M.Prakasam, B.Chevalier, and A.M.Umarji, Thermoelectric Properties of Chromium Disilicide Prepared by Mechanical Alloying, *J.Materials Science* 6018, 48 (2013).

46. D.Sivaprahasam, E. Bouchard, and R Gopalan, Processing of Nanopowders of *Fe-Co-Sb* Alloy by RF Plasma Technique for Thermoelectric Applications, *Materials Lett.*

47. D. Sivaprahasam, R. Gopalan, and G. Sundararajan, Nanocrystalline *Fe-Co-Sp* Thermoelectric Alloy Powder by RF Plasma Technique, *J. Alloys and Compounds*, Shortly to be submitted.

48. H. Subramaniam, D. Sivaprahasam, M. Battabyal, and R. Gopalan, Phase Stability and Thermoelectric Properties of $Cu_{10.5}Zn_{1.5}Sb_4S_{13}$ Tetrahedrite, *J. Alloy Comp*. 667, 323 (2016).

49. M. Battabyal, B. Priyadarshini, D. Sivaprahasam, N S. Karthiselva, and R. Gopalan, The Effect of Cu_2O Nanoparticle Dispersion on the Thermoelectric Properties of *n*-type Skutterudites, *J. Phys. D: Appl. Phys*., 48, 455309 (2015).

50. P. K. Rawat, B. Paul, and P. Banerji, Exploration of *Zn* Resonance Levels and Thermoelectric Properties in Iodine Doped *PbTe* with *ZnTe* Nanostructures, *ACS Applied Materials & Interfaces* 6, 3995 (2014).

51. A. Kumar, P.K. Rawat, and P. Banerji, Carrier Transport Phenomenon and Thermoelectric Properties in Melt-Grown Tellurium Doped *n*-type $Bi_{0.88}Sb_{0.12}$ Alloy, *Materials Science & Engineering B* 186,112 (2014).

52. P. K. Rawat, B. Paul, and P. Banerji, Nanotechnology, Thermoelectric Properties of $PbSe_{0.5}Te_{0.5}$: x (*PbI_2*) with Endotaxial Nanostructures: a Promising *n*-type Thermoelectric Material, *Nanotechnology* 24, 215401 (2013).

53. B. Paul and P. Banerji, Enhancement of Thermoelectric Power Factor Through Modification of Electronic Structure in *PbTe*: *Cr*, *AIP Conf. Proc* 1349, 851 (2012).

54. Diptasikha Das, K. Malik, A. K. Deb, S. Dhara, S. Bandyopadhyay, and Aritra Banerjee, Defect Induced Structural and Thermoelectric Properties of Sb_2Te_3 Alloy, *J. Applied Physics* 118, 045102 (2015).

55. VK Sharma, MK Chattopadhyay, KHB Shaeb, A Chouhan, SB Roy, Kumar Chattopadhyay, Large Magnetoresistance in $Ni_{50}Mn_{34}In_{16}$ Alloy, *Applied Physics Letters* 89(22), 2509 (2006).

56. Kulwinder Kaur and Ranjan Kumar, Effect of Pressure on Electronic and Thermoelectric Properties of Magnesium Silicide: a DFT Study, *Chin. Phys. B* 25(2), 056401 (2016).

57. Kulwinder Kaur and Ranjan Kumar, First Principle Investigation of the Electronic and Thermoelectric Properties of Mg_2C, *Chin. Phys. B* 25(2), 026402 (2016).

Submitted 15.01.2017

P. V. Gorskiy

P. V. Gorskiy

Institute of Thermoelectricity of the NAS and MES
Ukraine, 1 Nauky str., Chernivtsi, 58029, Ukraine

THE CORRELATION BETWEEN THE LATTICE THERMAL CONDCTIVITY OF THERMOELECTRIC MATERIALS BASED ON *Zn-Cd-Sb* AND THE PHASE DIAGRAM OF THE SYSTEM

Based on the analysis of phase diagrams of Zn-Sb, Cd-Sb and Zn-Cd-Sb systems, a correlation between the features of these diagrams and the lattice thermal conductivity of crystalline compounds existing in these systems was established. This correlation was analyzed with considerations of symmetry. Only those compounds and their modifications were considered which exist in crystalline state in the "generation" temperature range of 300-650 K which is relevant for thermoelectric application. Formulae for the components of lattice thermal conductivity tensors of all considered phases were derived with regard to symmetry elements which enter spatial groups to which the respective crystals belong. The lattice thermal conductivity was calculated with the use of the Boltzmann equation for phonons in relaxation time approximation. The relaxation time is determined with regard to normal processes of phonon-phonon scattering, as well as umklapp processes, taking into account different correlation between the frequency of interphonon collisions determined by these processes and phonon frequency. In this case, the symmetry elements determine the number of independent components of the velocity of longitudinal and transverse sound waves, the Gruneisen tensor, and the umklapp coefficient tensor characterizing the dependence of the frequency of umklapp collisions on the phonon frequency. In this way, the number of independent components of the lattice thermal conductivity tensor is determined for each phase. In the Zn-Cd-Sb system, phases with rhombic (including orthorhombic), hexagonal and cubic symmetry are possible. This means that the lattice thermal conductivity tensor can have three, two or only one independent component, respectively. In each case, analytical expressions for these components were obtained. In addition, analysis of the influence of point structural defects on the lattice thermal conductivity of Cd-Sb system was made.

Key words: phase diagram, lattice thermal conductivity, spatial symmetry, umklapp parameters, scattering by interstitial atoms

Introduction

Phase diagrams are known to reflect the equilibrium between different phases in a particular multicomponent system and determine the temperature and concentration intervals of their existence, since, as a rule, they are constructed by experimental or calculated methods in the "temperature-composition" coordinates. In so doing, the corresponding equilibrium curves in these diagrams reflect both the equilibrium between the liquid and solid states, for instance, with the same composition, and the equilibrium between the solid phases of different composition and crystal structure. The "liquid-crystal" equilibrium is decisive when choosing a technology for the production of semiconductor thermoelectric materials, for example, by growing single crystals from melts. The "crystal-crystal"

equilibrium, in turn, determines the composition and crystalline structure of the material that exists in the solid state in a particular temperature range. And since the crystal structure determines the group of spatial symmetry to which the material belongs (at least in the form of a single crystal), then it also determines the characteristics of the tensors of the kinetic coefficients of the material, namely, the thermal conductivity, the electrical conductivity, and the thermoelectric power. And these features determine the sphere of application of the material for thermoelectric energy conversion.

In turn, phase transitions between different solid phases in a system of two or more components are associated not only with a change in composition, but also with a change in the spatial symmetry of the material, even if the composition does not change. The investigation of the effect of such transitions on the lattice thermal conductivity of the *Zn-Cd-Sb* system is the purpose of this article.

The correlation between the components of the lattice thermal conductivity tensor of the *Zn-Cd-Sb* system and the features of its phase diagram

To date, the phase diagram of the *Zn-Cd-Sb* system has been studied most extensively in two sections of *CdSb-ZnSb* and *Cd₄Sb₃-Zn₄Sb₃* [1]. Both these sections are not quasibinary, since Cd_4Sb_3 is a metastable phase, and *ZnSb* melts with decomposition. In themselves, *ZnSb* and *CdSb* are orthorhombic crystals of D_{2h}^{15} group and, apparently, have the lowest symmetry. The first Brillouin zone of these crystals is a rectangular parallelepiped, so that the tensors of the kinetic coefficients of these crystals in the absence of a magnetic field are diagonal, and each of them has, generally speaking, three independent and different components, characterizing the degree of influence of deformations, and consequently anharmonicity. The same symmetry property is possessed by the velocity of sound propagation in these crystals, the Grüneisen parameter, which characterizes the degree of influence of deformations, and, consequently, the anharmonicity of the lattice vibrations, on the phonon energy spectrum, as well as the umklapp parameter characterizing the dependence of the probability of interphonon collisions with the umklapp on the phonon frequency [2]. At the same time, the Debye temperature determined by the temperature dependence of specific heat, just as the specific heat of crystal itself, is a scalar.

Therefore, in the case of the lowest symmetry the following expressions hold true for the components of lattice thermal conductivity tensor [3]:

$$\kappa_{l11} = \frac{\pi\rho\hbar}{32\gamma_{11}^2\theta^3 k_B T_D^2} \int_0^1 \frac{x^4 \exp(x/\theta)dx}{\left(\exp(x/\theta)-1\right)^2} \left[\frac{(v_{1l})^{8/3}(v_{2l}v_{3l})^{2/3}}{x^4+\mu_{11}x} + \frac{2(v_{1t})^{8/3}(v_{2t}v_{3t})^{2/3}}{x\left(3.125\theta^3+\mu_{11}\right)} \right], \tag{1}$$

$$\kappa_{l22} = \frac{\pi\rho\hbar}{32\gamma_{22}^2\theta^3 k_B T_D^2} \int_0^1 \frac{x^4 \exp(x/\theta)dx}{\left(\exp(x/\theta)-1\right)^2} \left[\frac{(v_{2l})^{8/3}(v_{1l}v_{3l})^{2/3}}{x^4+\mu_{22}x} + \frac{2(v_{2t})^{8/3}(v_{1t}v_{3t})^{2/3}}{x\left(3.125\theta^3+\mu_{22}\right)} \right], \tag{2}$$

$$\kappa_{l33} = \frac{\pi\rho\hbar}{32\gamma_{33}^2\theta^3 k_B T_D^2} \int_0^1 \frac{x^4 \exp(x/\theta)dx}{\left(\exp(x/\theta)-1\right)^2} \left[\frac{(v_{3l})^{8/3}(v_{1l}v_{2l})^{2/3}}{x^4+\mu_{33}x} + \frac{2(v_{3t})^{8/3}(v_{1t}v_{2t})^{2/3}}{x\left(3.125\theta^3+\mu_{33}\right)} \right]. \tag{3}$$

In these formulae, γ_{11}, γ_{22}, γ_{33} – are used to denote the components of the Gruneisen tensor, and μ_{11}, μ_{22}, μ_{33}, – the components of tensor of umkapp coefficients. Indices *l,t* refer to the longitudinal and transverse legs, the components of tensors of the Gruneisen parameter and umklapp coefficients are considered to be independent of polarization of phonons. Moreover, T_D is the Debye temperature determined by the specific heat, $\theta = T/T_D$.

At high temperatures, when the Peierls law and the Leibfried-Schlemmann formula are valid, formulae (1) – (3) go over into the following:

$$\kappa_{l11} = \frac{\pi\rho\hbar}{32\gamma_{11}^2\theta k_B T_D^2}\left[\left(v_{1l}\right)^{8/3}\left(v_{2l}v_{3l}\right)^{2/3}F\left(\mu_{11}\right)+\frac{\left(v_{1t}\right)^{8/3}\left(v_{2t}v_{3t}\right)^{2/3}}{3.125\theta^3+\mu_{11}}\right], \tag{4}$$

$$\kappa_{l22} = \frac{\pi\rho\hbar}{32\gamma_{22}^2\theta k_B T_D^2}\left[\left(v_{2l}\right)^{8/3}\left(v_{1l}v_{3l}\right)^{2/3}F\left(\mu_{22}\right)+\frac{\left(v_{2t}\right)^{8/3}\left(v_{1t}v_{3t}\right)^{2/3}}{3.125\theta^3+\mu_{22}}\right], \tag{5}$$

$$\kappa_{l33} = \frac{\pi\rho\hbar}{32\gamma_{33}^2\theta k_B T_D^2}\int_0^1\left[\left(v_{3l}\right)^{8/3}\left(v_{1l}v_{2l}\right)^{2/3}F\left(\mu_{33}\right)+\frac{\left(v_{3t}\right)^{8/3}\left(v_{1t}v_{2t}\right)^{2/3}}{3.125\theta^3+\mu_{33}}\right]. \tag{6}$$

Function $F(\mu)$ is determined as follows:

$$F\left(\mu\right) = \int_0^1\frac{xdx}{x^3+\mu}. \tag{7}$$

In accordance with the phase diagram of the ternary system *Zn-Cd-Sb* constructed in [4], formulae of the form (1) – (6) with the corresponding parameters are valid for *ZnSb*, *CdSb*, an orthorhombic solid solution or the so-called triple ω phase $Zn_xCd_{1-x}Sb$, a monoclinic modification of β-Zn_4Sb_3 into which the γ-Zn_4Sb_3 compound transforms at 766 K, as well as for orthorhombic antimony and the high-temperature orthorhombic modification of η-Zn_3Sb_2 at a temperature below 720 K. These formulae are also formally valid for β-Cd_4Sb_3 and η-Cd_3Sb_2 though the above compounds are metastable.

However, in the *Zn-Cd-Sb* system, even higher-symmetry compounds are possible, for example, hexagonal or cubic. In the case of hexagonal symmetry, two axes lying in a plane perpendicular to the hexagonal axis are equivalent. Therefore, for the velocities of longitudinal and transverse phonons, as well as the components of the tensors that appear in formulas (1) – (6), the following relations hold:

$$v_{1l} = v_{2l} \equiv v_{l\perp}, v_{3l} \equiv v_{l\parallel}, v_{1t} = v_{2t} \equiv v_{t\perp}, v_{3t} \equiv v_{t\parallel},$$
$$\gamma_{11} = \gamma_{22} \equiv \gamma_\perp, \gamma_{33} \equiv \gamma_\parallel, \mu_{11} = \mu_{22} \equiv \mu_\perp, \mu_{33} \equiv \mu_\parallel. \tag{8}$$

Taking them into account, we obtain the following expressions for independent components of lattice thermal conductivity tensor of the hexagonal phases of *Zn-Cd-Sb* system:

$$\kappa_{l11} = \kappa_{l22} \equiv \kappa_{l\perp} = \frac{\pi\rho\hbar}{32\gamma_\perp^2\theta^3 k_B T_D^2}\int_0^1\frac{x^4\exp\left(x/\theta\right)dx}{\left(\exp\left(x/\theta\right)-1\right)^2}\times$$
$$\times\left[\frac{\left(v_{l\perp}\right)^{10/3}\left(v_{l\parallel}\right)^{2/3}}{x^4+\mu_\perp x}+\frac{2\left(v_{t\perp}\right)^{10/3}\left(v_{t\parallel}\right)^{2/3}}{x\left(3.125\theta^3+\mu_\perp\right)}\right], \tag{9}$$

$$\kappa_{l33} \equiv \kappa_{l\parallel} = \frac{\pi\rho\hbar}{32\gamma_\parallel^2\theta^3 k_B T_D^2}\int_0^1\frac{x^4\exp\left(x/\theta\right)dx}{\left(\exp\left(x/\theta\right)-1\right)^2}\times$$
$$\times\left[\frac{\left(v_{l\parallel}\right)^{10/3}\left(v_{l\perp}\right)^{2/3}}{x^4+\mu_\parallel x}+\frac{2\left(v_{t\parallel}\right)^{10/3}\left(v_{t\perp}\right)^{2/3}}{x\left(3.125\theta^3+\mu_\perp\right)}\right]. \tag{10}$$

When the Peierls law and the Leibfried-Schlemmann formula are valid, formulae (9) and (10) go over into the following:

$$\kappa_{l\perp} = \frac{\pi\rho\hbar}{32\gamma_{\perp}^2\theta k_B T_D^2}\left[\left(v_{l\perp}\right)^{10/3}\left(v_{l\parallel}\right)^{2/3}F\left(\mu_{\perp}\right)+\frac{\left(v_{t\perp}\right)^{10/3}\left(v_{t\parallel}\right)^{2/3}}{3.125\theta^3+\mu_{\perp}}\right],$$ (11)

$$\kappa_{l\parallel} = \frac{\pi\rho\hbar}{32\gamma_{\parallel}^2\theta k_B T_D^2}\left[\left(v_{l\parallel}\right)^{10/3}\left(v_{l\perp}\right)^{2/3}F\left(\mu_{\parallel}\right)+\frac{\left(v_{t\parallel}\right)^{10/3}\left(v_{t\perp}\right)^{2/3}}{3.125\theta^3+\mu_{\parallel}}\right].$$ (12)

For single-crystal materials with a hexagonal symmetry, and, consequently, layered, and therefore superlattice, as a rule, inequality $\kappa_l > \kappa_{l\parallel}$ is valid. This inequality holds mainly because sound propagation speed in the direction perpendicular to hexagonal axis is higher than along the hexagonal axis, i.e. perpendicular to layers.

Formulae (9) – (12) are valid for hexagonal limited solid solutions of cadmium and zinc, as well as for hexagonal modifications β-Zn_4Sb_3 and β-Cd_4Sb_3, though the latter of said compounds is metastable.

For phases with cubic symmetry the following relations are valid:

$$v_{1l} = v_{2l} = v_{3l} \equiv v_l, v_{1t} = v_{2t} = v_{3t} \equiv v_t,$$
$$\gamma_{11} = \gamma_{22} = \gamma_{33} \equiv \gamma, \mu_{11} = \mu_{22} = \mu_{33} \equiv \mu .$$ (13)

Consequently, for these phases the components of the lattice thermal conductivity tensor are compared to each other, and it turns into a scalar:

$$\kappa_{l11} = \kappa_{l22} = \kappa_{l33} \equiv \kappa_l = \frac{\pi\rho\hbar}{32\gamma^2\theta^3 k_B T_D^2}\int_0^1\frac{x^4\exp\left(x/\theta\right)dx}{\left(\exp\left(x/\theta\right)-1\right)^2}\left[\frac{v_l^4}{x^4+\mu x}+\frac{2v_t^4}{x\left(3.125\theta^3+\mu\right)}\right].$$ (14)

When the Peierls law and the Leibfried-Schlemmann formula are valid, formula (14) goes over into the following:

$$\kappa_l = \frac{\pi\rho\hbar}{32\gamma^2\theta k_B T_D^2}\left[v_l^4 F\left(\mu\right)+\frac{v_t^4}{3.125\theta^3+\mu}\right].$$ (15)

Temperature dependences of the components of the lattice thermal conductivity tensors of cadmium and zinc antimonides obtained with the use of the derived relationships are given in Fig. 1a –b.

It can be seen from the plots that the approach used, in contrast to traditional approaches, makes it possible to obtain estimates of the components of the lattice thermal conductivity tensors of *ZnSb* and *CdSb*, consistent with the experimental data, and the degree of its anisotropy, which was mentioned in [3] (without citing specific temperature dependences). However, it should be borne in mind that total thermal conductivity of a single crystal, consisting of lattice and electron or hole components, is always determined experimentally.

These components in a variety of thermoelectric materials, in particular in cadmium and zinc antimonides, can be comparable. Therefore, in order to estimate the microscopic characteristics of phonon-phonon scattering, in particular, the umklapp coefficient, a preliminary separation of these components from each other is required. This separation is carried out exceptionally by calculation on the basis of experimental data on electrical condctivity, the Hall effect, and thermoEMF using the Wiedemann-Franz relation.

And temperature dependences of its anisotropy – in Fig.2a – b.
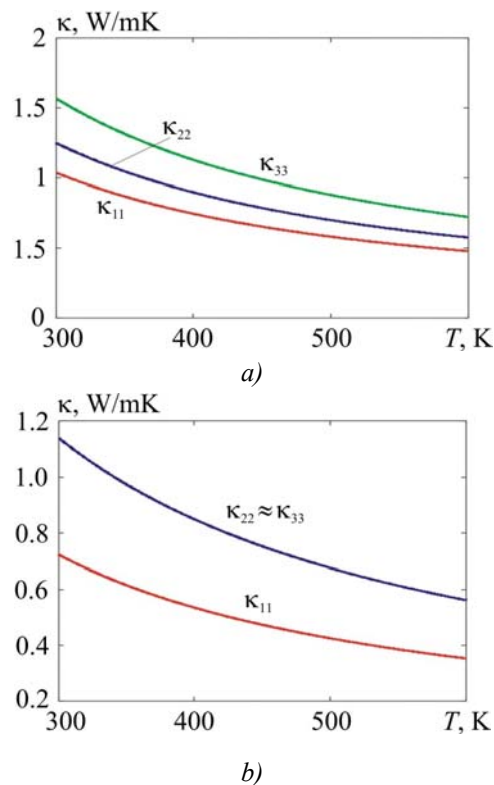

a)

b)

Fig. 1. Temperature dependences of the components of the lattice thermal conductivity
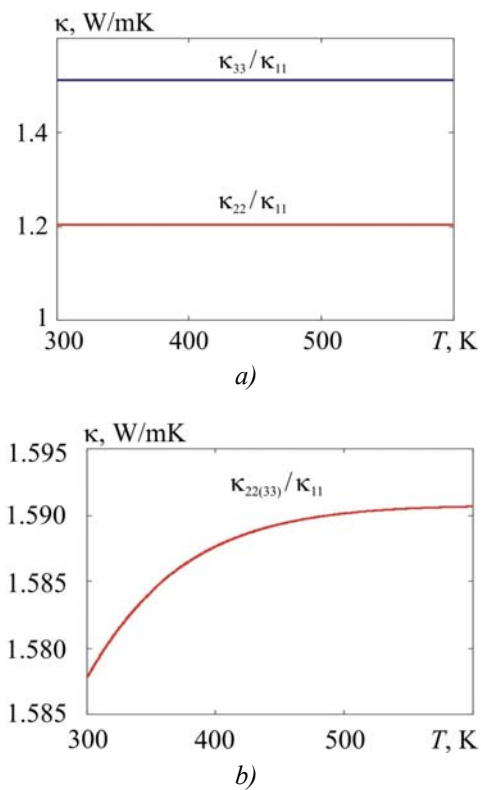*tensors of zinc antimonide ZnSb (a) and cadmium antimonide CdSb*

a)

b)

Fig. 2. Temperature dependences of thermal conductivity anisotropy
of zinc antimonide ZnSb (a) and cadmium antimonide CdSb

The influence of point defects on the lattice thermal conductivity of *Zn-Cd-Sb* system

As long as [5] deals with the possibility of increasing the thermoelectric figure of merit of zinc antimonide due to introduction into its composition of a certain atomic fraction of cadmium isovalent impurity, it is of certain interest to study the influence of such impurities on the lattice thermal conductivity of zinc antimonide. The authors of [5] note that cadmium isovalent impurity sufficiently strongly reduces the lattice thermal conductivity of zinc antimonide. Presumably, this decrease may be due to the fact that the presence of such an impurity leads to the appearance of an additional mechanism for scattering of phonons due to the difference in the masses of cadmium and zinc atoms. We consider this effect in the isotropic approximation, assuming that the impurity atoms are randomly distributed in the bulk of a single crystal. In this case, in accordance with the approach described in [6], the relaxation time due to scattering by impurity atoms can be represented as:

$$\tau_i = \frac{4\pi\rho^2 v_1 v_2 v_3}{N_i (\Delta M)^2 \omega^4}. \tag{16}$$

In this formula, N_i – volumetric concentration of impurity atoms, $\Delta M = M_{Cd} - M_{Zn}$ – mass difference of cadmium and zinc atoms. The density of crystal ρ in this case should be understood to mean its density in the presence of isovalent impurity. In turn, for $Cd_x Zn_{1-x} Sb$ composition N_i can be determined as follows:

$$N_i = \frac{\rho N_A x}{2 \left(x A_{Cd} + (1-x) A_{Zn} + A_{Sb} \right)}. \tag{17}$$

In this formula, N_A – Avogadro number, A_{Cd}, A_{Zn}, A_{Sb} – tabular atomic masses of cadmium, zinc and antimony, respectively, other notations are explained above.

Therefore, (16) can be finally rewritten as:

$$\tau_i = \frac{8\pi\rho v_1 v_2 v_3 \left(x A_{Cd} + (1-x) A_{Zn} + A_{Sb} \right)}{N_A x \left(M_{Cd} - M_{Zn} \right)^2 \omega^4}. \tag{18}$$

Thus, in the most general form with regard to the contribution of transverse phonon legs, the lattice thermal conductivity can be represented as:

$$\kappa_{l11} = \frac{\pi\rho\hbar}{32\gamma_{11}^2 \theta^3 k_B T_D^2} \int_0^1 \frac{x^4 \exp(x/\theta)dx}{(\exp(x/\theta)-1)^2} \times$$
$$\times \left[\frac{(v_{1l})^{8/3}(v_{2l}v_{3l})^{2/3}}{x^4(1+\mu_{il11})+\mu_{11}x} + \frac{2(v_{1t})^{8/3}(v_{2t}v_{3t})^{2/3}}{x(3.125\theta^3 + \mu_{11}) + \mu_{it11}x^4} \right], \tag{19}$$

$$\kappa_{l22} = \frac{\pi\rho\hbar}{32\gamma_{22}^2 \theta^3 k_B T_D^2} \int_0^1 \frac{x^4 \exp(x/\theta)dx}{(\exp(x/\theta)-1)^2} \times$$
$$\times \left[\frac{(v_{2l})^{8/3}(v_{1l}v_{3l})^{2/3}}{x^4(1+\mu_{il22})+\mu_{22}x} + \frac{2(v_{2t})^{8/3}(v_{1t}v_{3t})^{2/3}}{x(3.125\theta^3 + \mu_{22}) + \mu_{it22}x^4} \right], \tag{20}$$

$$\kappa_{l33} = \frac{\pi\rho\hbar}{32\gamma_{33}^2 \theta^3 k_B T_D^2} \int_0^1 \frac{x^4 \exp(x/\theta)dx}{(\exp(x/\theta)-1)^2} \times$$
$$\times \left[\frac{(v_{3l})^{8/3}(v_{1l}v_{2l})^{2/3}}{x^4(1+\mu_{il33})+\mu_{33}x} + \frac{2(v_{3t})^{8/3}(v_{1t}v_{2t})^{2/3}}{x(3.125\theta^3 + \mu_{33}) + \mu_{it33}x^4} \right]. \tag{21}$$

In these formulae, additional dimensionless parameters related to phonon scattering by impurities have the following values:

$$\mu_{il11} = \frac{3x(A_{Cd} - A_{Zn})^2 (v_{1l}v_{2l}v_{3l})^{2/3}}{128\gamma_{11}^2 [xA_{Cd} + (1-x)A_{Zn} + A_{Sb}]RT},\qquad(22)$$

$$\mu_{il22} = \frac{3x(A_{Cd} - A_{Zn})^2 (v_{1l}v_{2l}v_{3l})^{2/3}}{128\gamma_{22}^2 [xA_{Cd} + (1-x)A_{Zn} + A_{Sb}]RT},\qquad(23)$$

$$\mu_{il33} = \frac{3x(A_{Cd} - A_{Zn})^2 (v_{1l}v_{2l}v_{3l})^{2/3}}{128\gamma_{33}^2 [xA_{Cd} + (1-x)A_{Zn} + A_{Sb}]RT},\qquad(24)$$

$$\mu_{it11} = \frac{3x(A_{Cd} - A_{Zn})^2 (v_{1t}v_{2t}v_{3t})^{2/3}}{128\gamma_{11}^2 [xA_{Cd} + (1-x)A_{Zn} + A_{Sb}]RT},\qquad(25)$$

$$\mu_{it22} = \frac{3x(A_{Cd} - A_{Zn})^2 (v_{1t}v_{2t}v_{3t})^{2/3}}{128\gamma_{22}^2 [xA_{Cd} + (1-x)A_{Zn} + A_{Sb}]RT},\qquad(26)$$

$$\mu_{it33} = \frac{3x(A_{Cd} - A_{Zn})^2 (v_{1t}v_{2t}v_{3t})^{2/3}}{128\gamma_{33}^2 [xA_{Cd} + (1-x)A_{Zn} + A_{Sb}]RT}.\qquad(27)$$

In formulae (22) – (27), R is a universal gas constant, other notations are explained above.

Let us estimate, for instance, μ_{il11}. At $v_{1l} = 3.803 \cdot 10^3$ m/s, $v_{2l} = 4.034 \cdot 10^3$ m/s, $v_{3l} = 3.834 \cdot 10^3$ m/s, $A_{Cd} = 112.41$, $A_{Zn} = 65.39$, $A_{Sb} = 121.75$, $\gamma_{11} = 1.5$, $x = 10^{-3}$, $T = 300$ K we get $\mu_{il11} = 7.463 \cdot 10^{-4}$, which is almost four orders of magnitude less than umklapp parameter [3]. Even if we assume $x = 0.5$, i.e. consider the composition $Cd_{0.5}Zn_{0.5}Sb$, still we will have $\mu_{il11} = 0.332$, which is more than an order of magnitude less than umklapp parameter. Moreover, scattering by point defects alone, without the action of other scattering mechanisms, in particular scattering with umklapp, in itself does not provide a finite value of the lattice thermal conductivity, since the frequency dependence of the phonon scattering intensity on these defects is the same as for normal phonon-phonon scattering. Thus, the decrease in the lattice thermal conductivity during the transition from *ZnSb* to the ternary system $Cd_xZn_{1-x}Sb$ [5] cannot be explained by the presence of the "foreign" cadmium atoms themselves in the initial zinc antimonide lattice. It should be associated, on the one hand, with the rearrangement of this lattice, which leads to an increase in umklapp parameter, and on the other, to the appearance or increase in the concentration of such structural defects the phonon scattering intensity at which varies with a frequency more slowly than ω^4. These can include, for instance, phase inclusions (inhomogeneities), dislocations and packing defects. Formulae for the relaxation time of phonons during scattering by these defects are given in [6] for the case of a crystal with a simple cubic lattice with one atom in the unit cell. The generalization of these formulae for the case of lattices of cadmium and zinc antimonides is far from being trivial and is not the purpose of this article.

Conclusions

1. The correlation between the lattice thermal conductivity of materials of the *Zn-Cd-Sb* system and its phase diagram is due to the existence in this system of solid phases with different spatial symmetry.
2. Since phases with orthorhombic (including orthorhombic), hexagonal and cubic symmetries can

exist in the *Zn-Cd-Sb* system, the lattice thermal conductivity tensor for these phases can have three, two and one independent components, respectively.

3. In itself, the presence of "foreign" cadmium atoms in the ternary compound $Cd_xZn_{1-x}Sb$ at small x cannot explain the observed decrease in the lattice thermal conductivity of this compound in comparison with the lattice thermal conductivity of the initial *ZnSb*. Such a reduction is possible only if the addition of an isovalent cadmium impurity leads to reconstruction of the lattice, and, hence, to an increase in umklapp parameter, and also to an increase in the concentration of structural defects, the phonon scattering intensity at which increases with frequency more slowly than ω^4, namely phase inclusions (inhomogeneities), dislocations and packing defects.

The author considers it his pleasant duty to express gratitude to academician L.I.Anatychuk for the formulation of the problem.

References

1. V. B. Lazarev, V. Ya. Shevchenko, Ya. Kh. Grinberg, and V. V. Sobolev, $A^{II}B^{V}$ *Semiconductor Compounds* (Moscow: Nauka, 1978), 256p.

2. P. V. Gorskiy, V. P. Mikhalchenko, Reduction of Thermoelectric Material Lattice Thermal Condu ctivity Using Shape-Forming Element Optimization, 1, 19 – 27 (2013).

3. P. V. Gorskiy, Lattice Thermal Conductivity of Thermoelectric Materials Based on *Zn-Cd-Sb*, *J. Thermoelectricity* 5, 24 – 31 (2016).

4. L. A. Zabdur, Phase Equilibria in Ternary *Cd-Sb-Zn* System, *Calhad.* 21(3), 349 – 358 (1997).

5. M. I. Fedorov, L. V. Prokofyeva, Yu. I. Ravich, P. P. Konstantinov and A. A. Shabaldin, Thermoelectric Figure of Merit of *ZnSb* Intermetallide, *Semiconductors* 48(4), 448 – 453 (2014).

6. P. G. Klemens, Lattice Thermal Conductivity. – *In book: Solid State Physics. Advances in Research and Applications. Vol.7, p.* 1 – 98.

I. I. Sanduleac, A. I. Casian

Technical University of Moldova, 168,
Stefan cel Mare Ave., MD-2004, Chisinau, Moldova

I. I. Sanduleac

STATE OF THE ART AND NEW POSSIBILITIES TO INCREASE THETHERMOELECTRIC FIGURE OF MERIT OF ORGANIC MATERIALS

A. I. Casian

In this paper, a short review of promising thermoelectric organic materials is provided. It is shown that organic compounds, under appropriate synthesis and after accurate tuning of electronic properties by manipulating the internal molecular structure, may become serious substitutes of classical inorganic thermoelectric materials. A big step forward constitutes the implementation of new trends of nanotechnology in designing the thermoelectric structures. In this order, we provide the most important results, achieved in several low-dimensional thermoelectric structures, such as quantum-dot superlattices or molecular nanowires of conducting polymers. More specifically, the latter structures may become very promising thermoelectric materials, if we refer to the predicted values of ZT ~ 15. Whereas these predictions were made in the frame of simple one-dimensional physical model, in a more realistic physical model the values of ZT ~ 1.1 for an n- type and ZT ~ 4 for a p-type compound are predicted.

Key words: Thermoelectricity, organic compound, thermoelectric figure-of-merit, thermoelectric efficiency, the coefficient of performance.

Introduction

According to IEA (International Energy Agency) World Energy Outlook 2016, in 2040 the energy sector will look in the following way. It is expected a 30 % increase in energy demand, mostly from developing countries, 37 % of power generation will be from renewables, compared to 23 % in 2016, 150 million vehicles compared to 1.3 m, 50 % growth in demand for natural gas, overtaking the coal in the global energy mix. The level of oil consumption will constitute 103 million barrels per day, compared to 92.5 mb/d in 2015. The average annual growth of carbon emissions in energy sector will constitute 0.5 %, compared to 2.4 % per year since 2000 [1].

This situation will take place in 2040, if the nations will abide the pledges made as part of Paris Agreement, which entered into force on 4 November 2016. This is a major step forward in the fight against global warming. The agreement sets out a global action plan to put the world on track to avoid dangerous climate change by limiting global warming to well below 2 °C. One of the major Governments agreements is to undertake rapid actions thereafter in accordance with the best available science. In this order, one expects to slow down the projected rise in energy-related carbon emissions, from an average of 650 million tons per year since 2000, to around 150 million tons per year in 2040.

The era of fossil fuels appears far from over and underscores the challenge of reaching more ambitious climate goals. As a result of major transformations in the global energy system that will take place over the next decades, renewables and natural gas are the big winners in the race to meet energy demand growth until 2040. Therefore, to achieve the 2 °C target, the energy sector must be carbon-neutral by 2100. It is expected a growth of renewables from ~ $4.7 \cdot 10^{12}$ kWh in 2012 to ~ $10.6 \cdot 10^{12}$ kWh in 2040.

The use of thermoelectric efficient devices may constitute a cornerstone in this huge process of building a new technological future. Thermoelectricity offers new environment-friendly technological solutions of energy conversion, with the advantages of small size, high reliability, no pollutants and feasibility in a wide temperature range.

In the period of 60's – 70's, all attempts to improve thermoelectric figure-of-merit ZT led to the establishment of a threshold value of $ZT \sim 1$ in classical semiconductors [2]. Later, it turned out that ZT cannot be increased too much mainly because of the interconnectivity of the electrical conductivity and thermal conductivity of a material. Consequently, it concluded that researches that are more thorough are needed in the field of thermoelectric properties of materials. As a result, in 1970 the International Thermoelectric Society (ITS) is founded. In the period between 60's and 90's, no significant progress is achieved, the best thermoelectric materials being $Bi2Te3$ and its alloys with $ZT \sim 1$ for near room temperatures [3], and $PbTe$ for higher temperature range. There were no efficient thermoelectric materials for the temperature range 600 – 700 K [4]. Only at the beginning of the 90's the scientific community is attracting new attention to thermoelectric materials, mainly driven by the energy crisis and the problem of environmental conservation. As a result, many new discoveries are made, including the possibility to improve the thermoelectric properties by manipulating the crystal structure or composition of the material. Two main investigation areas are delimited: bulk thermoelectric materials and low dimensional systems [5]. During the mid of the 20'th century until now, many big ideas have served as guiding principles in focusing research and advancing knowledge. These include the use of heavy atom masses and complex unit cells, alloy scattering of phonons, bulk nanostructuring, phonon glass/electron crystal, quantum confinement of electrons, hierarchical nanostructuring, anharmonicity, and band engineering [6]. Recently, a large number of research demonstrated that organic materials, bulk or nanostructured, may become very promising thermoelectric materials [7].

In terms of internal structural arrangement, thermoelectric materials can be classified in two broad categories: bulk TE materials and nanostructured TE materials. In recent years, an increasingly strong interlacing of these categories is noticed. Bulk material approach is related to the structures with many atoms in the basic region of the crystal. In this case, the physical properties are more or less isotropic and do not change when the extraction or addition of any number of atoms is performed. In a low-dimensional system, the movement of electrons, phonons or photons is described by the wave vectors, which are defined in two dimensions (2D), or one dimension (1D). When the dimensionality is reduced, the quantum and surface effects are more pronounced, which leads to new physical properties, different from the bulk ones. In terms of the number of dimensions, different low dimensional systems can be distinguished, such as 2D quantum structures, quantum wires (1D) and quantum dots structures (0D). The density of energetic states dramatically changes, when the dimensionality is reduced. This phenomenon leads to significant changes in electronic and thermal transport properties [8, 10]. Note that recently [11] it has been shown that the thermal conductivity of indium tin oxide films with nanogranular structure may be strongly suppressed due to the enhancement of phonon scattering on grain boundaries and reaches ultra-low values $\sim 0.84 \pm 0.12$ Wm^{-1}K^{-1} at room temperature. Taking into account high values of the thermoelectric power factor [12], such films demonstrate promising thermoelectric properties.

Recently, the scientific community has focused more and more on the research of organic thermoelectric materials, particularly conjugated polymers. Among the most important benefits of these materials are: abundant raw materials, cheap and environmentally friendly production technology, flexibility and extensive possibilities to manipulate the molecular structure. Because of the instability of organic materials at high temperatures, the application of these materials as thermoelectric convertors is limited to low or moderate temperatures [13]. One of the big advantages

of organic compounds is their low thermal conductivity, compared to the majority of inorganic materials. This property is very important for a thermoelectric material, since the reduction of parasitic heat loss allows high *ZT* values. However, the electrical conductivity of most organic compounds is relatively low. At the same time, physical properties can be optimized effectively using chemical methods and molecular doping procedures. In recent years, a rapid development of the electronics on organic basis is noticed. This has led to the synthesis of hundreds of organic semiconductor compounds with high charge carrier mobility, similar to that of polycrystalline silicon [14].

Usually, the conjugated polymers manifest high doping reversibility, mechanical flexibility and satisfactory electric conductivity along the backbone. However, polymeric materials are often heterogeneous, because of the coexistence of crystalline and non-crystalline regions; the layering of the stack is difficult to control and the mass distribution of molecules is large. The overcome of these obstacles can be achieved by applying various synthesis schemes. The electrical conductivity, as well as the Seebeck coefficient, depends on the concentration of charge carriers, the chemical structure of monomers, as well as the spatial arrangement of the molecules. In the organic materials, like in the inorganic ones, the thermal transport consists of the contribution of the lattice and of the charge carriers. However, the Wiedemann-Franz law is often violated due to the strong coupling between electric charges and the lattice vibrations. As a result, the contribution of charge carriers to thermal conductivity is low. As an example, one reports that if the electrical conductivity of PA (polyacetylene), PANI (polyaniline) and PPY (polypyrrole) samples is increased by three orders of magnitude, the total thermal conductivity increases only from 0.1 $W \cdot m^{-1} K^{-1}$ to 1 $W \cdot m^{-1} K^{-1}$ [15].

Significant improvement of thermoelectric properties is reported for PEDOT: PSS thin films with high electrical conductivity, treated with hydrophilic solvents (ethylene glycol or DMSO): $ZT \sim 0.42$ at $T = 300$ K [16]. The value of power factor $P = 1.27$ $\mu Wm^{-1}K^{-2}$ was reported in PP-PEDOT thin films [7]. It is estimated that the thermoelectric figure-of-merit $ZT \sim 1.02$, but this result should be verified experimentally, by accurately measuring the thermal conductivity. The PEDOT nanowire/PEDOT hybrid composites have demonstrated a power factor P as high as 446.6 $\mu W \cdot m^{-1}$ K^{-2} and $ZT \sim 0.44$ at room temperature [17].

Recently, it has been demonstrated [18] that in freestanding PEDOT films both electrical conductivity and Seebeck coefficient were increased simultaneously by controlling the synthesis conditions, achieving a power factor ~ 7.9 $\mu W \cdot m^{-1}K^{-2}$. It is a very important result. First-principles calculations [19] based on density-functional theory (DFT) and the Boltzmann transport equation have shown that the polypyrrole (PPy), which is one of the conducting polymers, has promising thermoelectric properties.

Development of a thermoelectric generator from *p*-type optimized PEDOT: TOS and *n*-type non-optimized *TTF – TCNQ/PVC* was reported. This device can generate a power of $P \sim 0.128$ μW at $T = 10$ K and 0.27 μW at $T = 30$ K, a very important result for medical use [16]. At the same time, another promising research direction is the use of mixed organic-inorganic compounds [20]. As an example, in phenyl acetylene doped with silicon nanoparticles, $ZT = 0.57$ at $T = 300$ K was reported [21]. Research progress has been obtained in the study of thermoelectric property of Poly (M-ett) (M = metal, ett = ethylenetetrathiolate), which provides the best performance of *n*-type organicthermoelectric materials [22].

Highly conducting *Q*1*D* organic crystals

The small-molecule based organic compounds are another class of promising thermoelectric organic materials. This class of materials includes charge-transfer complex compounds and molecular

semiconductors. Particularly, our research is focused on the investigations of thermoelectric properties of charge-transfer quasi-one-dimensional organic compounds such as tetrathiafulvalene-tetracyanoquinodimethane (*TTF – TCNQ*), tetrathiotetracence-tetracyanoquinodimethan (*TTT(TCNQ)₂*) and tetrathiotetracene-iodide (*TTT₂I₃*) [23, 24, 25]. The abovementioned crystals belong to the class of quasi-one-dimensional (*Q1D*) organic crystals. The main characteristic of these compounds is the presence of a predominant direction in the internal structure. The molecules arrange in longitudinal chains, generating parallel segregated stacks. The distance between neighboring chains is much larger than the distance between two adjacent molecules along the chain. Due to this structural peculiarity, the physical properties of the crystal, such as electrical and thermal conductivity, are strongly anisotropic. In such a compound, the molecules from one chain play the role of acceptors and from another chain – of donors. As example, in *n*-type *TTF – TCNQ* and *TTT(TCNQ)₂*, *TTF* and *TTT* molecules are strong donors and *TCNQ* molecules – acceptors. In *p*-type *TTT₂I₃*, the electric charge is transferred from *TTT* molecular chains to iodine chains and the carriers are holes. The pronounced quasi-one dimensionality of internal structure imposes some peculiarities in the movement of charge carriers. Along the longitudinal direction, the overlap of π-electron wave functions generates a narrow conduction band, providing a metallic-type electrical conductivity. In transversal to the chain direction, due to the significant interchain distance, the overlap of electron wavefunctions is insignificant and the charge transport is of hopping type. However, because the interchain interactions are very small, we will describe the transport in longitudinal direction in the first approximation in a 3D band model.

The cornerstone idea of this physical crystal model is that two main electron-phonon interactions may compensate each other under some special conditions. As a result, for a narrow region of energetic states in the conduction band, the relaxation time of charge carriers increases significantly, being limited by scattering on impurity. However, in real-existing crystals the interchain interaction is present with more or less influence. Consequently, the relaxation time is limited not only by the impurity scattering, as one assumed in the 1D model, but also by the scattering on the neighboring molecular chains. Due to this, the simpler 1D physical model was improved by taking into consideration the interaction of the nearest chains in one plane (2D model) [26 – 28]. These works allowed us to conclude that for crystals with low purity level, the interchain interaction is insignificant. Contrarywise, for high-purity crystals, the abovementioned interchain interaction becomes important, diminishing significantly the relaxation time of the carriers. As a result, *ZT* is reduced considerably. In order to describe more accurately the thermoelectric properties of quasi-one dimensional organic crystals of *TTT(TCNQ)₂* and *TTT₂I₃*, a more complete physical model was elaborated, taking into account the interaction of carriers with the neighboring molecular chains (3D model) [29 – 31] and with impurities.

The Hamiltonian of the crystals has the form:

$$H = \sum_{k} E(\boldsymbol{k}) a_k^+ a_k + \sum_{q} \hbar \omega_q b_q^+ b_q + \sum_{k,q} A(\boldsymbol{k},\boldsymbol{q})(b_q + b_{-q}^+) a_k^+ a_{k-q}$$
$$+ \left(I_i V_{0i} \sum_{l=1}^{N_i} e^{-iqr_l} + I_d V_{0d} e^{-E_0/k_0 T} \sum_{m=1}^{N_d} e^{-iqr_m} \right) V^{-1} \sum_{k,q} a_k^+ a_{k-q}$$

(1)

The first term describes the energy of charge carriers in the tight binding and nearest neighbor approximations. For electrons, the energy *E*(*k*) is measured from the bottom of the conduction band. For holes – from the top of the valence band. a_k^+, a_k are the creation and annihilation operators for a charge carrier with the wave vector *k*. The second term describes the energy of acoustic longitudinal phonons, considered in the harmonic and tight-binding approximations. For not very high temperatures and weak electric fields, the optical phonons can be neglected. b_q^+, b_q are the creation and

annihilation operators for a phonon with the wave vector $\boldsymbol{q}$ and frequency $\omega(\boldsymbol{q})$. In these crystals, due to high molecule polarizability, two main interaction mechanisms of charge carriers with phonons take place. The first mechanism is of the deformation potential type, determined by the variation of transfer energies with respect to the intermolecular distances. The second interaction mechanism is similar to that of a polaron. In this case, the interaction is caused by the variation of induced polarization energy of molecules surrounding the charge carrier. Both abovementioned interactions are included in the matrix element $A(\boldsymbol{k}, \boldsymbol{q})$:

$$\left| A(\boldsymbol{k}, \boldsymbol{q}) \right|^2 = 2\hbar / \left(NM\omega_q \right) \left\{ w_1'^2 \left[\sin(k_x b) - \sin\left((k_x - q_x)b\right) \mp \gamma_1 \sin(q_x b) \right]^2 + \right.$$
$$\left. + w_2'^2 \left[\sin(k_y a) - \sin\left((k_y - q_y)a\right) \mp \gamma_2 \sin(q_y a) \right]^2 + w_3'^2 \left[\sin(k_y c) - \sin\left((k_y - q_y)c\right) \mp \gamma_3 \sin(q_y c) \right]^2 \right\} \quad (2)$$

where M is the mass of TTT or $TCNQ$ molecule, N is the number of molecules in the basic region of the crystal. w_1', w_2' and w_3' are the derivatives with respect to the intermolecurar distances of transfer energies w_1, w_2, w_3 of a carrier from a given molecule to the nearest ones along lattice vectors a, b, c. The parameters γ_1, γ_2 and γ_3 have the means of the ratios of amplitudes of second interaction to the first one in the direction of chains and in transversal directions. In (2) the upper sign corresponds to p-type TTT_2I_3 with the conducting x direction along $\boldsymbol{b}$. The lower sign corresponds to n-type $TTT(TCNQ)_2$ with the conducting x direction along $\boldsymbol{c}$.

Even the purest crystals contain a certain amount of impurities. In this physical model for the crystal, two most important types of impurities are considered (the last two terms in (1)): point-like neutral impurity centers and temperature-activated defects. The latter are related to different coefficients of thermal expansion for the chains of different composition. In (1) r_1, r_m are the radius vectors of impurities and defects; I_i, V_{0i}, N_i are, respectively, the energy of carrier interaction with an impurity, the volume of impurity action and the number of impurities; I_d, V_{0d}, N_d are the same for defects. E_0 is the activation energy of a such defect, V is the volume of the basic region of the crystal. At room temperature, the scattering of charge carriers on both types of impurity centers is described by the dimensionless parameter D_0, which is proportional to the impurity and defect concentration and may be very small in pure and perfect crystals.

The thermoelectric properties are investigated by considering a weak electrical field and a weak temperature gradient applied along the conductive chains. At room temperature, the kinetic energy of the charge carriers along the transversal directions is much smaller than the kinetic energy in the longitudinal direction. Due to this, it is possible to neglect the transversal kinetic energy of carriers in the scattering processes. So as the crystal model contains many interactions, in the linear approximation with respect to applied field the general expression for electrical conductivity tensor is deduced applying the method of two-particle retarded Green functions depending on temperature. The equation for the two-particle Green function contains the three-particle Green functions, for which new equations are written. In the latter the higher order Green functions are expressed through the two-particle ones and in such a way the chain of equations for the two-particle Green function is closed. After some transformations, the equation for Green function takes the form of a generalized Boltzmann kinetic equation. Considering carrier scattering on acoustic phonons at room temperature as elastic, the relaxation time of charge carriers is expressed through the probability of the scattering process. As a result, the linearized kinetic equation is solved analytically. Let us consider that the electrical field and the temperature gradient are applied in x direction and the transport is directed in the same x direction. Then the electrical conductivity σ_{xx}, Seebeck coefficient S_{xx}, electronic thermal

conductivity and the thermoelectric figure-of-merit $(ZT)_{xx}$ can be expressed analytically through the mass operator of the Green function. The latter is an analog of the inverse relaxation time of carriers.

Crystals of *p*-type *TTT₂I₃*

Modeling of the thermoelectric properties can be realized only numerically. In Fig. 1 (*a* and *b*) the longitudinal electrical conductivity and thermal conductivity of TTT_2I_3 crystals with different degree of purity as function of dimensionless Fermi energy $\varepsilon_F = E_F/2w_1$ are presented, where E_F is the Fermi energy.
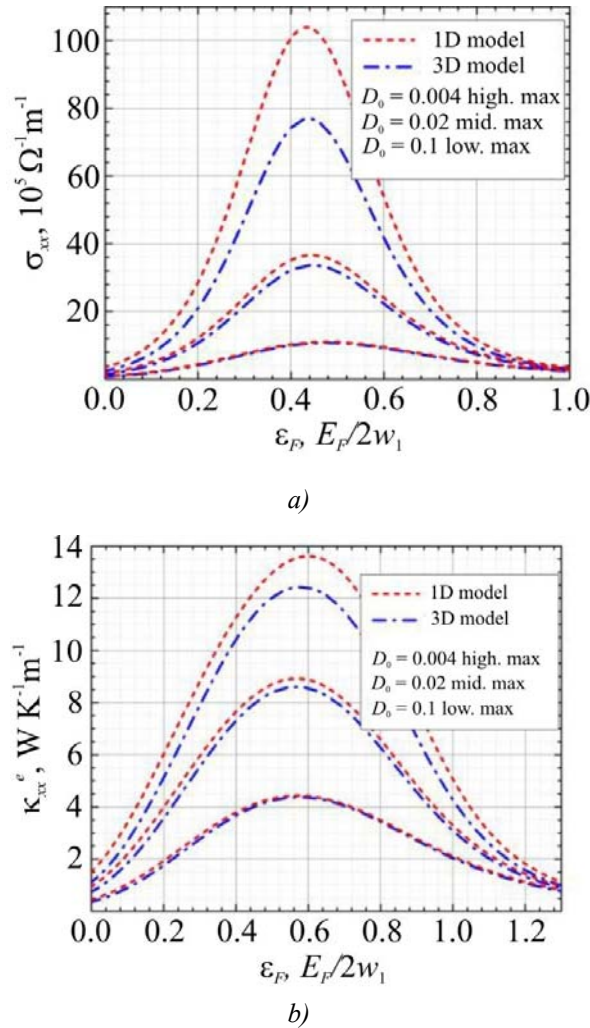

a)

b)

Fig. 1. a) Electrical conductivity σ$_{xx}$ and b) electronic thermal conductivity
along the direction of molecular chains as a function of dimensionless
Fermi energy for quasi-one-dimensional organic crystal of TTT₂I₃.

The crystal parameters are the same as in [30], only more perfect crystals are considered. The value $D_0 = 0.1$ corresponds to not very pure TTT_2I_3 crystals, grown from gaseous phase with stoichiometric conductivity 10^6 $\Omega^{-1}m^{-1}$ [25]. In this case, the 1D and 3D models practically coincide in the entire region of ε_F variation. The value $D_0 = 0.02$ corresponds to purer crystals with stoichiometric conductivity $\sigma_{xx} \sim 3 \cdot 10^{6} {}^{-1}m^{-1}$ not synthesized yet. It is seen that the deviation between the 1D and 3D models remains small. In this case, the scattering probability of carriers on neighbouring chains is much smaller than the scattering on impurities and the simpler 1D model is yet applicable. Only for ultra-pure hypothetic crystals, with $D_0 = 0.004$ and stoichiometric conductivity $\sigma_{xx} \sim 6.2 \cdot 10^6 m^{-1}$, the impurity scattering processes are smaller and the mentioned interchain interaction becomes important.

In this case, the more complete 3D physical model should be applied. In TTT_2I_3 crystals the stoichiometric concentration of charge carriers is $n = 1.2 \cdot 10^{21}$ cm^{-3}, to which corresponds $\varepsilon_F \sim 0.37$. It is seen that with the increase of carrier concentration, σ_{xx} grows rapidly.

From Fig. 1b it is observed that the electronic thermal conductivity is less sensitive to interchain interaction. Usually, the lattice thermal conductivity of organic crystals is low (for TTT_2I_3 $\kappa_{xx}{}^L \sim 0.6$ WK^{-1}m^{-1}). In the purest stoichiometric crystals $\kappa_{xx}{}^e \sim 9$ WK^{-1}m^{-1}, much higher than $\kappa_{xx}{}^L$. If the carrier concentration grows, $\kappa_{xx}{}^e$ increases considerably. Also, by comparing Fig. 1a and b, one can observe that the maxima of σ_{xx} are slightly displaced toward lower values of ε_F for TTT_2I_3 with respect to the maxima of $\kappa_{xx}{}^e$. This is related to the phenomenon of violation of the Wiedemann-Franz law in these crystals [32] and is favourable for the improvement of thermoelectric properties.

In Fig. 2a and b, the Seebeck coefficient S_{xx} and thermoelectric figure-of-merit $(ZT)_{xx}$ along the molecular chains as a function of dimensionless Fermi energy are presented.

For stoichiometric TTT_2I_3 crystals, S_{xx} weakly depends on crystal perfection and is close to $S_{xx} \sim 35 - 40$ µV/K, reported experimentally. It is observed (Fig. 2a) that S_{xx} is less sensitive to the interchain interactions and it increases considerably with the decrease of ε_F. If the hole concentration is diminished twice, from $n_h = 1.2 \cdot 10^{21}$ cm^{-3} (with $\varepsilon_F \sim 0.37$) down to $n_h = 0.6 \cdot 10^{21}$ cm^{-3} (with $\varepsilon_F \sim 0.12$), $S_{xx} \sim 260$ µV/K is expected for the purest crystals with $D_0 = 0.004$.

In stoichiometric case the figure-of-merit $(ZT)_{xx}$ is quite low (Fig. 2b, $(ZT)_{xx} \sim 0.1$ for $\varepsilon_F \sim 0.37$).
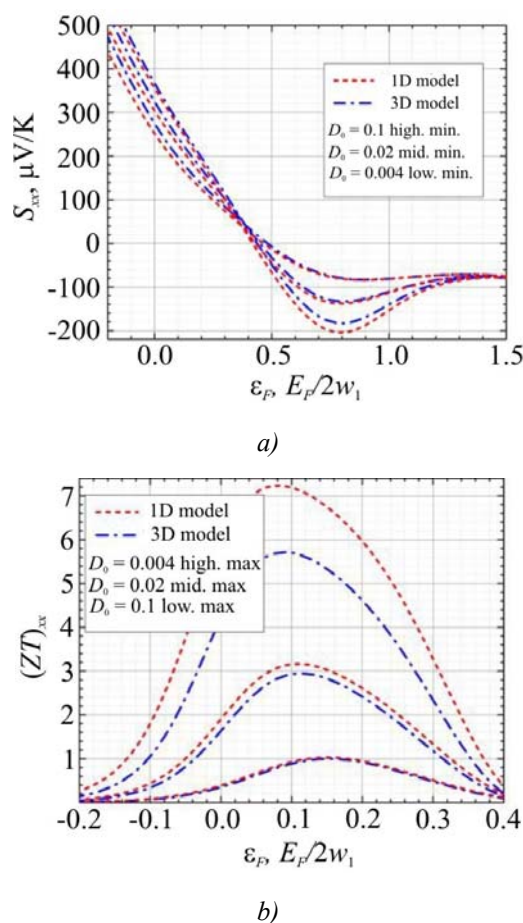

a)

b)

Fig. 2. a) The Seebeck coefficient S_{xx} and b) thermoelectric figure-of-merit $(ZT)_{xx}$
along the direction of molecular chains as a function of dimensionless
Fermi energy for quasi-one-dimensional organic crystals of p – type TTT_2I_3.

If the concentration of conducting holes is diminished twice, the Seebeck coefficient increases significantly and, even if the electrical conductivity decreases, this leads to a significant increase of $(ZT)_{xx}$ up to ~ 2.9 for crystals with $D_0 = 0.02$ and up to ~ 5 for those with $D_0 = 0.004$, very promising results. Thus, in order to increase $(ZT)_{xx}$ in TTT_2I_3 crystals, it is necessary to diminish the hole concentration and increase the crystal purity.

Crystals of *n*-type *TTT*(*TCNQ*)$_2$

The crystals of *n*-type $TTT(TCNQ)_2$ are less studied. Thus, the purity of reported crystals should not be very high. Due to this, somewhat higher values for D_0 were considered, meaning a more large concentration of impurities and defects than in TTT_2I_3 crystals. Other parameters are from [31].
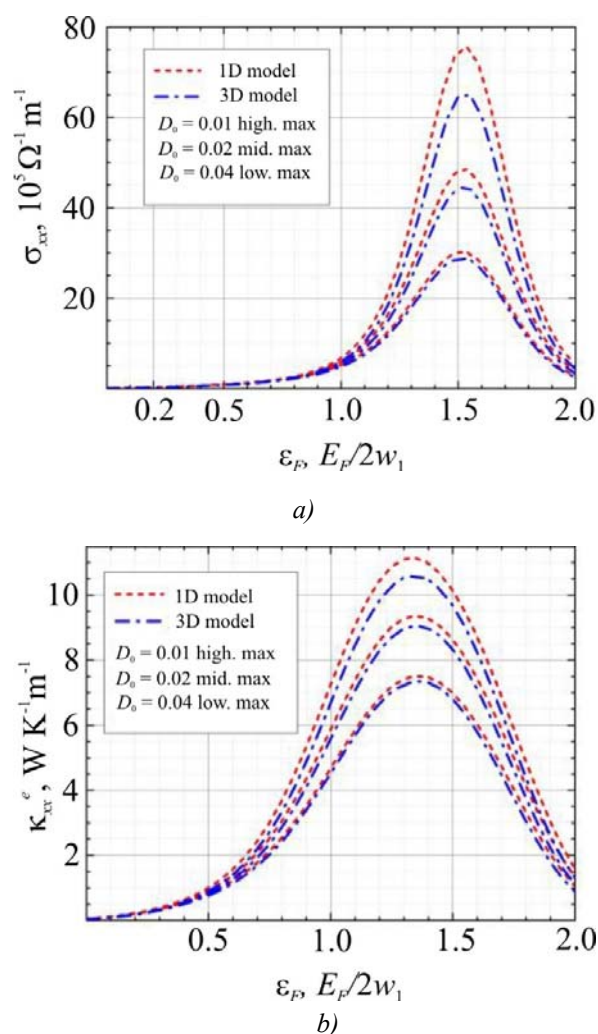

a)

b)

Fig. 3 a) Electrical conductivity σ_{xx} and b) electronic thermal conductivity along the direction of molecular chains as a function of dimensionless Fermi energy for quasi-one-dimensional organic crystal of n- type TTT(TCNQ)$_2$.

In the case of $TTT(TCNQ)_2$ the Seebeck coefficient is negative, because the charge carriers are electrons (Fig. 4*a*)

In stoichiometric crystals, $n_e = 1.1 \cdot 10^{21}$ cm^{-3} (or $\varepsilon_F \sim 0.35$), $S_{xx} \sim 120$ μV/K is expected. If the concentration of electrons is increased twofold ($\varepsilon_F \sim 1.05$) with respect to the stoichiometric value, $S_{xx} = -136$ μV/K, -160 μV/K and -180 μV/K is expected for the crystals with $D_0 = 0.04$, 0.02 and 0.01.
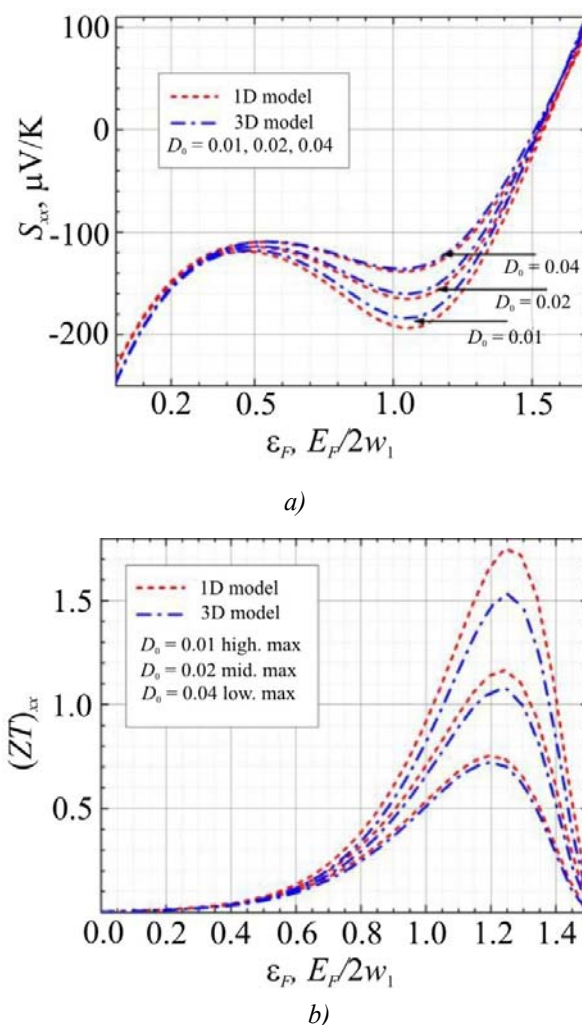
a)

b)

Fig.4. a) The Seebeck coefficient S_{xx} and b) thermoelectric figure-of-merit $(ZT)_{xx}$
along the direction of molecular chains as a function of dimensionless
Fermi energy for quasi-one-dimensional organic crystals of n – type TTT(TCNQ)$_2$.

It is observed (Fig. 4b) that in the case of stoichiometric crystals, the thermoelectric figure-of-merit *ZT* is quite low, even for crystals with high level of purity. This is explained by the simultaneous increase of electrical and thermal conductivity with increasing the purity of the crystal. However, if carrier concentration is properly tuned, the crystal enters the region of strong compensation of the abovementioned electron-phonon interactions. After that, if doped crystals are further purified, the electrical conductivity increases, but the thermal conductivity has a slower increasing rate. As a result, for *n*-type $TTT(TCNQ)_2$ and $D_0 = 0.01$ the following values are predicted: $ZT \sim 0.9$ for $\varepsilon_F = 1.05$ and $ZT \sim 1.1$ for $\varepsilon_F = 1.07$. In order to increase $(ZT)_{xx}$ in $TTT(TCNQ)_2$ crystals it is necessary to increase the electron concentration and increase the crystal purity.

Conclusions

Recent advances in the field of organic thermoelectric materials are reported. A more detailed evaluation of thermoelectric properties of quasi-one-dimensional organic crystals *p*-type TTT_2I_3 and *n*-type $TTT(TCNQ)_2$ is performed. It is expected that crystals of this type are very promising for thermoelectric applications, if the thermoelectric properties are optimized by accurate tuning of carrier

concentration and further purification of the crystal. Thus, the values of thermoelectric figure-of-merit $ZT \sim 5$ can be obtained in relatively pure TTT_2I_3 crystals, if the concentration of conducting holes is diminished twice with respect to the stoichiometric one. As it is well known, the thermoelectric properties of *n*-type materials are usually lower that in the case of *p*-type. However, the values of $ZT \sim 1$ are predicted for ultra-purified $TTT(TCNQ)_2$ crystals, if the concentration of conducting electrons is increased twice with respect to the stoichiometric one. The obtained results open up new possibilities for the implementation of organic compounds in new competitive thermoelectric devices. Partially the results have been implemented in the frame of the H2ESOT project [33], supported by FP7 program of EU Commission. For further improvement, a more detailed physical model should be elaborated.

References

1. http://www.iea.org/newsroom/news/2016/november/world-energy-outlook-2016.html
2. H. J. Goldsmid. Introduction to Thermoelectricity, *Springer Berlin Heidelberg*, p. 1 – 6 (2010).
3. H. J. Goldsmid. Electronic Refrigeration. In: *Pion, London* (1986).
4. T. M. Tritt. Thermoelectric Materials: Principles, Structure, Properties and Applications, *Encyclopedia of Materials: Science and Technology*, p. 1 – 11 (2002).
5. G. S. Nolas, J. Sharp, and H. J. Goldsmid. Thermoelectrics: Basic Principles and New Materials Developments, *Springer, New York* (2001).
6. D. T. Morelli. The Future of Thermoelectricity: What are the Next Big Ideas?, *Proceedings of ICT & ECT – 2015* (Dresden, Germany, 2015).
7. P. J. Taroni, I. Hoces, N. Stingelin, M. Heeney, E. Bilotti. Thermoelectric Materials: A Brief Historical Survey from Metal Junctions and Inorganic Semiconductors to Organic Polymers, *Israel Journal of Chemistry* **54** (5 – 6), p. 534 – 552 (2014).
8. M. N. Tripathi. Thermal and Thermoelectric Properties of Low-Dimensional Semiconductors, *Scholars' Press* (2013).
9. H. S. Lee. Thermoelectrics: Design and Materials, *John Wiley & Sons*, 440 p. (2016).
10. J. Mao. Size Effect in Thermoelectric Materials, *Quantum Materials* **1**, 16028 (2016).
11. V. I. Brinzari, A. I. Cocemasov, D. L. Nica, and G. S. Korotchenkov. Ultra-Low Thermal Conductivity of Nanogranular Indium Tin Oxide Films Deposited by Spray Pyrolysis, *Appl. Phys. Lett.* **110**, 071904 (2017).
12. G. Korotchenkov, V. Brinzari, and B. K. Cho. In_2O_3-based Multicomponent Metal Oxide Films and Their Prospects for Thermoelectric Applications, *Solid State Sci.* **52**, p. 141 – 148 (2016).
13. N. Dubey, M. Leclerc. Conducting Polymers: Efficient Thermoelectric Materials, *J.Polym. Sci.Part B: Polym. Phys.* **49**, p. 467 – 475 (2011).
14. C. Wang, H. Dong, W. Hu, Y. Liu, and D. Zhu. Semiconducting π – Conjugated Systems in Field-Effect Transistors: a Material Odyssey of Organic Electronics, *Chem. Rev.* **112**, p. 2208 – 2267 (2011).
15. H. Yan, N. Sada, and N. Toshima. Thermal Transporting Properties of Electrically Conductive Polyaniline Films as Organic Thermoelectric Materials, *J. Therm. Anal. Calorim.* **69**, p. 881 – 887 (2002).
16. G-H. Kim, L. Shao, K. Zhang, and K. P. Pipe. Engineered Doping of Organic Semiconductors for Enhanced Thermoelectric Efficiency, *Nat. Mater.* **12**, p. 719 (2013).
17. K. Zhang, J. Qiud, and S. Wang. Thermoelectric Properties of PEDOT Nanowire/ PEDOT Hybrids, *Nanoscale* **8**, p. 8033 (2016).

18. L. Zhang, T. Goto, I. Imae, Y. Sakurai, and Y. Harima. Thermoelectric Properties of PEDOT Films Prepared by Electrochemical Polymerization, *J. Polym. Sci., Part B: Polym. Phys*. **55**(6), p. 524 – 531 (2017).

19. Ch. Li, H. Ma, and Z. Tian. Thermoelectric Properties of Crystalline and Amorphous Polypyrrole: A Computational Study, *Applied Thermal Engineering* **111**, p. 1441 – 1447 (2017).

20. T. Zhao, D. Wang, and Z. Shuai. Doping Optimization of Organic-Inorganic Hybrid Perovskite $CH_3NH_3PbI_3$ for High Thermoelectric Efficiency, *Synthetic Metals*, (2017).

21. S. P. Ashby, J. Garcia-Canadas, G. Min, and Y. Chao. Measurement of Thermoelectric Properties of Phenylacetylene-Capped Silicon Nanoparticles and Their Potential in Fabrication of Thermoelectric Materials, *J.of Electronic Materials* **42**, p. 1495 (2013).

22. Y. Sun, W. Xu, C. Di, and D. Zhu. Metal-Organic Complexes – Towards Promising Organic Thermoelectric Materials, *Synth. Met*. (2016).

23. D. Jérome. Organic Conductors: From Charge Density Wave $TTF - TCNQ$ to Superconducting $(TMTSF)_2PF_6$, *Chem. Rev* **104** (11), p. 5565 – 5592 (2004).

24. L. Buravov, O. Eremenko, R. Lyubovski, and E. Yagubskii. Structure and Electromagnetic Properties of a New High-Conductivity Complex $TTT(TCNQ)_2$, *JETP* **20** (7), p. 208 – 209 (1974).

25. B. Hilti, C. W. Mayer. Electrical Properties of the Organic Metallic Compound bis (Tetrathiotetracene)-Triiodide, $(TTT)_2I_3$, *Helvetica Chimica Acta* **61** (40), p. 501 – 511 (1978).

26. A. Casian, I. Sanduleac. Organic Thermoelectric Materials: New Opportunities, *Journal of Thermoelectricity* **3**, p. 11 – 20 (2013).

27. A. Casian, I. Sanduleac. Effect of Interchain Interaction on Electrical Conductivity in Quasi-One-Dimensional Organic Crystals of Tetrathiotetracene-Iodide, *Journal of Nanoelectronics and Optoelectronics* **7**(7), p. 706 – 711 (2012).

28. A. Casian, I. Sanduleac. Thermoelectric Properties of Tetrathiotetracene Iodide Crystals: Modeling and Experiment, *Journal of Electronic Materials* **43**(10), p. 3740 – 3745 (2014).

29. I. Sanduleac, A. Casian. Nanostructured $TTT(TCNQ)_2$ Organic Crystals as Promising Thermoelectric *n*-Type Materials: 3D Modeling, *Journal of Electronic Materials* **45**(3), p. 1316 – 1320 (2015).

30. A. Casian, J. Pflaum, I. Sanduleac. Prospects of Low Dimensional Organic Materials for Thermoelectric Applications. *Journal of Thermoelectricity* **1**, p.16 – 26 (2015).

31. A. Casian, I. Sanduleac. Thermoelectric Properties of Nanostructured Tetrathiotetracene Iodide Crystals: 3D Modeling, *Materials Today: Proceedings* **2**(2), p. 504 – 509 (2015).

32. A. Casian. Violation of Wiedemann-Franz Law in Quasi-One-Dimensional Organic Crystals, *Phys. Rev. B* **81**, p. 155 – 415 (2010).

33. http://www.h2esot.com/

V. A. Romaka[1,2], L. P. Romaka[3], Yu. V. Stadnyk[3], V. Ya. Krayovskyy[2], A. M. Horyn[3]

[1]Ya. Pidstryhach Institute for Applied Problems of Mechanics and Mathematics, the National Academy of Sciences of Ukraine, 3 b, Naukova Str., Lviv, 79060, Ukraine;
[2]National University "Lvivska Polytechnika", 12, S. Bandera Str., Lviv, 79013, Ukraine;
[3]Ivan Franko National University of Lviv, 6, Kyryla and Mefodiya Str., Lviv, 79005, Ukraine

INVESTIGATION OF *TiNi₁₋ₓCuₓSn* THERMOELECTRIC MATERIAL

The crystalline structure, the temperature and concentration dependences of electrical resistivity, the Seebeck coefficient and magnetic susceptibility of $TiNi_{1-x}Cu_xSn$ thermoelectric material were investigated in the ranges of T = 80 – 400 K, x = 0.005 – 0.10. The mechanism for generation of donor nature structural defects upon the substitution of Cu atoms for Ni which reduce the compensation degree and determine the electrical conduction mechanisms of $TiNi_{1-x}Cu_xSn$ was identified. It was shown that thermoelectric power factor Z* reaches maximal values at concentration x ≈ 0.01 at intersection of the percolation level of conduction band by the Fermi level ε_F. The investigated $TiNi_{1-x}Cu_xSn$ semiconductor is a promising thermoelectric material, and ordering of its crystal structure provides stability and reproducibility of its characteristics.
Key words: resistivity, Seebeck coefficient, thermoelectric material.

Introduction

Thermoelectric materials obtained by heavy doping of *n-TiNiSn, n-ZrNiSn, n-HfNiSn* and *p-TiCoSb* intermetallic semiconductors with acceptor and/or donor impurities, possess high efficiency of thermal into electric energy conversion [1]. In [2] it is shown that maximum values of thermoelectric figure of merit [3] are achieved in *n*-type thermoelectric semiconductor materials under the condition of doping with donor impurities, and in *p*-type materials – with acceptor impurities. Due to such doping, at the lowest impurity concentrations, the Fermi level ε_F can get closer to the percolation levels of conduction band and valence band by the distance k_BT, which assures, on the one hand, high electric conductivity values, and, on the other hand, still high values of the Seebeck coefficient. At the same time, doping, for instance, of *p-TiCoSb* intermetallic semiconductor with donor impurity *Ni* ($3d^84s^2$) by substitution of *Co* ($3d^74s^2$) atoms (*Co* has a smaller number of $3d$-electrons than *Ni*) was not attended by the increase in the efficiency of thermal into electric energy conversion [4]. Here, ensuring the condition of the Fermi level ε_F approaching the percolation level of conduction band required overcompensation from the hole to electron semiconductor and a drift of the Fermi level from the valence band to conduction band, which is possible under the condition of considerable impurity concentrations which significantly reduced the value of the Seebeck coefficient.

However, recent results of integrated studies of crystalline and electronic structures, kinetic and magnetic characteristics of *TiNiSn₁₋ₓGaₓ* [5] and *ZrNiSn₁₋ₓGaₓ* thermoelectric materials [6] allowed

specifying the conditions for obtaining materials with maximum efficiency of thermal into electric energy conversion [2]. Thus, on doping of *n-TiNiSn* and *n-ZrNiSn* with *Ga* ($4s^2 4p^1$) acceptor impurity by substitution of *Sn* ($5s^2 5p^2$), mechanisms were revealed for a *simultaneous* generation in crystal of structural defects of both acceptor (*Ga* has less *p*-electrons than *Sn*) and donor nature due to the appearance and increasing the number of vacancies in position *4b* of *Sn* atoms. It appeared that simultaneous formation in thermoelectric material of donor-acceptor pairs contributes to improving the thermoelectric figure of merit.

This paper investigates thermoelectric material $TiNi_{1-x}Cu_xSn$ obtained by substitution of *Ni* ($3d^8 4s^2$) atoms by *Cu* ($3d^{10} 4s^1$), which generates in crystal structural defects of donor nature (*Cu* has more *3d*-electrons than *Ni*). The synthesized thermoelectric material $TiNi_{1-x}Cu_xSn$ in conformity with conditions [2] must possess high efficiency of thermal into electric energy conversion. On the other hand, the results of investigation of similar thermoelectric material $ZrNi_{1-x}Cu_xSn$ [1] have confirmed the formulated conditions [2] for obtaining maximum values of thermoelectric figure of merit.

Investigation procedures

The object to be investigated included structural, energy, kinetic and magnetic characteristics of thermoelectric material $TiNi_{1-x}Cu_xSn$. The samples were synthesized by melting batch mixture of the source components in electric arc furnace in an inert atmosphere with subsequent homogenizing annealing for 720 hours at a temperature of 1073 K. The *X*-ray structural analysis method was used to obtain the data arrays (diffractometer Guinier-Huber image plate system, $CuK\alpha_1$), and FullProf program [7] was employed for the calculation of structural characteristics. The chemical and phase compositions of the samples were controlled by microprobe analyzer (EPMA, energy-dispersive X-ray analyzer). The temperature and concentration dependences of the electrical resistivity (ρ) and the Seebeck coefficient (α) were measured with respect to copper and magnetic susceptibility (χ) (Faraday's method) of $TiNi_{1-x}Cu_xSn$ samples in the ranges: $T = 80 - 400$ K, $N_D^{Cu} \approx 3.8 \cdot 10^{19}$ cm^{-3} ($x = 0.005$) $- 1.9 \cdot 10^{21}$ cm^{-3} ($x = 0.10$) and magnetic field strength $H \leq 10$ кE.

Research on structural features of $TiNi_{1-x}Cu_xSn$

A microprobe analysis of the concentration of atoms on the surface of $TiNi_{1-x}Cu_xSn$ samples up to composition $x = 0 - 0.10$ has established their conformity to the initial batch compositions, and *X*-ray phase and structural analyses have shown that *X*-ray diffraction patterns have no traces of other phases apart from the main phase which is indexed in structural type *MgAgAs* [8] (face-centered cubic lattice, spatial group *F*43*m* (№ 216), Pearson symbol *cF*12).

Taking into account a larger atomic radius of *Cu* ($r_{Cu} = 0.128$ nm) as compared to *Ni* ($r_{Ni} = 0.124$ nm), it would be logical to expect a monotonous increase in the values of unit cell period $a(x)$ in $TiNi_{1-x}Cu_xSn$. Exactly this result of change in the values of $a(x)$ was obtained at computer simulation of $TiNi_{1-x}Cu_xSn$ crystalline structure (Fig. 1, dependence 2). However, *X*-ray diffraction studies of $TiNi_{1-x}Cu_xSn$ showed that the introduction of *Cu* atoms into the structure of *TiNiSn* by replacing *Ni* atoms in the concentration range $x = 0 - 0.01$ was not accompanied by a monotonous increase in the values of the period $a(x)$ (Fig. 1, dependence 1), indicating more complex structural changes in the crystal than simply substituting *Cu* atoms for *Ni*. From Fig. 1 it is seen that in the concentration range $x = 0 - 0.005$ the values of unit cell period $a(x)$ drastically increase, but in the range $x = 0.005 - 0.01$ they drastically decrease as well, and at concentrations $x \geq 0.01$ there is practically monotonous reduction of $a(x)$ values which is close to the results of

computer simulation of $TiNi_{1-x}Cu_xSn$ structure. It is clear that structural changes in $TiNi_{1-x}Cu_xSn$ in the concentration range $0 \le x \le 0.01$ will lead to unpredictable changes in the electronic structure of thermoelectric material and determine its properties. Let us try to identify structural changes in $TiNi_{1-x}Cu_xSn$ that caused this, at first sight, unpredictable behavior of unit cell period $a(x)$.

In our work [9] it is shown that crystalline structure of n-$TiNiSn$ is disordered (local amorphization) due to partial, up to ~1% ($z \approx 0.01$), occupancy by Ni atoms of $4a$ position of Ti ($3d^2 5s^2$) atoms, which generates in crystal structural defects of donor nature ("a priori doping"), as long as Ni has more $3d$-electrons, and the compound formula takes on the form $(Ti_{1-z}Ni_z)NiSn$. In the energy gap of n-$TiNiSn$ at the distance of 16.9 meV from the percolation level of conduction band there appears impurity donor level ε_D^1 caused by structural defects generated in the crystal.
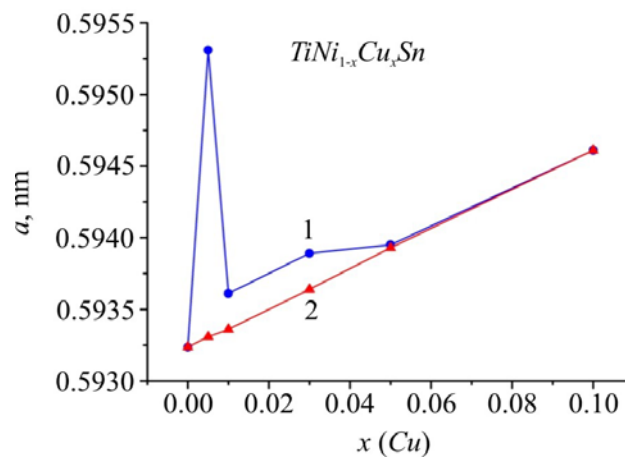

Fig. 1. Change in the values of unit cell period a(x) of $TiNi_{1-x}Cu_xSn$ semiconductor solid solution:
1 – experimental results; 2 – results of simulation of substitutional solid solution

At the same time, refinement of $TiNi_{1-x}Cu_xSn$ crystalline structure by powder method with a simultaneous refinement of the isotropic parameters of atomic displacement and occupancy of Ti crystallographic position ($4a$) has shown that the lowest value of coefficient of mismatch between crystalline structure model and the array of Bragg reflections within $MgAgAs$ structural type was obtained for a model where occupancy of position of Ti atoms for $x \ge 0.01$ is 100%. In other words, in the concentration range of Cu $0 \le x \le 0.01$ impurity atoms there is a displacement from $4a$ position of small Ni atoms by greater Ti ($r_{Ti} = 0.146$ nm) atoms, which *puts in order $TiNi_{1-x}Cu_xSn$ crystalline structure and "heals" structural defects of donor nature.*

Alongside with displacement of Ni atoms from position $4a$ there is a process of simultaneous substitution in $4c$ position of Ni atoms by greater Cu atoms. Taking into account that the difference in atomic radii between Ti and Ni is ($r_{Ti} - r_{Ni}$) = 0.022 nm, and between Ni and Cu ($r_{Cu} - r_{Ni}$) = 0.004 nm, a change in $a(x)$ values at concentration range $x = 0 - 0.005$ will be determined by the process of displacement of Ni from $4a$ position by large Ti atoms, as long as the contribution of this substitution to total change of $a(x)$ value is 5 times that at substitution of Cu atoms for Ni. Exactly such structural changes in $TiNi_{1-x}Cu_xSn$ at concentration range $x = 0 - 0.005$ will cause rapid growth of the values of unit cell period $a(x)$ (Fig. 1, dependence 1). After the displacement of the main part of Ni atoms from Ti position $(4a)$ (structure ordering) a change in $a(x)$ values will be determined by the occupancy by Cu atoms of Ni position ($4c$), which only now will lead to a monotonous growth of $a(x)$ values, as predicted in the simulation of $TiNi_{1-x}Cu_xSn$ structure. Note that *ordering* of $TiNi_{1-x}Cu_xSn$ crystalline structure makes it stable to temperature and temporal changes, creating prerequisites for obtaining material with stable characteristics.

Changes in crystalline structure of $TiNi_{1-x}Cu_xSn$ during its ordering will necessarily lead to a respective transformation of electronic structure. It is clear that donor impurity level ε_D^1 present in *n-TiNiSn* as a result of displacement of ~ 1 % of *Ti* atoms by *Ni* atoms [9], must disappear at concentrations $x > 0.01$. On the other hand, since *Cu* atom possesses a greater number of 3*d*-electrons than *Ni*, the substitution of *Cu* for *Ni* atom generates in 4*c* position a structural defect of donor nature, which will cause the emergence in the energy gap of another donor impurity level ε_D^2. The presence of a large number of donors ε_D^2 will determine the kinetic characteristics of $TiNi_{1-x}Cu_xSn$ which is bound to appear in the investigation of the dependences of resistivity and the Seebeck coefficient.

Research on the kinetic, energy and magnetic characteristics of $TiNi_{1-x}Cu_xSn$

The temperature and concentration dependences of the electric resistivity ρ and the Seebeck coefficient α of $TiNi_{1-x}Cu_xSn$ are presented in Figs. 2 – 4. The dependences $\ln\rho(1/T)$ and $\alpha(1/T)$ for *n-TiNiSn* (Fig. 2) are typical for heavily doped and compensated semiconductors [10], and the high-temperature activation areas testify that the Fermi level ε_F is located in the energy gap from which thermal activation of electrons to percolation level of conduction band takes place. The result obtained for *n-TiNiSn* is fully consistent with the results of [10] where it is shown that in a semiconductor the Fermi level ε_F is located at the distance of 16.9 m·eV from the bottom of conduction band ε_C.

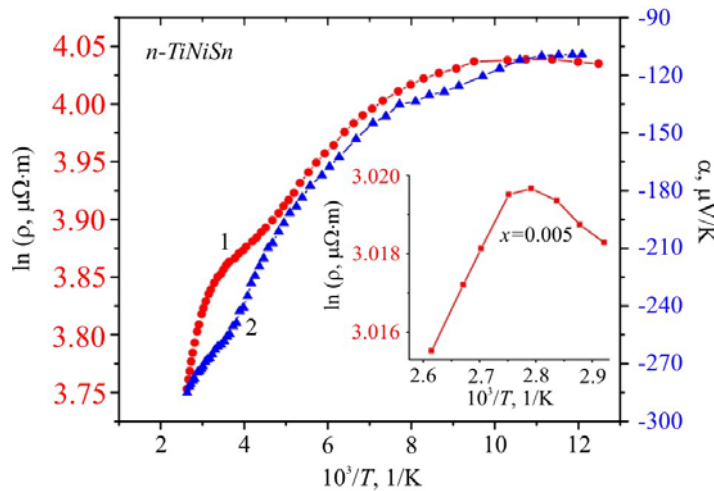*Fig. 2. Temperature dependences of electric resistivity lnρ(1/T) (1)*
and the Seebeck coefficient α(1/T) (2) of n-TiNiSn.
Inset: dependence lnρ(1/T) of $TiN_{x0.995}Cu_{0.005}Sn$

Doping of *n-TiNiSn* semiconductor with the lowest concentration of *Cu*, $x = 0.005$ donor impurity leads, as is shown by the dependence $\ln\rho(1/T)$ of $TiNi_{0.995}Cu_{0.005}Sn$ (Fig. 2, inset), to conduction metallization in the temperature range of $T = 80 - 360$ K (Fig. 3*a*, curve 1). It means that at the concentrations of $TiNi_{0.995}Cu_{0.005}Sn$ impurity and at temperatures $T = 80 - 360$ K the Fermi level ε_F intersected the percolation level of conduction band. From this we can conclude that drastic approach of the Fermi level ε_F to the percolation level of conduction band shows that the generated impurity donor level ε_D^2 is located at the distance of k_BT from the bottom of conduction band, and the temperatures $80 \leq T \leq 360$ K are sufficient for intersection by the Fermi level ε_F of the percolation level of conduction band.

However, further temperature increase at $T > 360$ K is suddenly accompanied by a reverse metal-dielectric conductivity transition [10], and the electric resistivity values of $TiNi_{0.995}Cu_{0.005}Sn$

decrease with a rise in temperature (Fig. 2, inset). Such behavior of $\ln\rho(1/T)$ $TiNi_{0.995}Cu_{0.005}Sn$ dependence makes it clear that at temperatures $T > 360$ K the Fermi level ε_F goes beyond the band of continuous energies to the energy gap. Note that the sign of the Seebeck coefficient of $TiNi_{0.995}Cu_{0.005}Sn$ at all temperatures remained negative (Fig. 3*b*), which gives us the right to identify dielectric-metal and metal-dielectric conductivity transitions at intersection by the Fermi level ε_F of the percolation level of conduction band.

This, at first sight, unexpected behavior of the Fermi level of ε_F $TiNi_{0.995}Cu_{0.005}Sn$ in the temperature range of $80 \leq T \leq 360$ K actually has a very simple explanation. Indeed, donor concentration of the impurity donor level ε_D^1 ($z = 0.01$) [9] exceeds the concentration of donors ε_D^2 generated in a semiconductor at the lowest concentration of *Cu*, $x = 0.005$ donor impurity. At the same time, as shown by the results of the experiment, the depth of donor level ε_D^1 [9] is much larger than ε_D^2. The inverse metal-dielectric conductivity transition is caused by depletion of impurity donor level ε_D^2 at temperatures $T \geq 360$ K [10].
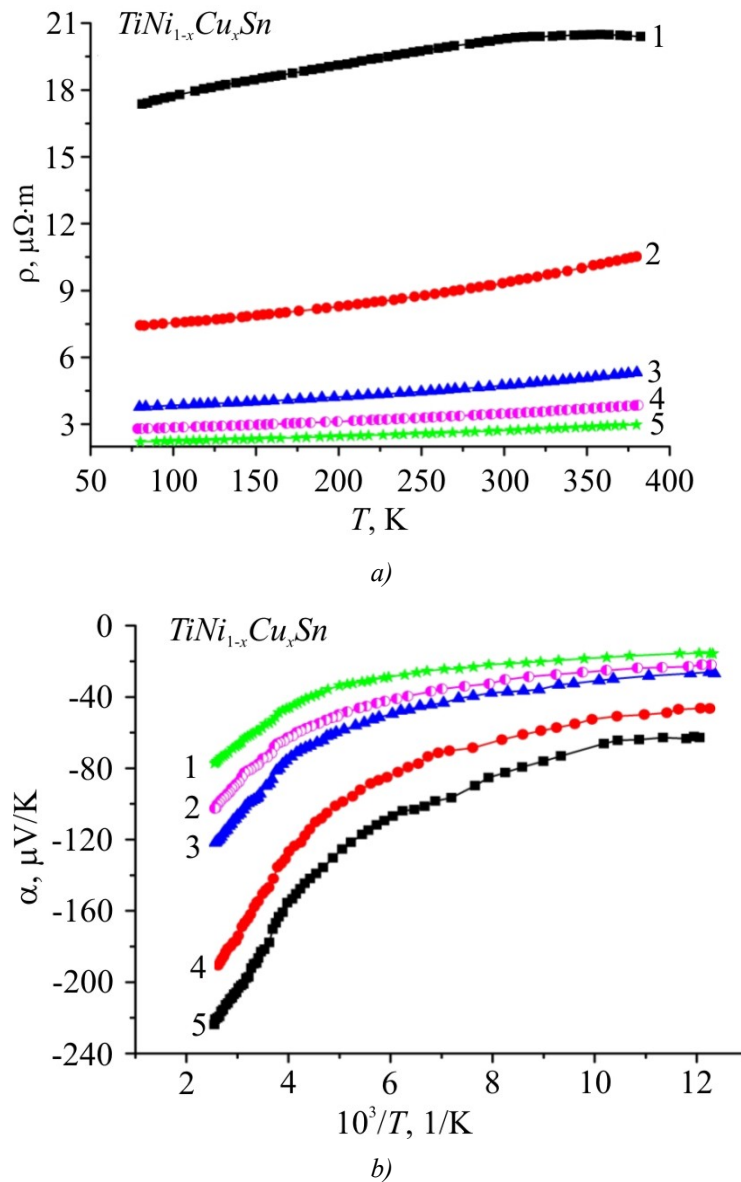

a)

b)

Fig. 3. Temperature dependences of electric resistivity ρ(T) (a)
and the Seebeck coefficient α(1/T) (b) of TiNi₁₋ₓCuₓSn:
1 – x=0.005; 2 – x=0.01; 3 – x=0.03; 4 – x=0.05; 5 – x=0.10

As long as concentration of donors at donor level ε_D^1 is higher than ε_D^2, and after temperatures $T \geq 360$ K there is thermal activation of electrons from the deeper donor level ε_D^1, this is represented in the appearance of activation area on the dependence $\ln\rho(1/T)$ of $TiNi_{0.995}Cu_{0.005}Sn$ (Fig. 2, inset).

The fact that *Cu* atoms introduced into *n-TiNiSn* generate structural defects of donor nature is also demonstrated by the dependences of change in the values of resistivity $\rho(x,T)$ and the Seebeck coefficient $\alpha(x,T)$ over the entire concentration and temperature ranges (Fig. 4).

Thus, introduction of the lowest in the experiment concentrations of *Cu* drastically reduces the value of resistivity $\rho(x)$ at $T = 80$ K from the values of $\rho(x = 0) = 56.5$ μΩ·m to $\rho(x = 0.005) = 17.4$ μΩ·m and $\rho(x = 0.01) = 7.4$ μΩ·m, which is due to increase in the number of free electrons at ionization of donors generated in the crystal. In so doing, the sign of the Seebeck coefficient of $TiNi_{1-x}Cu_xSn$ remains negative for all concentrations, and electrons are majority carriers.
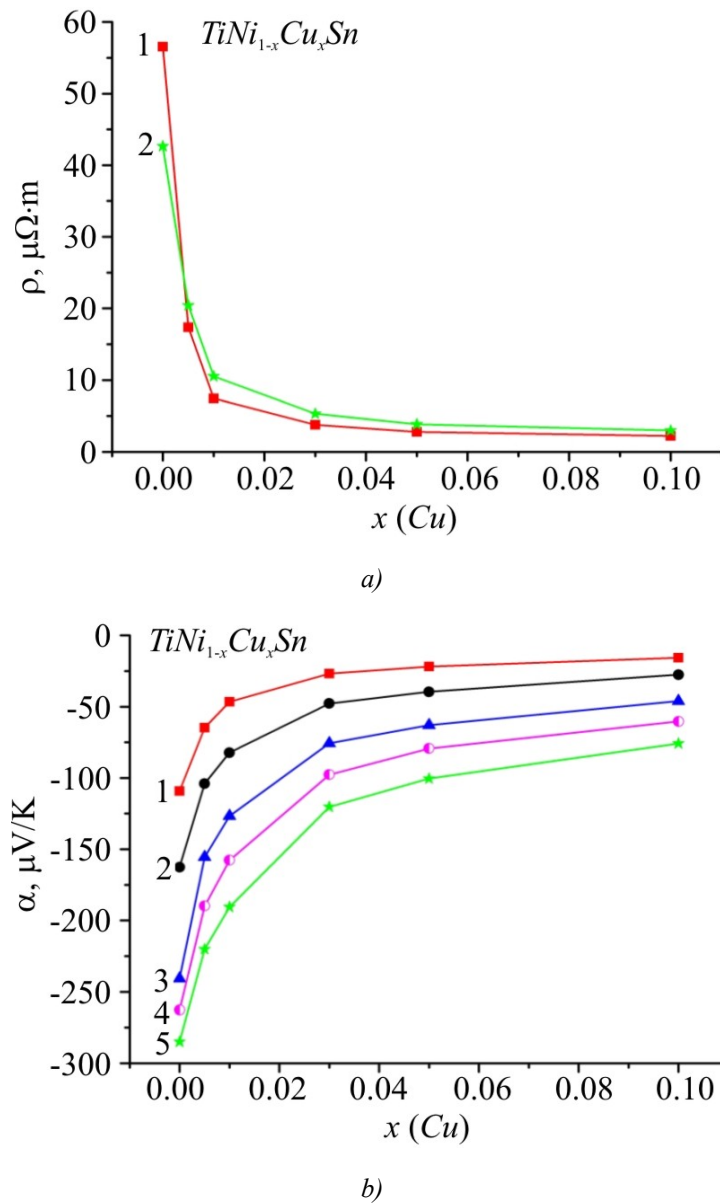

a)

b)

Fig. 4. Change in the values of electric resistivity ρ(x) (a) and the
Seebeck coefficient α(x) (b) of TiNi₁₋ₓCuₓSn at different temperatures;
a: 1 – T=80 K, 2 – T=380 K; b: 1 – T=80,
2 – T=160, 3 – T=250, 4 – T=300, 5 – T=380 K

The results of kinetic investigations of $TiNi_{1-x}Cu_xSn$ are consistent with the results of experimental measurements of magnetic susceptibility χ at a temperature of $T = 300$ K (Fig. 5). Investigations showed that all the samples of $TiNi_{1-x}Cu_xSn$ are Pauli paramagnetics wherein magnetic susceptibility is determined exceptionally by electronic gas and is proportional to density of states at the Fermi level $g(\varepsilon_F)$.

As can be seen from Fig. 5, dependence $\chi(x)$ of $TiNi_{1-x}Cu_xSn$ at $x > 0$ monotonously increases, hence increases the density of states at the Fermi level, which is possible only under the condition of generation of semiconductor thermoelectric material of structural defects of donor nature. Precisely this result was predicted by the studies of the structure and kinetic characteristics of $TiNi_{1-x}Cu_xSn$.

Maximum values of thermoelectric power factor Z^* ($Z^* = \alpha^2 \cdot \sigma$, where α is the Seebeck coefficient, σ is electric conductivity) are achieved under the condition when the Seebeck coefficient values are still high and the electric conductivity values of $TiNi_{1-x}Cu_xSn$ semiconductor solid solution have become even greater [2].

Under these conditions, on the dependences $Z^*(x)$ of $TiNi_{1-x}Cu_xSn$ at all investigated temperatures, an extremum appears at the concentrations of the impurity atoms Cu $x \approx 0.01$. Fig. 6 shows a dependence $Z^*(x)$ at a temperature of $T = 380$ K from which it follows that the values of $Z^*(x)$ are greater than in n-$TiNiSn$ undoped semiconductor.
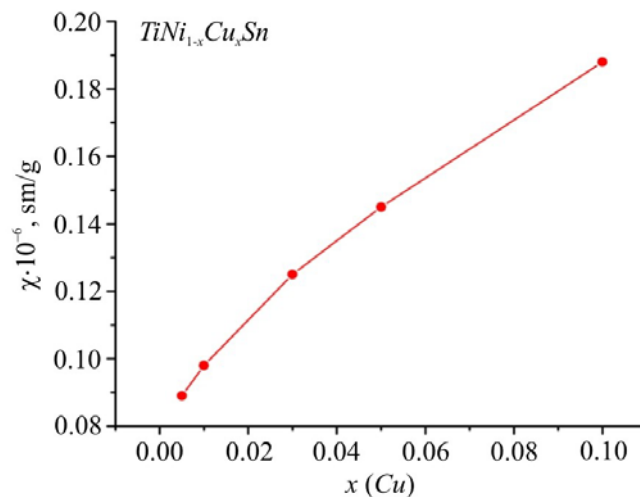

Fig. 5. Change in the values of magnetic susceptibility $\chi(x)$
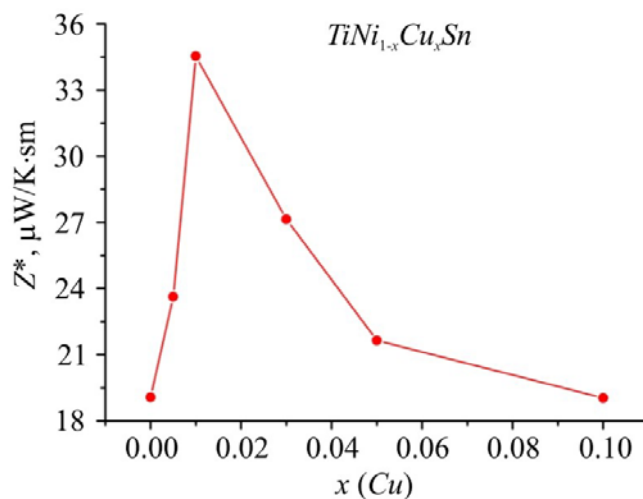*of $TiNi_{1-x}Cu_xSn$ at a temperature of $T = 300$ K*

Fig. 6. Change in the values of thermoelectric power factor $Z^*(x)$
of $TiNi_{1-x}Cu_xSn$ at a temperature of $T = 380$ K

The appearance of maximum on the dependence $Z^*(x)$ at the concentration of impurity atoms $TiNi_{1-x}Cu_xSn$, $x \approx 0.01$, is expected, since, as has been shown by the research on the kinetic characteristics, exactly at these concentrations the Fermi level ε_F is at the distance k_BT from the percolation level of conduction band, which assures, on the one hand, high values of electric conductivity, and on the other hand – still high values of the Seebeck coefficient.

Taking into account that calculations show slight (by $\sim 3\,\%$) increase in thermal conductivity κ for $TiNi_{1-x}Cu_xSn$, $x = 0.01$, the values of thermoelectric figure of merit Z will be also higher than in n-$TiNiSn$ undoped semiconductor, which makes the investigated semiconductor solid solution a promising thermoelectric material.

Conclusions

Thus, as a result of integrated research on the crystalline structure, the kinetic and magnetic characteristics of $TiNi_{1-x}Cu_xSn$ semiconductor thermoelectric material, we have identified the mechanism for generation of structural defects of donor nature at substitution of Cu atoms for Ni that reduce the compensation ratio and determine the electric conductivity mechanisms of material. The investigated $TiNi_{1-x}Cu_xSn$ semiconductor is a promising thermoelectric material, and crystalline structure orderliness is a guarantee of stability and reproducibility of characteristics.

References

1. V. A. Romaka, V. V. Romaka, and Yu. V. Stadnyk, *Intermetallic Semiconductors: Properties and Application* (Lviv:Lvivska Polytechnika, 2011), 488 p.
2. Romaka V. A., Fruchart D., Stadnyk Yu. V., Tobola J., Gorelenko Yu. K., Shelyapina M. G., Romaka L. P., Chekurin V. F. A condition of maximum power characteristic to intermetallic semiconductors of the *MgAgAs* structure type / Semiconductors, Vol. 40, № 11, 2008, p. 1289 – 1395.
3. L. I. Anatychuk. *Thermoelements and Thermoelectric Devices* (Kyiv: Naukova Dumka, 1979), 768 p.
4. Yu. V. Stadnyk, V. A. Romaka, M. G. Shelyapina, D. Fruchart, Yu. K. Gorelenko, L. P. Romaka, A. V. Tkachuk, and V. F. Chekurin. Impurity Band Effect on $TiCo_{1-x}Ni_xSb$ Conduction. Donor Impurities, *J. Alloys and Compounds* 421, p. 19 – 23 (2006).
5. V. A. Romaka, P. Rogl, L. P. Romaka, Yu. V. Stadnyk, V. Ya. Krayovskyy, D. Kaczorowski, and A. M. Horyn. Features of Structural, Energy and Kinetic Characteristics of $TiNiSn_{1-x}Ga_x$ Thermoelectric Material, *J.Thermoelectricity* 3, 24 – 33 (2016).
6. V. A. Romaka, L. P. Romaka, Yu. V. Stadnyk, V. Ya. Krayovskyy, V. V. Romaka, and A. M. Horyn, Research on Electrical Conductivity Mechanisms of Thermoelectric Material Based on *n-ZrNiS*n Doped with *Ga, J.Thermoelectricity* 4, 44 – 58 (2016).
7. T. Roisnel, J. Rodriguez-Carvajal. WinPLOTR: a Windows Tool for Powder Diffraction Patterns Analysis, *Mater. Sci. Forum, Proc. EPDIC7* 378 – 381, 118 – 123 (2001).
8. V. V. Romaka, L. P. Romaka, V. Ya. Krayovsky, and Yu. V. Stadnyk. *Stannides of Rare-Earth and Transition Metals* (Lviv: Lvivska Polytechnika Publ., 2015), 224 p.

9. V. A. Romaka, P. Rogl, V. V. Romaka, E. K. Hlil, Yu. V. Stadnyk, and S. M. Budgerak. Features of a priori Heavy Doping of the *n-TiNiSn* Intermetallic Semiconductor, *Semiconductors* **45**(7), 879 – 885 (2011).

10. B. I. Shklovsky, A. L. Efros. Fully Compensated Crystalline Semiconductor as a Model of Amorphous Semiconductor, *JETP* **62**(3), 1156 – 1165 (1972).

Submitted 12.11.2016

**L. I. Anatychuk[1,2], R. R. Kobylianskyi[1,2], I. A. Konstantynovych[1,2], R. V. Kuz[1,2],
O. M. Manik[2], O. V. Nitsovych[1,2], R. G. Cherkez[1,2]**

[1]Institute of Thermoelectricity of the NAS and MES Ukraine,
1 Nauky str., Chernivtsi, 58029, Ukraine;
[2]Yu.Fedkovich Chernivtsi National University,
2 Kotsyubynsky str.,Chernivtsi, 58012, Ukraine

TECHNOLOGY FOR MANUFACTURING THERMOELECTRIC MICROTHERMOPILES

The present paper gives the results of development of technology for manufacturing thermoelectric microthermopiles which simplifies considerably and mechanizes the method for manufacturing thermoelectric heat flux sensors and microgenerators for power supply to low-power medical equipment. It was established that proposed technology reduces the percentage of rejected thermoelectric material plates and thus reduces the cost of thermoelectric microthermopiles. The efficiency of using such technology for manufacturing thermoelectric microthermopiles with the legs of small cross-section from 0.02 × 0.02 mm to 1.0 × 1.0 mm and the length up to 30 mm was experimentally confirmed.
Key words: manufacturing technology, thermoelectric microthermopile, heat flux sensor, thermoelectric microgenerator.

Introduction

General characterization of the problem. It is known that as early as the first stages of designing thermoelectric microgenerators (for instance, for power supply to low-power electronic devices, telemetry and navigation systems, IR-detectors, as well as military and medical equipment) it was established that thermopiles for them must have unusual design that differs markedly from traditional generator modules [1 − 3]. For instance, for isotopic thermoelectric microgenerators with electric power in the range of $0.05 \div 2.5$ W, temperature difference on the module $100 \div 200$ K and operating voltage $5 \div 15$ V it is necessary to use thermopile legs of the length up to $10 \div 20$ mm and cross-section from 0.2×0.2 mm to 0.5×0.5 mm. However, for power supply to low-power medical equipment at small temperature differences on the module to 10 K and electric power in the range of $0.05 \div 5$ mW one must use thermopile legs of cross-section from 0.02×0.02 mm to 1×1 mm. In so doing, the number of legs in the thermopile must be from several hundreds to several thousands and more. Fulfillment of such requirements is a rather complicated technological problem [4 − 8].

The attempts of creating such microthermopiles were reduced to using film technologies [9]. Film thermopiles were created in the form of tapes which then can be folded into a compact roll. To manufacture such thermopiles, magnetron sputtering and other techniques were employed in combination with photolithography methods. Thermoelectric materials based on *Bi-Te* were used in the thermopiles. However, the results of testing film thermopiles revealed a number of their significant shortcomings, namely the substrates on which the thermopiles were formed shunted thermal flux which caused the reduction of efficiency; the difference in linear expansion coefficient between films and substrate (generally polyamide 5 μm) gave rise to thermal stresses in the thermopiles, which led to failures in their operation; recrystallization processes in the films led to degradation of thermopiles and

deterioration of their thermoelectric properties; creation of reliable thermal contacts between the thermopile, heat source and package caused difficulties which led to additional losses of temperature difference on thermopile faces. The totality of the above problems resulted in the abandonment of film thermopiles in thermoelectric microgenerators.

Therefore, *the purpose of this work* is to develop special technology for manufacturing thermoelectric microthermopiles with increased density of components (up to several thousand legs of small cross-section from 0.02×0.02 mm to 1.0×1.0 mm and length up to 30 mm) to produce thermoelectric heat flux sensors and microgenerators for power supply to low-power medical equipment.

Technology for manufacturing thermoelectric microthermopiles with increased density of components [10, 11]

The technology for manufacturing thermoelectric microthermopiles given in [10] was taken as a basis. The technology for manufacturing a thermoelectric microthermopile [11] proposed here comprises preparation of *n*- and *p*-type plates with deposition on the end surfaces of anti-diffusion layers, making cuts in these plates, coating of the internal surfaces of plates with cuts by electrically insulating compound and connection of the plates so as to form between them a gap of $10 \div 30$ μm, filled with compound; after polymerization of compound the external parts of the plates are removed to form a plate consisting of interconnected *n*- and *p*-type legs; the plates of *n*- and *p*-type legs are arranged one above the other and connected by compound to form a thermoelectric microthermopile, whose legs are connected by metalized anti-diffusion layers; heat spreaders on the hot and cold surfaces of thermoelectric microthermopile are created by high-temperature compound with thermally conductive fillers.
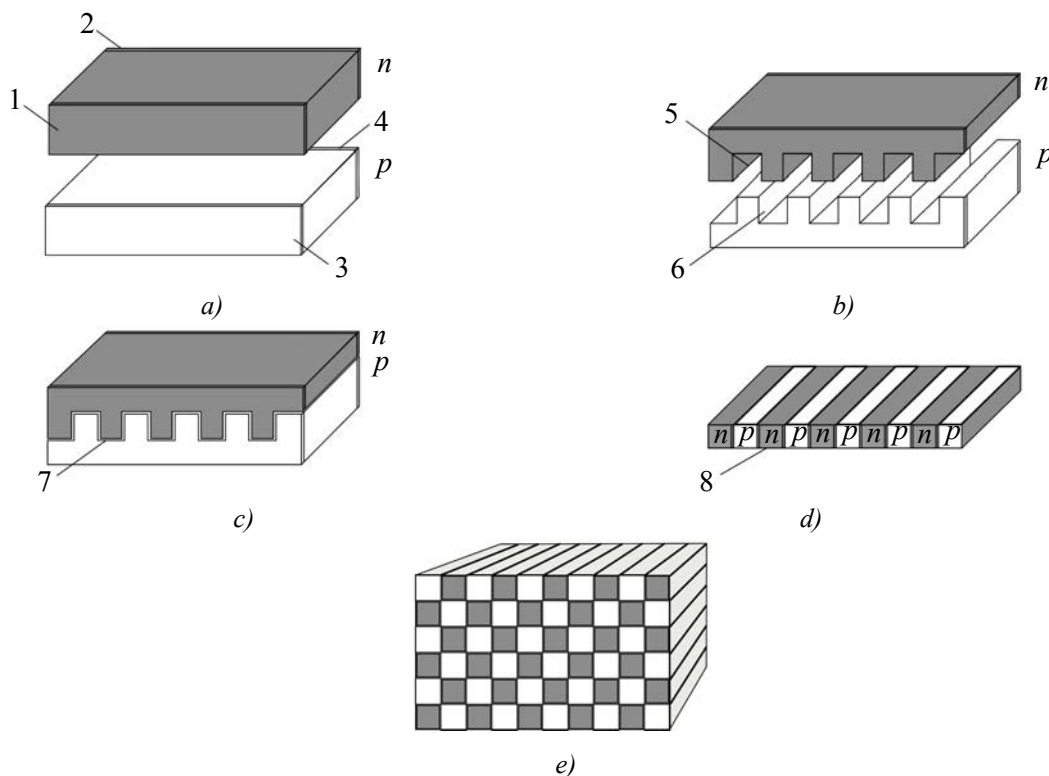

Fig. 1. Schematic of technology for manufacturing thermoelectric microthermopiles
with increased density of components [11].

Fig. 1 shows a schematic demonstrating the idea of proposed technology for manufacturing thermoelectric microthermopiles with increased density of components [11]. The technology is as follows. At first, rectangular plates of *n*- and *p*-type are manufactured with deposition on the end surfaces of anti-diffusion layers 1 – 4 (Fig. 1*a*). Cuts of necessary size 5 – 6 are made in the plates on specially elaborated equipment (for instance, multi-wire cutting machine) (Fig. 2*b*). The internal surfaces of the plates are coated with high-temperature compounds with the operating temperature 300 – 400 °C, following which the plates are connected in such a way as to form a gap of 10 – 30 μm filled with compound 7 (Fig. 2*c*). After polymerization of compound the external parts of the plates are removed to form plate 8 which consists of interconnected *n*- and *p*-type legs (Fig. 1*d*). Then the plates of *n*- and *p*-type legs are arranged one above the other and connected by compound to form a thermoelectric microthermopile (Fig. 1*e*). Connection of legs is done by metalized anti-diffusion layers. Heat spreaders on the hot and cold surfaces of thermopiles are created by high-temperature compound with thermally conductive fillers – diamond or corundum powders.

Testing of proposed technology has proved the efficiency of its use for manufacturing thermoelectric microthermopiles with the legs of small cross-section from 0.02×0.02 mm to 1.0×1.0 mm. Such technology simplifies considerably and mechanizes the method for manufacturing thermoelectric microthermopiles with a large number of legs of *n*- and *p*-type conductivity.

Improvement of technology for manufacturing thermoelectric microthermopiles [12]

The disadvantage of the above technology for manufacturing thermoelectric microthermopiles is significant percentage of rejected thermoelectric material plates due to microcracks that may arise when grinding.

Said problem is solved by using an improved technology for manufacturing thermoelectric microthermopiles [12] which consists in the removal of the external parts of connected plates in three stages: grinding of plates on the one side, gluing such plates with their ground sides together and grinding of both external sides of the newly-formed double plates.

The proposed technology allows joint formation of the legs with small cross-section from 0.01×0.01 mm to 1.0×1.0 mm and makes it possible to combine them into thermoelectric microthermopiles with the length of legs up to 30 mm.

Fig. 2 shows a schematic which demonstrates the idea of proposed technology for manufacturing a thermoelectric microthermopile [12]. The technology is as follows. At first, rectangular plates of *n*- and *p*-type conductivity are manufactured with deposition on the end surfaces of anti-diffusion layers 1 – 4 (Fig. 2*a*). Cuts of necessary size 5 – 6 are made in the plates on specially elaborated equipment (for instance, multi-wire cutting machine) (Fig. 2*b*). The internal surfaces of the plates are coated with high-temperature compounds with the operating temperature 300 – 400 °C, following which the plates are connected in such a way as to form a gap of 10 – 30 μm filled with compound 7 (Fig. 2*c*). After polymerization of compound the external parts of connected plates are removed in three stages: grinding of plates on the one side to form plate 8 (Fig. 2*d*), gluing of such plates with their ground sides together to form plate 9 (Fig. 2*e*) and grinding of both external sides of newly-formed double plates 9 to form plate 10 consisting of interconnected *n*- and *p*-type legs (Fig. 2*f*). Then the plates of *n*- and *p*-type legs are arranged one above the other and connected with compound to form a thermoelectric microthermopile 11 (Fig. 2*g*). Connection of legs is done by metallized anti-diffusion layers. Heat spreaders on the hot and cold surfaces of thermopiles are created by high-temperature compound with thermally conductive fillers – diamond or corundum powders.
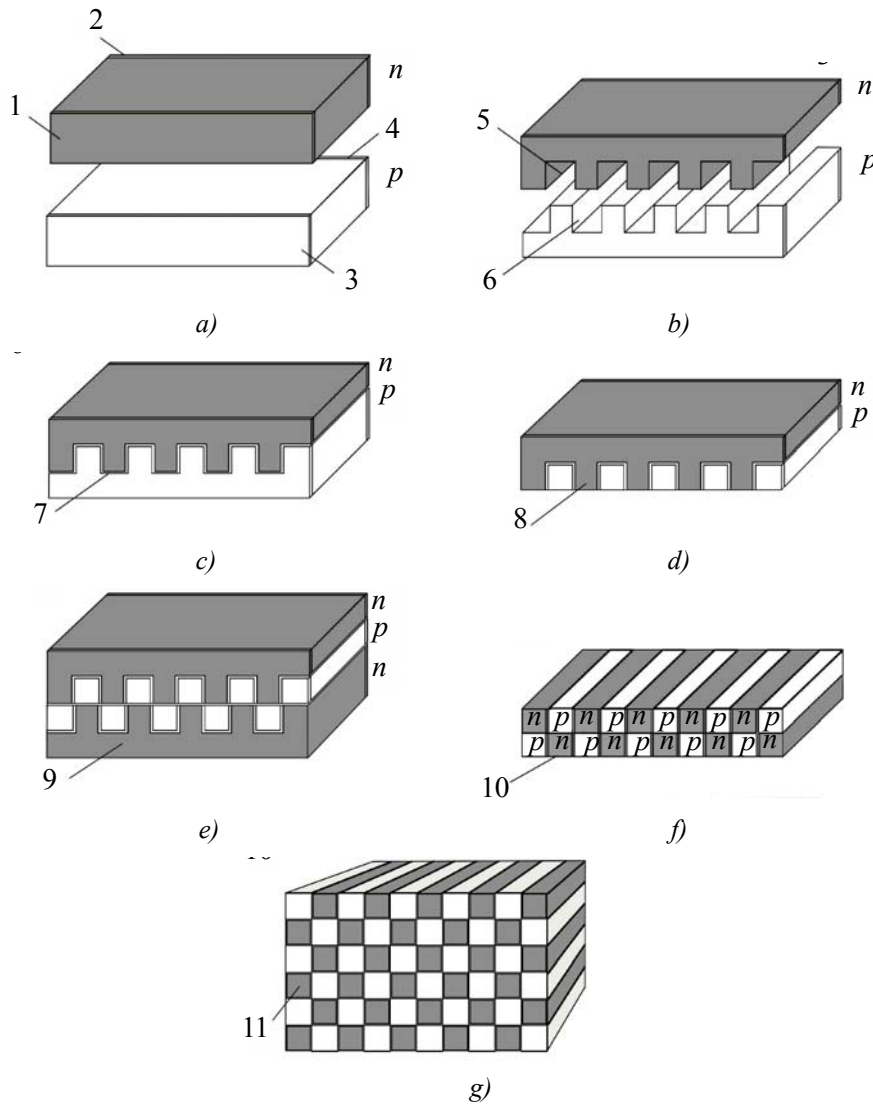
Fig. 2. Schematic of technology for manufacturing thermoelectric microthermopiles [12].

Experimental tests of proposed technology have proved the efficiency of its use for manufacturing thermoelectric microthermopiles with the legs of small cross-section from 0.01×0.01 mm to 1.0×1.0 mm. Such technology reduces considerably the percentage of rejected thermoelectric material plates due to decrease in the number of microcracks that may arise when grinding, and, thus, reduces the cost of thermoelectric microthermopiles. This, in turn, improves the reliability of produced thermoelectric heat flux sensors and microgenerators for power supply to low-power medical equipment.
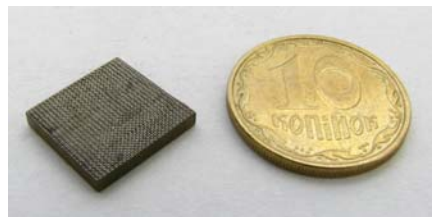
Fig. 3. Appearance of a thermoelectric thermopile produced by the above technology of size
(10 × 10 × 2) mm with cross-section of the legs 0.02 × 0.02 mm.

Fig. 3 shows a thermoelectric microthermopile produced by the above technology of size $(10 \times 10 \times 2)$ mm with cross-section of the legs 0.02×0.02 mm.

Based on the above technology, a series of thermoelectric microthermopiles has been manufactured with the size $(10 \times 10 \times 2)$ mm and the legs of small cross-section from 0.02×0.02 mm to 1.0×1.0 mm. In this way the efficiency of using said technology for manufacturing thermoelectric microthermopiles with increased density of components was experimentally verified.

Conclusions

1. A special technology was developed for manufacturing thermoelectric microthermopiles with increased density of components (up to several thousand) based on high-performance semiconductor materials that simplifies considerably and mechanizes the method for manufacturing thermoelectric heat flux sensors and microgenerators for power supply to low-power medical equipment.

2. The efficiency of using proposed technology for manufacturing thermoelectric microthermopiles with the legs of small cross-section from 0.02×0.02 mm to 1.0×1.0 mm and the length of legs up to 30 mm was experimentally confirmed.

3. It was established that the proposed technology reduces the percentage of rejected thermoelectric material plates due to decrease in the number of microcracks that may arise when grinding and, thus, reduces the cost of thermoelectric microthermopiles.

References

1. L. I. Anatychuk. *Thermoelements and Thermoelectric Devices: Reference Book* (Kyiv: Naukova Dumka, 1979), 768 p.
2. L. I. Anatychuk. *Thermoelectricity, Vol.1, Physics of Thermoelectricity* (Kyiv, Chernivtsi: Institute of Thermoelectricity, 1998), 376 p.
3. L. I. Anatychuk. *Thermoelectricity, Vol.2, Thermoelectric Power Converters* (Kyiv, Chernivtsi: Institute of Thermoelectricity, 2003), 376 p.
4. O. A. Geraschenko. *Foundations of the Heat Flux Measurement* (Kyiv: Naukova Dumka, 1971), p.192.
5. O. A. Geraschenko, T. G. Grischenko, L. V. Dekusha. Methods of Designing Optimal Heat Flux Converters, *Problems of Energy Saving* 3, 36 – 42 (1990).
6. B. M. Demchuk, O. J. Luste. Information and Energy Description of Thermoelectric Multiple Thermopiles, *J.Thermoelectricity* 2, 54 – 56 (2003).
7. L. I. Anatychuk, B. M. Demchuk, O. J. Luste. *Patent № 67369A*, Thermopile, 2004.
8. B. M. Goltsman, Z. M. Dashevsky, V. I. Kaidanov, N. V. Kolomoyets. Film *Thermoelements: Physics and Application* (Moscow: Nauka, 1985), 232 p.
9. B. M. Demchuk, O. J. Luste. Method of Assembling a Thermopile, *Certificate of Authorship № 1145857*, 1984.
10. L. I. Anatychuk, I. A. Konstantynovych. *Patent of Ukraine № 93217*, InCl H_01L 35/00, Method for Manufacturing Thermoelectric Microthermopile; Application № u201403210; filed 31.03.14; publ. 25.09.14, Bul. № 18.
11. L. I. Anatychuk, R. R. Kobylianskyi. *Application for a Utility Model № u201612914 of 19.12.2016.* Method for Manufacturing a Thermoelectric Microthermopile, Institute of Thermoelectricity; Yu. Fedkovych Chernivtsi National University.

Submitted 23.01.2017

B. S. Dzundza, O. B. Kostiuk, V. I. Makovyshyn, M. Yu. Perehinchuk

Vasyl Stefanyk Precarpathian National University,
57, Shevchenko Str., Ivano-Frankivsk, 76018, Ukraine

THERMOELECTRIC PROPERTIES OF THIN FILMS
BASED ON PURE AND DOPED LEAD TELLURIDE

The influence of technological factors of production, namely the time and temperature of deposition, on the surface morphology and the thermoelectric properties of thin films based on pure lead telluride and bismuth- doped PbTe:Bi with the content of bismuth 1 at. % (n-type) and $Pb_{17}Ag_2Te_{20}$ (p-type) compounds is investigated. The films were obtained in vacuum at different temperatures on fresh chips (0001) of mica-muscovite. It has been established that samples of PbTe: Bi with thickness of 0.3-0.5 μm have maximum thermoelectric power. It reaches $25 \mu W/K^2 cm$, which is much higher than that of pure lead telluride. For p-type films based on $Pb_{17}Ag_2Te_{20}$ compounds the thermoelectric power is much lower, despite the high values of the Seebeck coefficient, due to low conductivity values.
Key words: thin film, lead telluride, doping, thermoelectric properties.

Introduction

Films based on lead telluride are promising for the creation on their basis of active elements of micro and optoelectronics: detectors and infrared sources of optical spectrum [1], thermoelectric energy converters [2, 3]. The properties of thin polycrystalline films are strongly dependent on the surface morphology and electronic processes occurring at interphase boundaries [4 – 7]. The problem of obtaining films with predetermined properties and ensuring the stability of their electrical parameters in time is still relevant and unresolved. Moreover, when the films are exposed to air, due to the acceptor effect of oxygen, a layer rich in *p*-type carriers is formed on the surface, which prevents from obtaining a stable *n*-type material based on pure lead telluride [8, 9].

Doping of main matrix with donor impurities yields stable in time *n*-type material based on lead telluride [8]. For *p*-type material, complex compounds based on *PbAgTe* can be used.

The purpose of the work is to obtain stable in time films based on *PbTe* deposited on fresh chips (0001) of mica-muscovite and to study the influence of technological factors of production on the surface morphology of the films and their thermoelectric properties.

Experimental procedure

Films to be studied were obtained by vapour deposition of pre-synthesized *PbTe*, *PbTe:Bi*, $Pb_{17}Ag_2Te_{20}$ material in vacuum on the substrates of fresh chips (0001) of mica-muscovite. The temperature of the evaporator was $T_{ev} = 600\ ^oC$, and the temperature of substrates varied in the range of T_s=150 – 250 ^oC. The temperature of the films was set by deposition time within (20 – 2100) ^oC and measured by microinterferometer MII-4.

Measurement of the electrical and thermoelectric parameters of films was made in air at room temperatures in permanent magnetic fields on the designed automated installation, which provides measuring electrical parameters, as well as recording and primary processing of data, with the possibility of plotting time and temperature dependences. The measured sample had four Hall and two

current contacts. Silver films were used as ohmic contacts. Current through the samples was ≈ 1 mA. Magnetic field was directed perpendicular to the surface of films at 1.5 T induction.

The resulting samples were studied by methods of atomic force microscopy (AFM) on a Nanoscope 3a Dimension 3000 (Digital Instruments USA) in periodic contact mode. Measurements were made in the central part of the samples using serial silicon probes NSG-11 with a nominal radius of curvature to 10 nm (NT0MDT, Russia). According to the results of AFM studies, in addition to the surface morphology, the size of individual nanocrystals in the lateral direction and their height were determined by the watershed method using the Gwyddion program.

Surface morphology of films

Analysis of the results of AFM studies (Figs. 1 – 3) allows establishing certain common factors in the formation of epitaxial nanostructures, depending on their thickness and substrate temperatures. Thus, for instance, low deposition temperatures $T_s = 150 \, °C$ contribute to formation of nanocrystals with a predominance of growth rate in the tangential direction to substrate surface. This is indicated by the fact that their linear dimensions in the plane of the substrate azimuth exceed considerably the dimensions in the normal to surface direction. The rise in growth temperature to $T_s = 200 \, °C$ leads to formation of more homogeneous nanocrystals both in the form and linear dimensions in the lateral and normal directions to substrate surface (Fig. 1, Table). Thus, for films based on pure lead telluride the dimensions of crystallites in the lateral and normal directions are commensurate, for *Bi*-doped films the predominance of lateral dimensions remains, though much less pronounced. For *PbAgTe* films there are many coarse grains with flat tops (Fig. 3). A further rise in the deposition temperature leads to the formation of new growth stages on nanocrystals.

Table

Technological conditions of deposition and main morphological characteristics of resulting films. Evaporation temperature is 600 ^oC, deposition temperature is 200 ^oC.

Compound	Deposition time, s	Thickness (d), nm	Horizontal diameter of grains (D), nm	Average height of grains (H), nm	Average roughness (Sa), nm
PbTe	600	810	39	51.5	8.43
PbTe	445	540	24	26.2	5.57
PbTe	150	270	31	39.3	3.79
PbTe:Bi	300	320	45	16.2	1.81
PbTe:Bi	900	670	97	47.1	2.21
PbTe:Bi	1800	1620	107	60.3	3.12
Pb$_{17}$Ag$_2$Te$_{20}$	60	405	150	13.7	1.23
Pb$_{17}$Ag$_2$Te$_{20}$	35	270	100	14.1	1.86

Interesting is the dependence of the morphology of epitaxial structures on their thickness. For thin films based on pure *PbTe*, the formation of nanostructures with rounded faces and without a clear cut (Fig. 1a) is characteristic. With the increase in the time of deposition and, accordingly, the thickness of the condensate to ~ 1 microns, the growth of well-formed nanocrystals of different heights 20 – 80 nm (Fig. 1b) with linear dimensions at the base up to 100 nm takes place. For the *PbTe:Bi* films, the resulting structures consist of nanosized pyramidal form crystallites. The average size of crystallites perpendicular to the direction of the surface is ~ 50 nm, and in the lateral ~ 100 nm (Fig. 2, Table). Thin films based on

$Pb_{17}Ag_2Te_{20}$ compounds are characterized by rather homogeneous crystallites with rounded faces and flat tops, the sizes in the normal direction are rather small ~ 14 nm. As the film thickness increases to ~ 0.5 μm, the structure of the films becomes heterogeneous, with the predominance of grains in the form of flat cut pyramids of height of ~ 5 nm with a base of 300 – 500 nm, on the background of which there are single grains of height ~ 20 nm with sharp tops and a base of 80 – 100 nm. In this case, the average surface roughness is several times lower than for pure *PbTe* films and is 1 – 2 nm.

a) *b)*
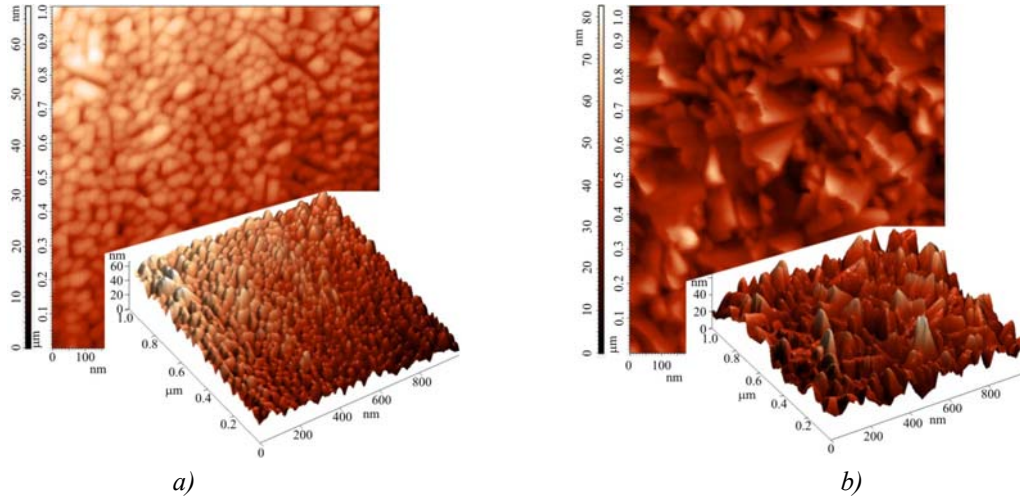
Fig. 1. AFM image of the surface of PbTe films on chips (0001)
of mica-muscovite, thickness: nm – 270 (a), 810 (b).

a)

b)
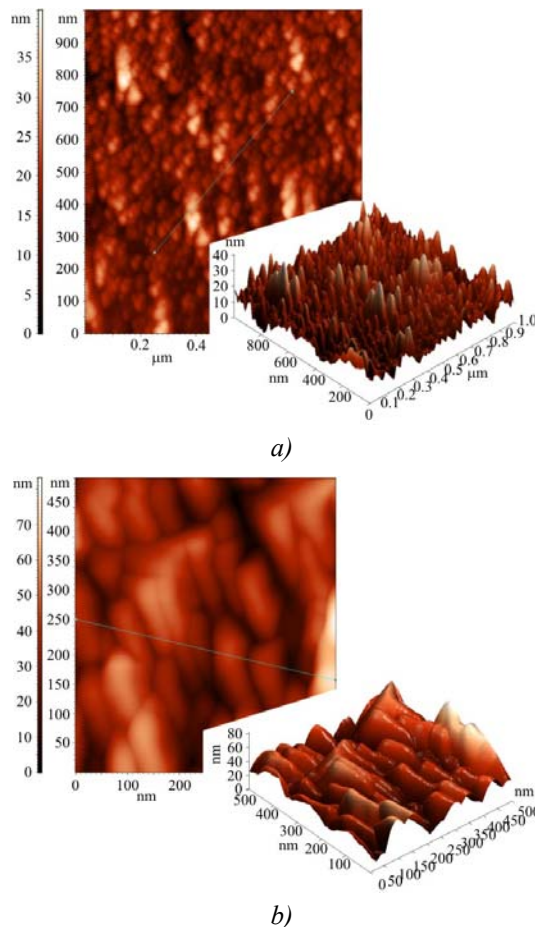
Fig. 2. AFM image of the surface of PbTe:Bi films on chips (0001)
of mica-muscovite, thickness d: nm – 320 (a), 1620 (b).

a)

b)
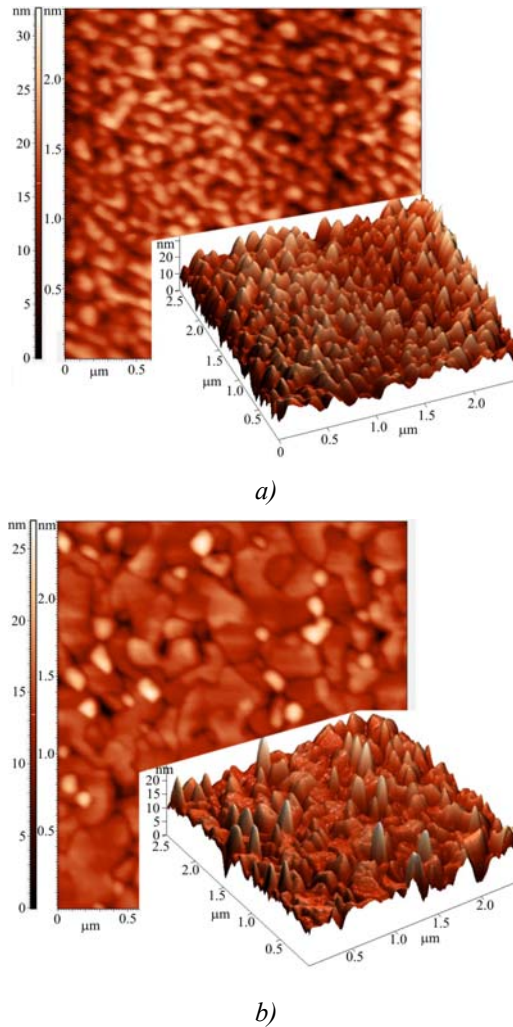
Fig. 3. AFM image of the surface of $Pb_{17}Ag_2Te_{20}$ films on chips (0001)
of mica-muscovite, thickness d: nm – 270 (a), 405 (b).

Analysis of thermoelectric properties of the films

The resulting dependences of the electric conductivity σ and the Hall concentration of current carriers n_H, the Seebeck coefficient S and the thermoelectric figure of merit $S^2\sigma$ on the film thickness are represented in Fig. 4.

From the previous works it can be concluded that deposition temperature has a significant impact on the thermoelectric parameters of material under study. For films based on pure lead telluride the electric conductivity, the Hall concentration of charge carriers and the thermoelectric power increase with a rise in deposition temperature, and the thermoelectric power has a clear peak at deposition temperature 200 ^{o}C. With a further rise in the temperature of the substrate, the growth rate increases more than twice to reach 2.25 nm/s (Fig. 2), and the thermoelectric parameters somewhat degrade. The thermoelectric power of films based on pure lead telluride is relatively low and reaches the maximum 6.2 μW/K^{2}cm at thicknesses close to 400 nm. To increase the thermoelectric power, 1 at. % of bismuth doping impurity was introduced into lead telluride. Taking into account clear peak of thermoelectric power, subsequent studies versus the thickness of doped condensate were conducted for samples obtained at T_s = 200 ^{o}C.

Introduction of bismuth doping impurity somewhat reduced deposition rate to 0.85 nm/s, but thermoelectric parameters of such samples are much better.
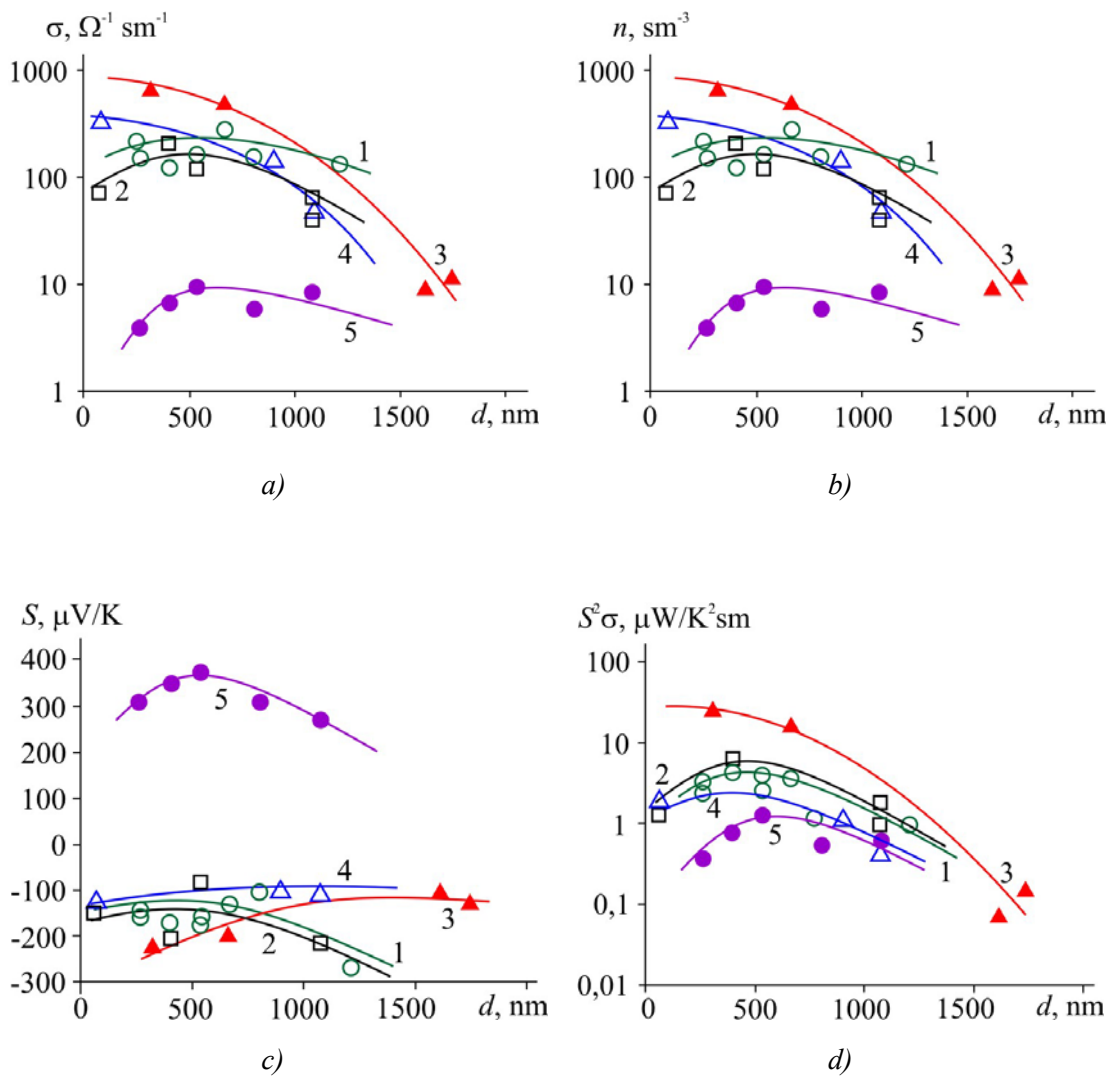
Fig. 4. Dependences of the electric conductivity σ(a), the Hall concentration n (b),
the Seebeck coefficient (c) and the thermoelectric power $S^2\sigma$ (d) on the thickness
of films obtained on fresh chips of mica. 1,○ – PbTe films obtained at Ts = 200 °C; 2,
□ – PbTe films obtained at Ts = 250 °C; 3, ▲ – PbTe:Bi films obtained at
Ts = 200 °C; 4,△ - PbTe:Bi films obtained at Ts = 150 °C;
5,● – $Pb_{17}Ag_2Te_{20}$ films obtained at Ts = 200 °C.

Specifically, bismuth doping resulted in the increase of the Hall concentration of charge carriers by more than an order of magnitude, the increase in the electric conductivity by more than three times with practically unvaried Seebeck coefficient, which made it possible to achieve a significant increase in thermoelectric power up to 25 µV/K. One should also note the thickness dependence of thermoelectric power which demonstrates a clear peak at thicknesses close to 320 – 400 nm. The growth of thermoelectric figure of merit is due to improvement of structural perfection of films (Fig. 5), which leads to reduction of scattering effect at grain boundaries and considerable increase in the electric conductivity. With rather small thicknesses, the role of carrier scattering on the surface of film is increased and the conductivity is considerably reduced.

For the films of p-type $Pb_{17}Ag_2Te_{20}$ such high values of thermoelectric power could not be reached, despite the sufficiently high Seebeck coefficient values of 300 – 400 µV/K, because of low electric conductivity to 10 $\Omega^{-1}cm^{-1}$.

The thickness dependence of thermoelectric power also demonstrates a clear peak with the

thicknesses close to 500 nm, which is related to essential change of film structure at these thicknesses.
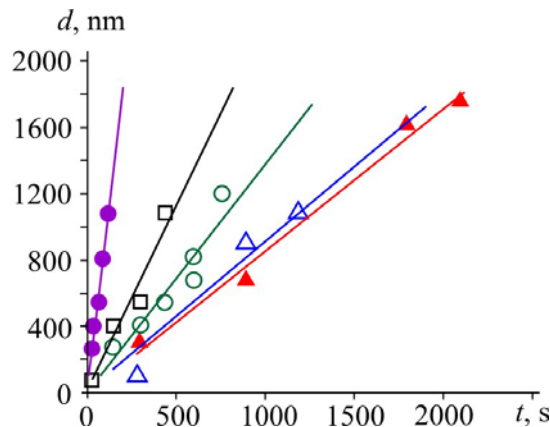

Fig. 5 Dependence of film thickness on deposition time. ○ – PbTe films obtained at Ts = 200 °C; □ – PbTe films obtained at T_s = 250 °C; ▲ – PbTe:Bi films obtained at Ts = 200 °C; △ – PbTe:Bi films obtained at T_s = 150 °C; ● – $Pb_{17}Ag_2Te_{20}$ films obtained at T_s = 200 °C.

Conclusions

1. The effect of technological factors on the structure, surface morphology and thermoelectric properties of vapour phase thin films based on pure and bismuth-doped lead telluride *PbTe*:*Bi* and $Pb_{17}Ag_2Te_{20}$ compounds obtained by vapour phase methods on mica substrates is investigated.

2. It is established that *PbTe*:*Bi* samples with the content of *Bi* 1 at. % and a thickness close to 320 – 400 nm have maximum thermoelectric power 25 µW/K^{2}cm which is much better than that of pure tin telluride. For films based on $Pb_{17}Ag_2Te_{20}$ the peak of thermoelectric characteristics is observed at somewhat larger thickness – close to 500 nm.

3. It is shown that thin films based on *PbTe* have improved thermoelectric parameters as compared to the bulk samples.

References

1. V.M.Shperun, D.M.Freik, and R.I.Zapukhliak, *Thermoelectricity of Lead Telluride and its Analogs* (Ivano-Frankivsk: Plai, 2000), 250 p.
2. E.P.Sabo, Technology of Chalcogenide Thermoelements. Physical Fundamentals. Structure and Properties of Materials, *J.Thermoelectricity* 1, 61 (2002).
3. T.Kajikawa, Current Status of Research and Dvelopments in Technology of Thermoelectric Generation in Japan, *J.Thermoelectricity* 1, 18 – 30 (2009).
4. M.Green, *Surface Properties of Solids* (Moscow: Mir, 1972).
5. Y. P. Saliy, D. M. Freik, I. K. Yurchyshyn, and I. M. Freik, Periodicity of the Distribution of Intrinsic Defects in Epitaxial *PbTe* Films, *J. Nano- and Electronic Physics* **5**(3), 03038 – 1 (2013).
6. D.M. Freik, Y.P. Saliy, I.M. Lishchynskyy, V.V. Bachuk, and N.Y. Stefaniv, Evolution of Growth

Processes of Paraphase Nanostructures of Lead Telluride, *J.Nano- and Electronic Physics* **4**(2), 02011 – 1 (2012).

7. L.I.Anatychuk, *Thermoelements and Thermoelectric Devices: Reference Book* (Kyiv: Naukova Dumka, 1979), 768 p.

8. D.M.Freik, I.V.Horichok, N.I.Dykun, and Yu.V. Lysiuk, Influence of Manufacturing Technology on the Thermoelectric Properties of Nonstoichiometric and Doped Lead Telluride and Solid Solutions on its Basis, *J.Thermoelectricity* 2, 43 (2011).

9. D.M.Freik, M.A.Galushchak, and L.I.Mezhilovskaya, *Physics and Technology of Thin Films* (Lviv: Vyshcha Shkola, 1988), 182p.

Submitted 12.11.2016

Djelaili Abdelbaqi, Korti Abdel Illah Nabil

ETAP laboratory, Department of Mechanical Engineering,
University of Tlemcen, Algeria

PERFORMANCE OF A HYBRID SOLAR WALL INTEGRATED INTO THE SOUTH FACADE DEDICATED FOR THE PASSIVE HEATING OF BUILDINGS

Actually building designers have to think about new strategies to achieve the best sustainable building designs. Well-planned passive heating strategies in building design may reduce significantly building's energy consumption. In this, paper a proposed designe of south façade of a room by integrating a hybrid solar wall and a window in case to heat passively a room is studied. The simulations for three-dimensional model of BIPV Trombe wall system have been carried out for December 10th, 2015. The temperature and velocity distribution of indoor air in different position inside the room are obtained from the simulation results. The obtained results show that the temperature difference between the inlet and the outlet of the solar wall can reach 9 °C. The 3D analysis of the proposed model show clearly that the window's thermal effect on the passive heating can't be neglected. Meanwhile, the simulation daily electrical efficiency conversion and average indoor air temperature of this system can reach 18 % and 28 °C respectively for maximum solar radiation of 470 W/m².

Key words: natural ventilation, trombe wall, photovoltaique cells, hybrid solar wall.

Introduction

Control of natural ventilation answers to multiple issues. First, it allows the building to have a sufficient quality indoor air for the health of occupants, replacing stale air by the occupants and the various sources of pollution (kitchens, bathrooms, workshops, etc.) by fresh air. Secondly, it contributes to the sustainability of buildings by removing moisture that could cause damage.

Any solution for ventilation must be adapted to the local context, both climate, urban, technical and economic. Our prototype provides passive heating of a room based on the phenomenon of natural convection. The solar energy utilization in the field of the habitat to reduce its energy consumption was the subject of several studies. A technique of heating being based on a solar system of collecting, storage and restitution of heat was developed with the C.N.R.S. (France) by Professor Trombe [1].

The use of solar energy in the area of habitat to reduce its energy consumption has been the subject of several studies. Ramadan Bassiouny et al [2] also studied (2008) the influence of certain parameters on the thermal behavior of the solar chimney to optimize its design. The results obtained show that the width of the chimney has a very important influence on the ACH (air changes per hour) compared to that of the inlet section. The results show that there is an optimum intake section beyond what ACH begins to decrease. It was concluded that increasing the intake size three times only improves the ACH by almost 11 %. However, increasing the width of the stack by a factor of three improves by nearly 25 % ACH, keeping fixed the intake section. The same researchers studied in 2009 [3] subsequently a solar chimney placed on a sloping roof to see the influence of the inclination on the thermal behavior of the chimney. The results show the inclination significantly affects the rate of ventilation and the airflow, which crosses the chimney. This study shows that the optimum angle of

inclination of the stack is between 45° and 75° to 28.4° latitude.

Guohua Gan et al [4] studied numerically natural ventilation through a vertical solar chimney by a CFD model. The simulation is performed using two fields, the first (*s*) identical to that of the cavity size of the stack, and the second (*L*) is extended. It has shown that the use of two areas for effective simulation for a variety of ventilation, however, the use of a single field identical to that of the cavity of the chimney size is favored for long chimneys where wall strength is dominant. Photovoltaic cells are adapted to receive the electrical gain using a hybrid solar wall, Basak kundakci and Zerrin Yilmaz [5] are studying the design parameters that influence the thermal efficiency of a solar wall such as the south facade.

A numerical model carried out by Bourdeau and Jaffrin [6] and Bourdeau et al [7] showed that the use of a wall of 3.5cm thickness can replace a wall of concrete 15cm. The use of the pcm reduces 90 % of mass of wall of storage and increases their effectiveness by a factor of 20 % [8].

Zlaweski et al [9] concluded that the solar energy that crosses the glazing is approximately 78 K·W·H/m²; the wall in PCM absorbs that 37.7 K·W·H/m², which accounts for 49 % of incidental energy. The wall in PCM generates 23.5 K·W·H/m² in the open cavity and this quantity accounts for 68 % of absorptive energy. Thus, the effectiveness of this wall does not exceed 30 %.The aim of this work is to produce a three-dimensional numerical model of the passive heating of a Place with a hybrid solar wall. This prototype is designed for cooling the *PV* cell and provide a passive heating to our home for the cold period of the year.

Physical model

Fig. 1 illustrates a schematic of the physical domain, with an attached hybrid solar wall of length L, and width d. The domain considers having a window (1 m × 1 m), and it is at 1 m height from the floor. The considered dimensions for this room were 3.5 m × 3 m × 3 m (Fig. 1), and the hybrid solar wall was considered 1.8 m length and 1.2 m width and the air gap was taken as 0.5 m.

The PV-Trombe wall system, as shown in Fig. 1, is composed of a semi-transparent PV cell panel, a thermal mass wall acting as a thermal absorber and an air duct in between. There are also two air vents for winter heating. The PV-TW wall system works as the original Trombe wall and its detailed description can be found in [10].
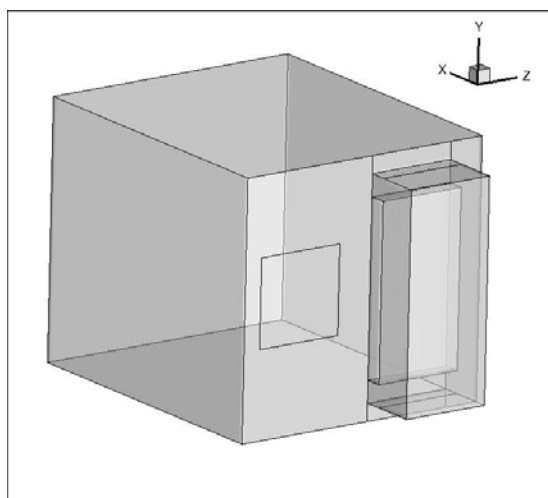

Fig. 1: A general schematic of the physical domain.

Boundary conditions:

Our area to be treated is a room in three dimensions (Fig. 2), has a hybrid solar wall and a window on the south façade. All walls of the studied rooms are adiabatique, except the south wall. The convection and the radiation heat flux effect are added at the south wall and the concrete roof.

Where the solar radiation values are from real climatic data of a typical day of Tlemcen. The convection heat transfer coefficient due to wind is defined by the equation (1) recommended by McAdams [11]:

$$h = 5.67 + 3.86V_{wind} \tag{1}$$

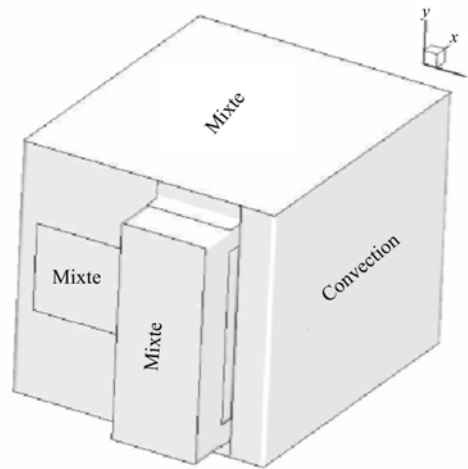where V_{wind} is the wind velocity.

Fig. 2: Boundary condition adapted in CFD model.

The air inside the hybrid solar wall is heated by the greenhouse effect. The warm air, which is more light because it is less dense, rises, which causes the aspiration of the fresh air. The circulation of the air is made naturally without mechanics; this circulation ensures also the free cooling of our photovoltaique cell. The outlet at the top of solar wall is in the opposite direction of the inlet (in the bottom of the solar wall). The size of the inlet section of the solar wall is identical to that of the exit section. Simulation is carried out under the laminar mode, and the air is considered initially stable.

Results and discussion

The following sections present the numerical results obtained from three-dimensional unsteady-state turbulent simulations using the standard k − ε model with an enhanced wall function for the attached solar chimney model.

The simulation has been carried out with data of a day during wintertime December 10th in Tlemcen (Altitude 750 m, Latitude 35° 28' and Longitude 17°1'). The hourly variation of global and diffuse horizontal solar radiation during the 24 hours of the selected day is shown in Fig. 3.

After designing the models using Gambit software, their networking is made by organized networks. The boundary conditions of the models are defined model based on Fig. 2, although these conditions can be altered by "Fluent software" in the next stages of the analysis.

The commercial CFD software package, FLUENT, which is based on the finite volume approach was used for the simulation in three dimensions using the segregated solver.
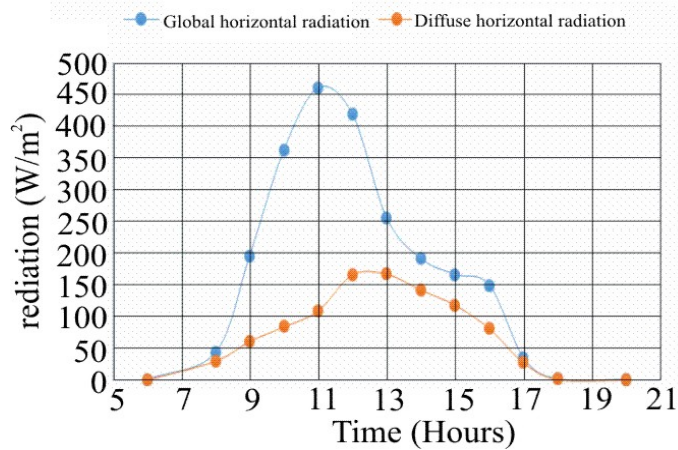
Fig. 3 The hourly solar radiation in Tlemcen during December the 10th.

In the second stage, the models are utilized in "Fluent software" (Fluent 6.3.26), the solution condition is described as followings:

- Solver: Pressure based.
- Space: 3D.
- Formulation: Implicit.
- Time: unsteady.
- Operating pressure: 101325P.
- The convergence criterion was set equal to 10 – 6 for all parameters.

To verify the precision of the developed numerical model we propose to compare the obtained results with those obtained experimentally by Basak kundakci and Zerrin Yilmaz [4] who studied a trombe wall system with single glass, double glass and *PV* panels. Fig. 4 represents the hourly change in surface temperature of the *PV* cell recorded for two successive days. A comparison shows that our results that appear in doted black curve agree well with that of literature [4]. This prove the good accuracy of the method proposed in this work.
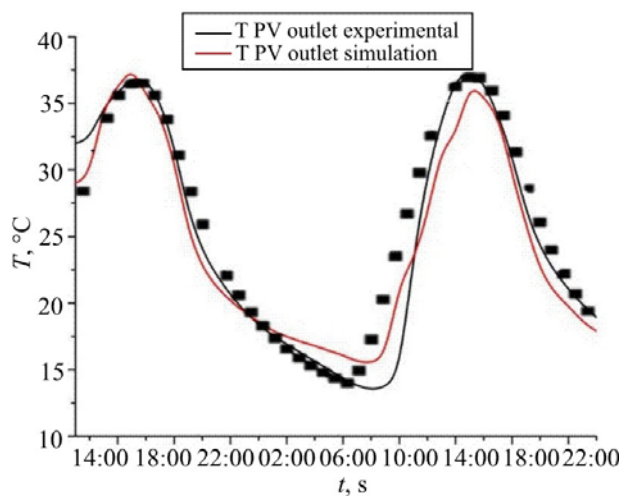

Fig. 4: Validation of results.

Fig. 5 and Fig. 6 show the temperature contour recorded every tow hour starting at 07:00. The higher values of solar radiation increase the air temperature inside the chimney

and the air temperature difference between the inlet and the outlet of the hybrid solar wall increased too (Fig. 5).

The air temperature rise in the proposed model is proportional to the solar irradiation intensity. An increase in solar intensity increases the *PV* cell temperature and consequently increases the air temperature inside the hybrid solar wall. We can see clearly that the important values of temperature are recorded near the *PV* cell and the window. The air inside the room is warmed naturally by the solar chimney effect explained bellow.

Fig. 4 show that the window has more significant effect in the passive heating of the air inside the room. The thermal effect of adapting a window in the south wall cannot be neglected, the raison that prove that the study of a similar problem could be in three dimension.
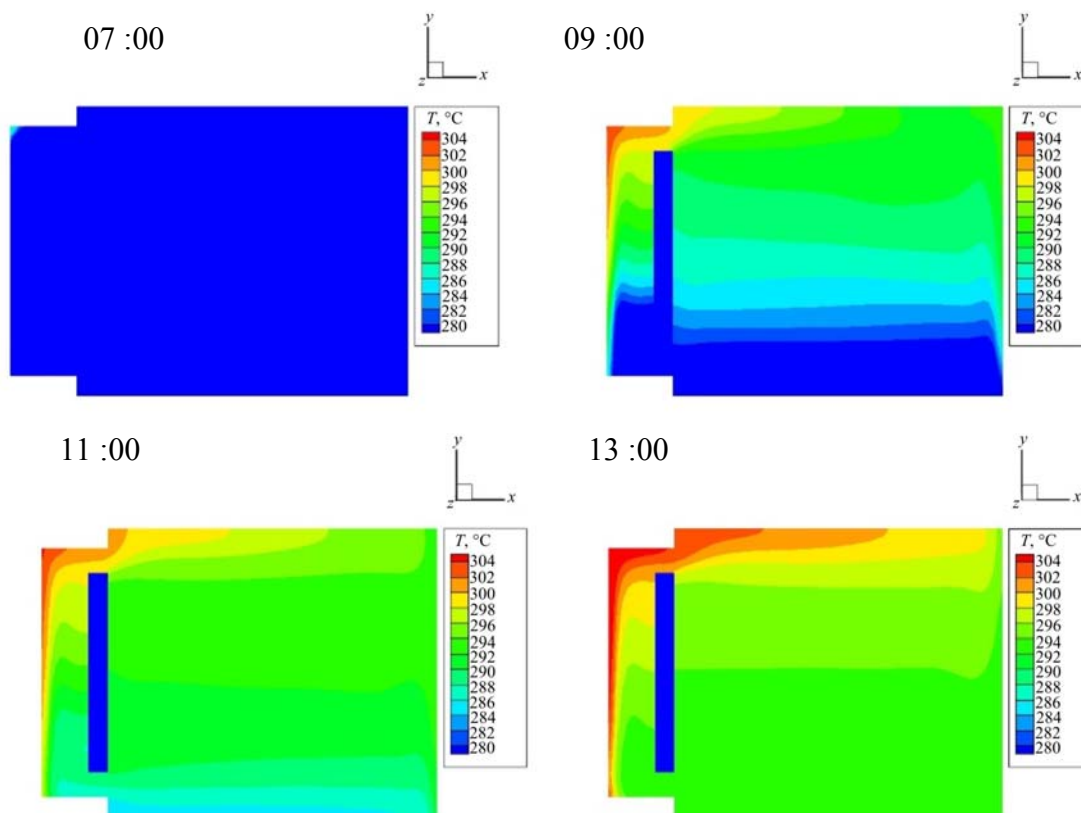

Fig. 5: Temperature contour recorded every
two hours (z=2.4m).

Fig. 7 showed the air temperature distribution inside the hybrid solar wall near the *PV* cell (a) and the air temperature distribution inside the room near the window (b). The figure indicates the significant temperature changes corresponding to solar intensity variations. Further, as intensity increases, there is an increase in all temperatures. During all the day, we notice that the *PV* records the most important temperature. As seen in the Fig. 7 the temperature, reach 304K near the *PV* and 300K near the window.

The Fig. 8 shows the evolution of the temperature fields inside the test room. The heat generated in the level of the *PV* cell and the window has a significant impact on the temperature

distribution inside the room as seen in Fig. 8. The highly temperature recorded inside the room are located on the top near the ceiling ($\leq$ 302 K).
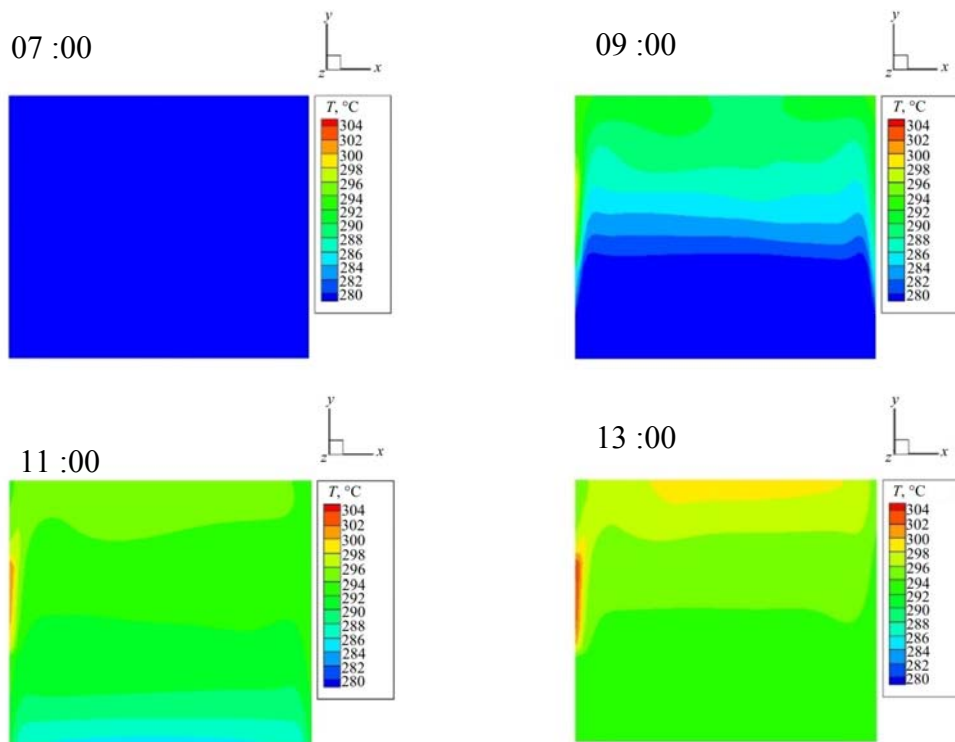
07 :00

09 :00

11 :00

13 :00

Fig. 6: Temperature contour recorded every two hours (z=1m).
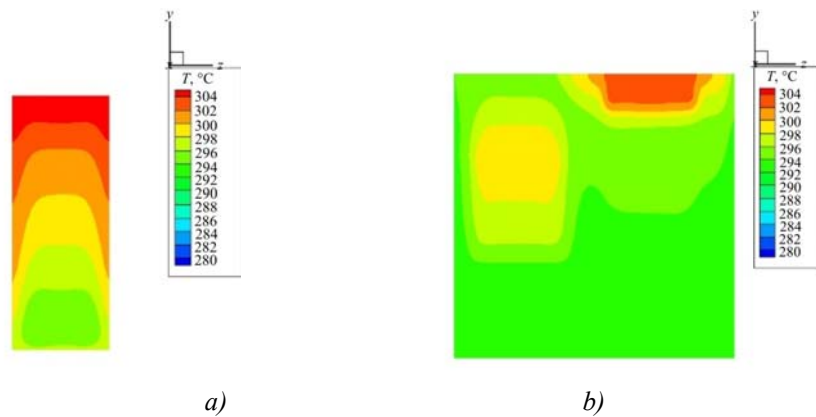
a)

b)

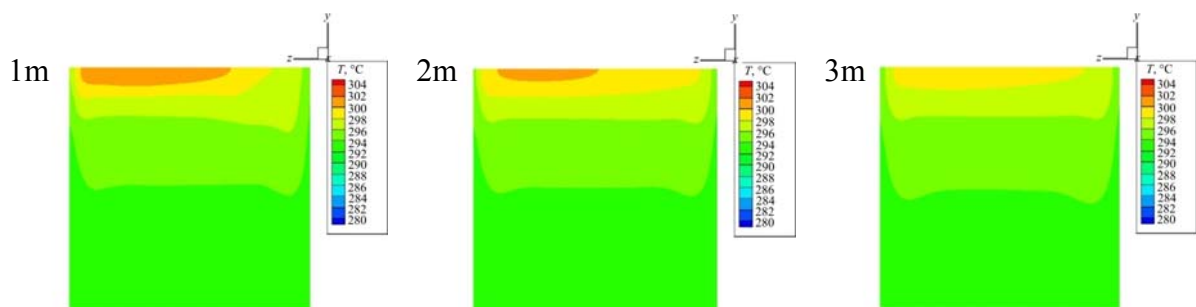*Fig. 7: Temperature contour near the PV cell (a) and the window (b)*

1m

2m

3m

Fig. 8: Temperature contour in 1, 2 and 3m along the X-axis from the south façade respectively
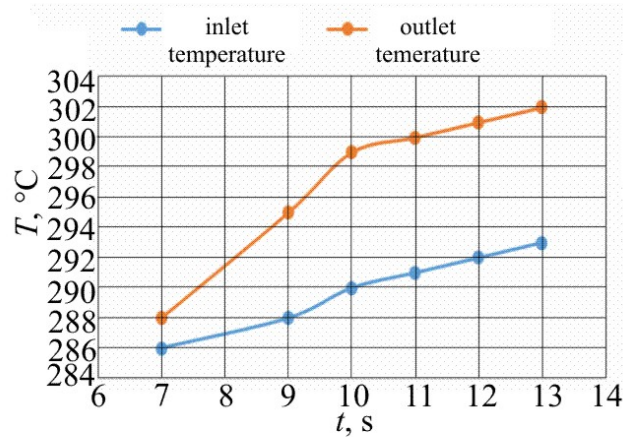
Fig. 9 Temperature variation at inlet an outlet of
the hybrid solar wall

As seen in Fig. 9 the following inlet and outlet hybrid solar wall temperatures are compared. The fresh air inside the room will be changed with one wormed naturally by the greenhouse effect inside the hybrid solar wall during the day. The air temperature in the inlet and the outlet of the hybrid solar wall reach the maximum value at 13^{00} which is 302K and 293K respectively.

Fig. 10 shows the hourly electrical efficiency change with *PV* cell surface temperature during the selected day December 10th. Where PV cell conversion efficiency related to the cell temperature as:

$$\eta_{pv} = \eta_0 \left(1 - 0.0045\left(T - 298.15\right)\right) \tag{2}$$

η_0 is the electrical efficiency under standard conditions (1000 W/m², 25 °C) [12].
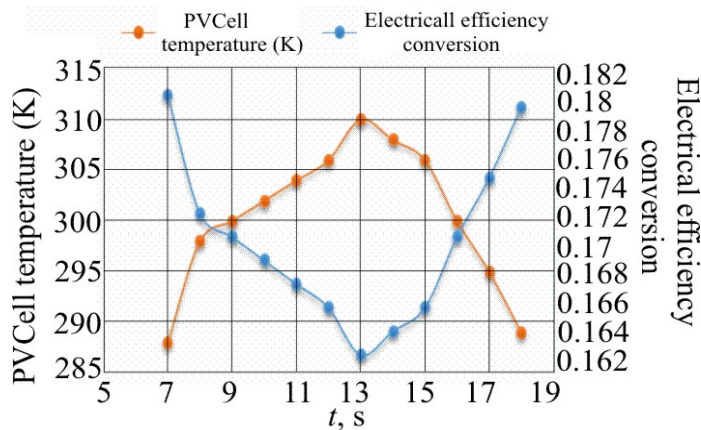

Fig. 10: The hourly change in the efficiency and
the temperature of the PV cell in both of models

The *PV* cells has the ability to produce electricity during the day as long as it was exposed to the solar radiation. As seen in Fig. 10, the electrical efficiecy conversion has its highest value that was recorded at 06^{00} which is 18.02 % while the surface temperature of the *PV* cells has its lowest value of 14°C. The electrical efficiency drops to its lowest value of the day at 13^{00} which is 16.3 % when the

surface temperature of the *PV* cells increases to its highest value of 37°C. Then, the electrical efficiency conversion increases to 17.94 % at 18^{00} as the surface temperature of the *PV* cells decreases to 16°C.

Conclusion

The aim of this work is to present a thermal performance of hybrid solar wall integrated in a passive solar building in Tlemcen. The numerical simulation using the segregated solver with real climatic data conditions of Tlemcen city.

This study shows firstly that the solar wall is an effective solution for the passive heating of the buildings. By adapting a solar wall, the temperature of air of the room can reach the 28 °C when the ambient temperature is lower than 21 °C.

Secondly, the results obtained show that our hybrid solar wall ensures a good cooling of the photovoltaic cell that enabled us thereafter to reach a better electric output.

It is interesting to note that the excess heat released by the PV-Cell is used for heating passively our room; despite the PV cell is cooled down by the fresh air aspired from the room.

There exist several improvements to increase the effectiveness of our solar wall, like the use increase the insolation of surrounding wall to limit the heat losses towards the outside, or the integration of the pcm to prolong the operating time of our wall of storage.

References

1. D. M. Utzinger. 'Analysis of Building Components Related to Direct Solar Heating of Building', M. S. Thesis, University of Winconsin, Madison, (1979).
2. Ramadan Bassiouny, Nader S. A. Koura. An analytical and numerical study of solar chimney use for room natural ventilation, Energy and Buildings 40 (2008) 865 – 873.
3. Ramadan Bassiouny, Nader S. A. Korah. Effect of solar chimney inclination angle on space flowpattern and ventilation rate, Energy and Buildings 41 (2009) 190 – 196.
4. Guohui Gan. Simulation of buoyancy-driven natural ventilation of buildings-Impact of computational domain, Energy and Buildings 42 (2010) 1290 – 1300
5. Basak Kundakci Koyunbaba , Zerrin Yilmaz, The comparison of Trombe wall systems with single glass, double glass and PV Panels, Renewable Energy 45 (2012) 111 – 118.
6. Bourdeau, L., Jaffrin, A.. 1979. Actual performance of a latent heat diode wall. In: Proceedings of Izmir International Symposium II on Solar Energy Fundamentals and applications, Izmir Turkey.
7. Bourdeau, L.. 1980. Study of two passive solar systems containing phase change materials for thermal storage. In: Hayes, J., Snyder, R. (Eds.), Proceedings of the Fifth National Passive Solar Conference, 19 – 26 October, Amherst, Newark, DE, American Solar Energy Society, p. 297.
8. Knowles, T., 1983. Proportioning composites for efficient thermal storage walls. Solar Energy 31 (3), 319 – 326.
9. Laurent Zalewski, Annabelle Joulin, Steten el Lassue, Yvan Dutil, Daniel Rousse, Experimental study of small-scale solar wall integrating phase change material, Solar Energy 86 (2012) 208 – 219
10. Ji Jie, Yi Hua, He Wei, Pei Gang, Lu Jianping, Jiang Bin. Modeling of a novel Trombe wall with *PV* cells, Building and Environment, in press.
11. Mc Adams, W.H. 1954. Heat Transmission, third edition, McGraw-Hill, New York
12. Zondag HA, de Vries DW, van Helden WGJ, van Zolingen RJC, van Steenhoven AA. The thermal and electrical yield of a PV-thermal collector. Sol Energy 2002; 72(2):113 – 28.

**Guram Bokuchava[1], Karlo Barbakadze[1],
Giorgiy Darsavelidzee[1], Boris Shirokov[2]**

[1]Sukhumi Ilia Vekua Institute of Physics and Technologya
7, Mindeli Str., 0186, Tbilisi, Georgia
[2]The National Scientific Centre "Kharkiv Institute of Physics and Technology"
1, Akademicheskaya Str., 61108, Kharkiv, Ukraine

ACHIEVEMENTS OF SUKHUMI ILIA VEKUA INSTITUTE OF PHYSICS AND TECHNOLOGY IN THE FIELD OF THERMOELECTRIC MATERIALS SCIENCE AND INSTRUMENT MAKING

The paper presents the stages of the development and manufacture of various-purpose thermoelectric generators at Sukhumi Ilia Vekua Institute of Physics and Technology (SIPT). Analytical and experimental studies conducted at SIPT in the late 1950s revealed great prospects for the creation of high-efficiency thermoelectric generators for nuclear power plants of terrestrial and space application. In 1964, a thermoelectric converter for the world's first nuclear power plant, "Romashka," was built at SIPT. In 1966, a single-stage thermoelectric converter "Buk" was created, followed in 1969 by a two-stage TEG "Buk" with an electric power of 2.8 kW. C Since the beginning of 2000, the institute has resumed work on the development of high-temperature thermoelectric materials and devices based on SiGe. The effect of reactor radiation on the thermoelectric characteristics of SiGe and other materials was analyzed. To develop radiation –resistant materials for high-temperature thermoelements, p-type B_4C and n-type $Si_{0.7}Ge_{0.3}$ were chosen. New thermoelectric converters are being developed on the basis of relatively inexpensive SiGe alloys containing 5 – 10 at. % Ge.
Key words: thermoelectric generator, SiGe alloys, "Romashka", "Buk", radioisotope fuel, boron carbide

Introduction

In chronological order, the main achievements of SIPT in thermoelectric materials science and instrument making are set forth, namely preparation of bulk *Ge*, *Si* and *SiGe* crystals (1955 – 1958), synthesis of thermoelectric alloys, development of technology of high-temperature interconnects, creation of high-temperature thermopiles together with I.Kurchatov Nuclear Energy Institute, Podolsk Research Institute and Kharkiv Institute of Physics and Technology, development and creation of nuclear power plant "Romashka" (1964), creation of an experimental prototype of a single-stage thermoelectric generator "Buk" (1966). The problem of developing low-resistance and stable interconnects to *Pb* and *Ge* tellurides, obtaining heat-resistant thermoelement legs and creating high-efficiency thermopile with anti-sublimation coating has been successfully solved. The results of the works were used to create a two-stage thermoelectric generator for the nuclear power plant of space application "Buk".

In the 1970s, a number of TEGs were created at SIPT, operating on radioisotope fuel in different temperature ranges.

In the 1980s, low-power TEGs were developed for use in microelectronics, medicine, and military field. TEGs "Gamma" for working in deep water conditions, environmentally friendly

refrigerators, microcoolers that stabilize the temperature of high-sensitive photodetectors were also developed.

In 2003 – 2013, a number of international projects were carried out concerning the problems of thermoelectric instrumentation and optoelectronic devices based on *SiGe*.

At the present time, thermopiles and generators are being developed on the basis of *SiGe* alloys with a relatively low content of *Ge* (5 – 10 at. %) in TEGs intended for use in the furnaces of central gas heating systems, as well as for cathode protection of main pipelines of energy carriers. A joint project is being developed for creation of a three-stage thermoelectric generator with participation of Sukhumi Ilia Vekua Institute of Physics and Technology, Institute of Thermoelectricity of the NAS Ukraine and the National Scientific Center "Kharkiv Institute of Physics and Technology" of the NAS Ukraine.

In the early 1950s, Sukhumi Institute of Physics and Technology (SIPT) began to pursue research in the field of physics and technology of semiconductor materials. This was due to the need for creation of new high-purity materials – germanium and silicon – for the rapidly developing semiconductor electronics.

SiGe alloys, as a thermoelectric material, were first proposed by A. F. Ioffe in 1954 [1]. In 1956, for the first time at SIPT, studies began on technology for production of *Ge-Si* alloys. The work was continued by several researchers in the USSR and the USA.

In 1958, in connection with the need for outer space exploration, the institute was commissioned to develop a nuclear-fueled thermoelectric power converter. The choice of SIPT for this task was due to its successes and achievements in obtaining semiconductor-grade germanium and silicon and germanium-silicon alloys, obtaining for the first time in the USSR a germanium single crystal in 1954 and a silicon single crystal in 1956. In the years 1958 – 1960, devices and equipment for the synthesis and study of *SiGe* alloys were developed and manufactured; efficient thermoelectric alloys $Si_{0.93}$ $Ge_{00.7}$ of *n*- and *p*-type conductivity were obtained; technology for manufacturing high-temperature interconnects was developed (~1000 °C) and high-temperature thermopiles were made. In 1964, for the first time in the world under the direction of I. Gverdtsiteli, a thermoelectric generator for the nuclear power plant "Romashka" was developed and created (Fig. 1).
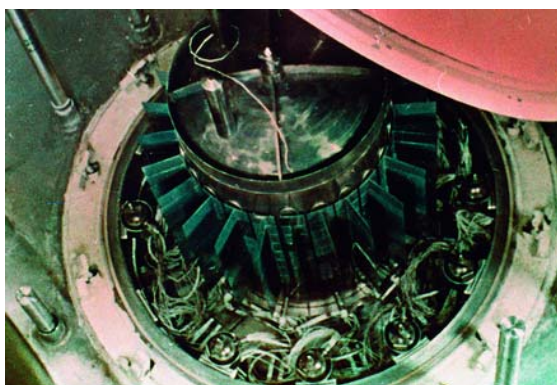

Fig. 1. "Romashka"

In creation of "Romashka" together with SIPT participated: I. Kurchatov Nuclear Energy Institute, Podolsk Research Institute and Kharkiv Institute of Physics and Technology.

The source of thermal energy for the "Romashka" plant was a nuclear reactor operating on fast neutrons. The released thermal energy was converted into electrical energy by means of thermoelements. The tests of the "Romashka" plant confirmed the high reliability of the entire system and the stability of the main operating parameters. In 1964, the results of these works were presented

in Geneva at the III International Symposium on the Peaceful Uses of Atomic Energy (Report № 873) and aroused the great interest of world-famous specialists. These materials were published in a well-known scientific journal [2].

Thermoelectric materials science and instrument making at SIPT developed along two lines. The first one is creation of high-power TEGs of space application for nuclear power plants and their full-scale production. The second is production of medium and low power TEGs operating on isotope fuel for the needs of different sectors of economy. In 1962, studies began on the development of a thermoelectric generator for space power unit "Buk". High-performance $Si_{0.68}Ge_{0.32}$ alloys of *n*- and *p*-type conductivity, low-resistance interconnects and thermopiles with high mechanical strength were developed. On their basis, in 1966, a single-stage experimental thermoelectric generator "Buk" was created and successfully tested (Fig. 2).
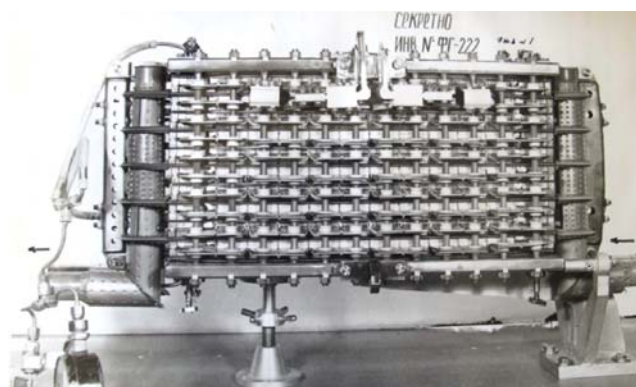

Fig. 2. "Buk"

After its testing, it was decided to create a more efficient two-stage TEG for the "Buk". Its first stage was to be made of $Si_{0.7}Ge_{0.3}$ alloys of *n*- and *p*-type conductivity and the second stage was to be based on thermoelectric alloys $PbTe$ (*n*) and $GeTe$ (*p*). The problem lied in the development of low-resistance and stable interconnects to $PbTe$ and $GeTe$ alloys, obtaining thermally stable thermoelement legs and creating on their basis the high-performance thermopile with anti-sublimation coating. These problems were successfully solved, and in 1968 a highly efficient two-stage TEG for the "Buk" plant with a capacity of 2.8 kW was created. Its first stage operated in the temperature range 715 – 530 °C, and the second – 530 – 350 °C. Unlike the "Romashka", in the "Buk" plant the reactor was separated from the TEG and connected to it by a two-circuit coolant (heat-supplying and heat-releasing) based on *Li-K*. This made it possible to practically exclude the effect of radiation on the structural units of the TEG.

In 1975, after many years of integrated research, "Buk" was put into serial production and more than 30 samples successfully worked in space vehicles of the "Cosmos" series.

In 1972, the technology of production of low-temperature thermoelectric materials (Bi_2Te_3-Bi_2Se_3 *n*-type and Bi_2Te_3-Sb_2Te_3 *p*-type) was developed at SIPT for manufacturing thermopiles on their basis, which significantly expanded the operating temperature range of TEGs developed at the institute. In 1975, a number of TEGs were created (Limon, Beta, Reut, Gong, Gorn, etc.), operating on radioisotope fuel in different temperature ranges, with power output of 8 – 70 Watt.

In the 1980s, SIPT was engaged in works on low-power TEG Hermes, Signal, etc., for use in microelectronics, medicine, and the military field.

In 1989, the modernized TEG "Buk" was completed and put into serial production at the institute with a doubled service life, due to the improvement of interconnects.

In thermoelectric instrument making, a significant step was the development of the TEG "Gamma" based on low-temperature thermoelectric materials for operation in deep-water conditions. In it, a thermoelectric annular module developed at the institute was used.

In the late 1980s, SIPT, in cooperation with other institutes, began developing a program similar to the American SP-100. The program included creation of a ~ 100 kW TEG, with a 7-year service life. In this direction, a modular TEG "Gloria" was created, capable of generating various capacities for replication. The work was suspended due to conversion. In the late 1980s, SIPT began to develop environmentally friendly cold devices based on the Peltier effect, using high-performance low-temperature thermopiles. Micro-refrigerating devices containing up to 100 thermocouples were developed and manufactured, which ensure temperature stabilization of highly sensitive photodetectors.

The main results of reactor tests of $Si_{0.7}Ge_{0.3}$ alloys at temperatures in the range of 773 – 973 K with a fast neutron fluence set to ~4.0×1020 sm^{-2} are presented in [3]. The studies were carried out on the water-to-water power reactor of the Institute for Nuclear Research of the Academy of Sciences of Ukraine under conditions that are as close as possible to the real operating conditions of nuclear power plants. As a donor impurity, samples of heavily doped $Si_{0.7}$ $Ge_{0.3}$ alloy with electron conductivity (*n*-type) used phosphorus (*P*), and a *p*-type alloy was doped with boron (*B*).

Summarizing the experimental results obtained, we can make the following practically important conclusions. The threshold values of fast neutron fluences on achieving which in silicon-germanium alloys there begins a sharp increase in the electric resistance and thermoelectromotive force, make $\Phi \approx 6 \cdot 1018$ sm^{-2} for the electron and $\Phi \approx 1 \cdot 1018$ sm^{-2} – for the hole material. For the first time for $Si_{0.7}Ge_{0.3}$ alloys, the dose dependences $\alpha = f(\Phi)$ and $\rho = f(\Phi)$ were observed to saturate at fluences $\Phi \approx 1 \cdot 1020$ sm^{-2} in the electron material and $\Phi \approx 2 \cdot 1019$ sm^{-2} in the hole one. By the end of the reactor irradiation, the coefficients of the thermoelectromotive force increased by a factor of ~1.8 – 2 in the electron material and by a factor of 1.4 – 1.7 in the hole one, compared with the initial value; the electrical resistivity in the electron material increased by a factor of 20 – 23, and in the hole one by a factor of 6 – 8. The radiation resistance of a boron-doped $Si_{0.7}Ge_{0.3}$ hole alloy can be considerably increased by substitution of isotope 11B for isotope 10B. It can be assumed that thermoelectric modules made of $Si_{0.7}Ge_{0.3}$ alloy in the radiation field of the reactor will be notable for the service life which can be further increased by programmed intra-zone regeneration annealings.

It is known [4] that boron carbide (B_4C) is a promising high-temperature thermoelectric material with good transfer properties. Bipolarons are charge carriers in B_4C and their concentration is ~ 10^{21} sm^{-3}. Electrical conductivity is activated with temperature. The transfer of heat is accomplished by phonons and strongly depends on the localization of boron and carbon atoms (stoichiometry). To reduce χ, the boron concentration was increased to $B_{6.5}C$. The Seebeck coefficient for boron carbide already reaches ~ 180 μV /°C at a temperature of 300K, and σ increases with a rise in temperature.

It can be concluded that the thermoelement created on the basis of $^{11}B_4C$ will not only be more efficient, but it will probably be resistant to radiation. In addition, B_4C has an electronic defect structure and is characterized as an acceptor-type semiconductor with a band gap $\Delta E = 1.2$ eV without degradation of the thermoelectric parameters.

Taking into account all the above, it becomes possible to create high-efficiency high-temperature (≥1000 °C) radiation-resistant TEGs based on $^{11}B_4C$ *p*-type and *SiGe* *n*-type by changing the parameters of operating conditions. It is clear that the problem of connection between thermoelements must be solved. In order to implement the proposals, studies of thermal efficiency (*ZT*) were performed on the basis of isotope ^{11}B at high temperatures of B_4C. All thermoelectric parameters (ρ, S, χ) were

investigated. The possibility of creating a high-temperature thermoelectric generator based on B_4C and *SiGe* materials was demonstrated [5]. The main problem encountered by researchers during their research and development on thermoelectric converters with a nuclear heat source is to improve or create high-quality materials both with high efficiency of *Z* conversion at high temperatures and with high radiation resistance. Production of materials was carried out using two methods: hot pressing in vacuum and crystallization caused by CVD. Boron carbide was used for *p*-leg of the thermoelectric converter, and the radiation-resistant *Si-Ge* alloy doped with phosphorus was used for *n*-leg of the thermoelectric converter.

This idea was implemented by two institutes: the National Scientific Center "Kharkiv Institute of Physics and Technology" (NSC-KIPT) and Sukhumi Institute of Physics and Technology (SIPT) within the framework of the STCU project Gr-20j "Development of radiation-resistant thermoelectric elements based on boron carbide (B_4C) and silicon-germanium (*SiGe*) alloys" (2003 – 2005, collaborator – Prof. Fernand D.S.Marquis, USA).

NSC – KIPT was engaged in the works on development of processes for production of boron carbide and silicon-germanium alloys by the gas-phase and plasma-chemical methods, SIPT – on production of boron carbide and silicon-germanium alloys by hot pressing in vacuum, and also on the study of the thermal and electrophysical properties of the materials obtained.

The effect of boron content on the thermoelectric properties of boron carbide samples obtained by hot pressing and gas-phase (including plasma-chemical) methods was studied.

From the results of measuring thermoelectric characteristics, the figure of merit *Z* of materials of samples obtained by hot pressing methods, as well as by gas-phase and plasma-chemical deposition methods was calculated. Over the entire temperature range (300 – 1300 K) the figure of merit of boron carbide samples obtained by the CVD-methods exceeds the figure of merit of the hot-pressed samples, and with a rise in temperature this difference is somewhat increased. The samples obtained by the CVD-methods have nearly equal values of *Z*, but the figure of merit of plasma-chemical samples is 10 –15 % higher than that of the samples obtained by the gas-phase method.

It is established that for the composition $B_{6.5}C$ the figure of merit of *p*-leg reaches $1 \cdot 10^{-4}$ 1/degree for the gas-phase manufacturing method and $1.3 \cdot 10^{-4}$ 1/degree – for plasma-chemical. The figure of merit of the pair ($Si_{0.7}Ge_{0.3}$ + 0.3 %P) gas − ($B_{6.5}C$) gas is $2.2 \cdot 10^{-4}$ 1/degree, and the efficiency – 4.4 %. When *p*-type leg is made of plasma-chemical $B_{6.5}C$, the figure of merit of this pair is $2.5 \cdot 10^{-4}$ 1/degree, and the efficiency – 5.0 % [6].

In order to determine the thermoelectric compatibility, the calculation of the thermoelectric efficiency of the $Si_{0.7}Ge_{0.3}$ alloy of *n*-type and boron carbide B_4C and $B_{6.5}C$ of *p*-type of different densities was carried out.The most optimal in compatibility with $Si_{0.7}Ge_{0.3}$ *n*-type in *Z* is a sample of boron carbide (*p*-type), made on the basis of 11B with a high boron content, i.e. BxC, where x ≥ 6.3. The 11B isotope in boron carbide samples also provides high radiation resistance, which is of considerable importance in the case of their use as a heat source of a nuclear reactor.

In 2008 – 2010, international STCU/GNSF project №4655 "Development of technology and creation of a prototype of high-temperature heliothermoelectric generator" was carried out. An experimental heliothermoelectric generator (HTEG) was developed. HTEG (up to 1000 °C) was created on the basis of a highly concentrated Cassegrain optical system and a thermoelectric generator based on $Si_{1-x}Ge_x$ alloys (x = 0.05 – 0.10) for electrical energy production.

The thermopiles with 32 legs were manufactured by collective interconnection method. Their energy and thermomechanical properties were studied.

Two-stage optical furnaces of the Cassegrain type were manufactured and their energy and thermomechanical characteristics were studied.

In 2009 – 2010, STCU / GNSF project №4996 "Development of *Si-Ge* nanostructured alloys by explosive compaction method and creation of energy-efficient thermopiles on their basis" was carried out. The raw materials used were powders of standard nanostructured *Si* and *Ge* obtained by grinding.

Experimental thermoelements and thermopiles have been created. Their structural and thermoelectric parameters have been investigated.

At present, the institute is developing thermoelectric alloys of *SiGe n*- and *p*-type with a low content of *Ge* (5 – 10 at. %). It is known [7] that the thermal resistance of *Si-Ge* alloys containing up to 10 at. % *Ge* increases sharply with increasing *Ge* content. This material is promising for creating thermoelectric generators, where waste heat is used for direct use, in heating furnaces and in central gas heating systems. Such a thermoelectric generator can operate in the open air and generate an electric power of ~ 1 W from the working area of 1 sm^2. The generated electrical energy can be used to operate these systems, as well as for the individual needs of consumers.

These alloys were obtained by co-grinding the original components into ultrafine powder and hot pressing in a vacuum of 10 *Pa* at 1250 – 1370 °C under a pressure of 480 kg·sm^{-2} for 20 – 40 minutes. As the main components of the alloys, polycrystalline *Si* and *Ge* were used, and the alloying components for the *p*-type alloy were amorphous *B*, and for the *n*-type alloy, amorphous phosphorus and polycrystalline *GaP*. Homogenizing isothermal annealing of the samples was carried out at 1200 – 1360 °C for 20 – 100 hours in vacuum and in the open air.

Fig. 3 shows *X*-ray profiles of the diffraction maximum (444) of samples of the $Si_{0.95}Ge_{0.05}$ alloy prior to and after annealing at 1360 °C for 34 hours. The alloy was pressed at 1355 °C for 40 min. The porosity of the material is 2%. Prior to annealing, the diffraction maximum of the sample corresponds to *Si-Ge* alloy with *Ge* content of 6 at.% and pure *Si*. After annealing, the sample is a homogeneous *Si-Ge* alloy with *Ge* content of 4.6 at.%. As a result of high-temperature pressing, fine powder particles collect together and form larger grains of alloys with sizes up to 10 μm.
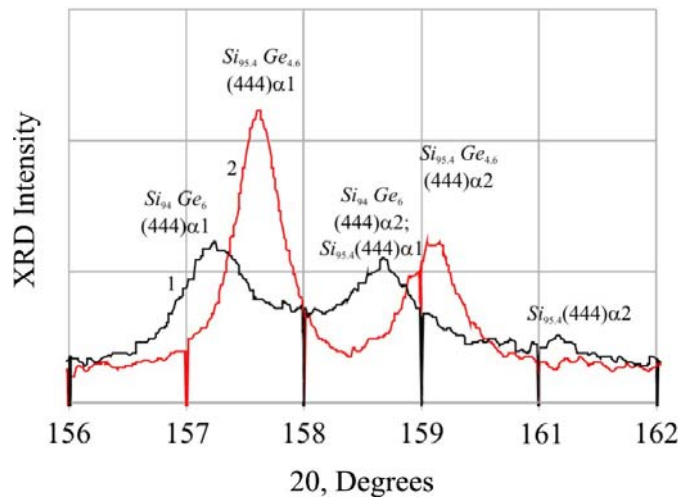

Fig. 3. X-ray profiles of the diffraction maximum (444) of the sample:
1 – prior to annealing; 2 – after annealing

The microhardness of this sample varies within 10.64 – 11.86 GPa (the average value is 11.29 GPa), and the microhardness of the molten $Si_{0.95}Ge_{0.05}$ alloy is 11.30 GPa [8]. In accordance with microhardness, this material is a fairly homogeneous alloy.

Fig.4 shows the microstructure of $Si_{0.95}Ge_{0.05}$ + *GaP* 3 w. % alloy pressed at 1290 °C for 30 min prior to and after annealing at 1350 °C for 25 hours.The porosity of the material is 17 %. Prior to annealing, the sample contains fine particles and pores. Around large pores there are large homogeneous

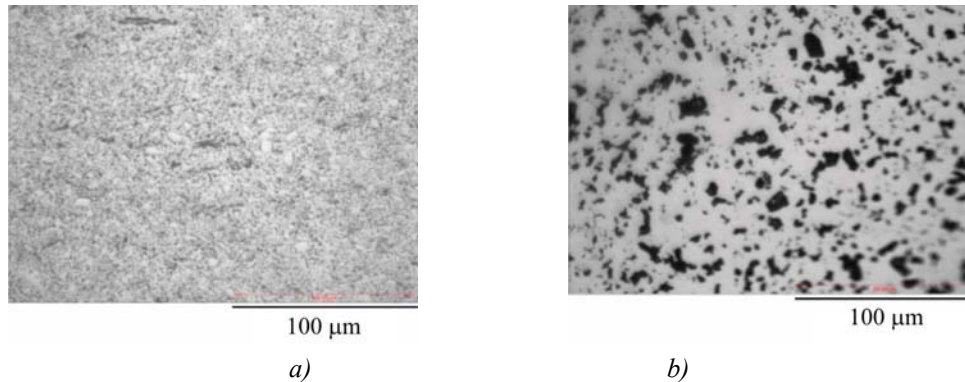regions enriched with germanium. After annealing, the material structure is uniform and contains pores up to 20 μm.

a)   *b)*

Fig. 4. Microstructure of samples: a) prior to annealing; b) after annealing

Table shows the results of studying the concentration n and the mobility μ of the current carriers and the electrical conductivity σ of $Si_{0.95}Ge_{0.05}$ alloys doped with *B*, *P* or *GaP*. The alloys were pressed at 1335 °C for 30 min. The porosity of the material is 3 %. From the results obtained, when compressing powders, a deep dissolution of impurities takes place. The values of the measured parameters correspond to the results of known studies, but the mobility of holes of the p-type sample is 3 times higher [9]. As a result of isothermal annealing at 1300 ° C for 30 hours, the values of n, μ and σ of the samples studied did not change significantly.

Table

Electrophysical characteristics of Si-Ge alloys

Alloys	Type	n, 10^{20}. cm^{-3}	μ, cm^2. v^{-1}. sc^{-1}	σ, Ω^{-1}. cm^{-1}
$Si_{0.95}Ge_{0.05}$ + *B* 0.2 w. %	*p*	0.6	250	1725
$Si_{0.95}Ge_{0.05}$ + *P* 0.5 w. %	*n*	2.0	74	2000
$Si_{0.95}Ge_{0.05}$ + *GaP* 2 w. %	*n*	1.6	67	1400

The temperature dependences of α, σ, λ and *Z* were measured for three samples of each of the obtained alloys $Si_{0.95}Ge_{0.05}$ + *GaP*3 w.% and $Si_{0.95}Ge_{0.05}$ + *B* 0.2 w. %, pressed at 1325 °C for 30 min. Material porosity is 7 %. The data obtained from one sample of n-type alloy and one sample of *p*-type alloy is shown in Figs. 5 and 6.

The efficiency Z is calculated by the formula $Z = \alpha^2 \sigma / \lambda$.

The nature of the changes in the measured parameters, depending on the temperature of the materials being studied, is similar to the character of such changes in the same parameters of all other thermoelectric *Si-Ge* alloys.The efficiency of investigated alloys is 20 % lower compared to *n*- and *p*-type $Si_{0.68}Ge_{0.32}$ alloys comprising 6.4 times more germanium. The values of α and λ of the *n*-type

alloy in question are close to the nanostructured $Si_{0.95}Ge_{0.05}$ *n*-type alloy [10], but its electrical conductivity is 1.8 times lower. The reason for this is the oxidation of the resulting ultra-fine powder, as the operations for its manufacture and use were carried out in the air.
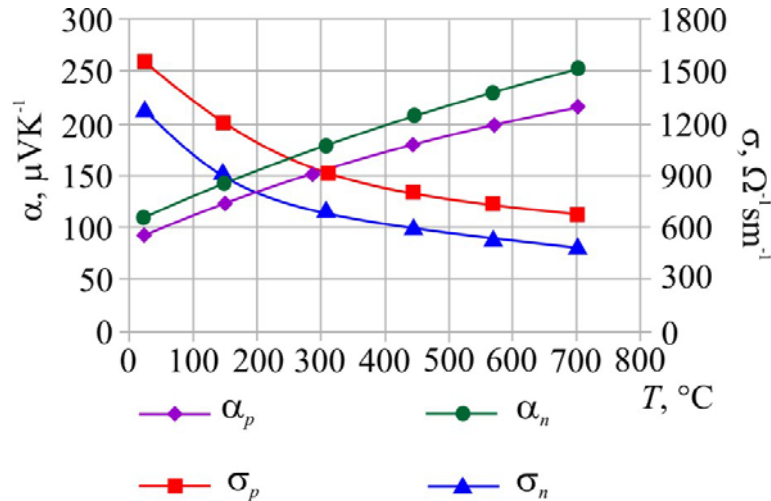

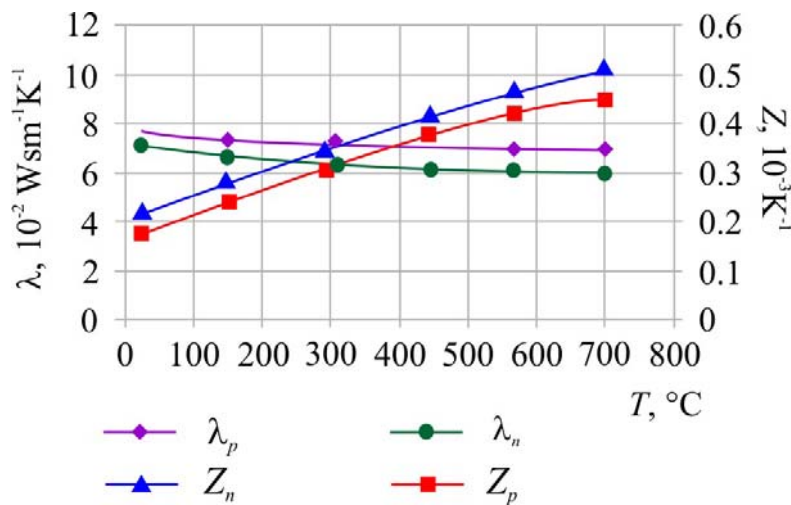*Fig. 5. Temperature dependence of σ and α*
of n- and p-type samples

Fig. 6. Temperature dependence of λ and Z
of n- and p-type samples

Further optimization of carrier concentration and technological regimes of the investigated alloys will increase their efficiency. The described method of obtaining alloys does not require expensive equipment and is easily realized. The use of the thermoelectric alloy *SiGe* synthesized by this method is suitable both for direct use (creation of thermoelectric converters) and for production of nanostructured materials.

The institute conducts research on the production of polycrystalline and single-crystal *SiGe* alloys with a content of up to 10 at.% *Ge* by the Czochralski method, intended for thermoelectric converters and optoelectronic devices.

With regard to new theoretical developments [11] and accumulated rich experience in creating two-stage thermoelectric generators, a joint project of a three-stage thermoelectric generator on the basis of high-performance thermoelectric materials is under development nowadays with participation

of Sukhumi Ilia Vekua Institute of Physics and Technology, Institute of Thermoelectricity NAS of Ukraine and the National Scientific Centre "Kharkiv Institute of Physics and Technology" NAS of Ukraine.

Conclusions

This paper gives an overview of the results of research in the field of materials science and thermoelectric instrument making, conducted at Sukhumi Ilia Vekua Institute of Physics and Technology from the 50s of the last century to the present time.

Since the early 50s of the 20th century, technological devices have been designed and *Ge*, *Si* and *SiGe* semiconductor bulk crystals have been synthesized, methods for synthesis and subsequent hot pressing of thermoelectric *SiGe* alloys used in the future when creating high-temperature thermoelectric generators for the "Romashka" nuclear power plant (1964), and also for the construction of single-stage (1966) and two-stage (1972) thermoelectric generators for the "Buk" nuclear power unit have been developed.

For a long time (1970 – 1990), various thermoelectric converters operating in low, medium and high temperature regions with different applications have been developed and developed.

In the first years of this century, in cooperation with the Kharkiv Institute of Physics and Technology, the possibility in principle of creating high-temperature thermoelectric converters with *p*- and *n*-legs made of boron carbide and *SiGe* alloys obtained by various methods was shown.

Together with the Institute of Nuclear Research of the NAS of Ukraine, reactor tests of $Si_{0.7}Ge_{0.3}$ alloys were carried out in the temperature range from 773 to 973 K with a fast neutron fluence set up to $4 \cdot 1020$ cm^{-2} and threshold values of fluences for *p*- and *n*-legs of thermoelectric converters were determined. The possibilities of increasing their radiation resistance and resource capacity were estimated.

In recent years, a technology has been developed to create a high-temperature heliothermoelectric generator based on the highly concentrated Cassegrain optical system and thermoelectric $Si_{1-x}Ge_x$ alloys ($x = 0.05$-0.10).

The nanostructured *SiGe* alloys have been developed by explosive compaction method and energy-efficient thermopiles have been developed on their basis. Their structural and thermoelectric parameters have been investigated.

References

1. A. V. Ioffe and A. F. Ioffe, *Dokl. Akad Nauk SSSR* 98(5), 757 (1954).
2. M. L. Milionshikov, A. S. Abramov, I. G. Gverdtsiteli, L. V. Gorlov, et al., High-Temperature Reactor-Converter "Romashka", *J. Nuclear Energy* 17(35), 329 – 335 (1964).
3. G. Bokuchava, G. Murgulia, and V. Kashia, Study of Reactor Irradiation on Thermoelectric Properties of Highly Doped *n*- and *p*-$Si_{0.7}Ge_{0.3}$, *Atomic Science and Engineering Issues*, Series "Radiation defects physics and radiational material science" 86, Ukraine, NSC "Kharkiv Institute of Physics and Technology" 3, 68 – 72 (2005).
4. *Ch. Wood, Proceedings of the 9th International Symposium on Boron, Borides and Related Compounds (Duisburg, 3, 236 – 248, 1987).*
5. G. Bokuchava, G. Karumidze, B. Shirokov, To the Problem of Creation of High Temperature Thermoelectric Generator, *Georgian International Journal of Science and Technology* **1**(3), 19 – 24 (2008).

6. A. Zhuravlev, B. Shirokov, A. Shiyan, G. Bokuchava, and G. Darsavelidze, Vapour Phase Methods in the Developments of Thermoelectric Converters and Heteroepitaxial Structures. *Proc. of International Conference "Modern Materials and Technologies"* (Tbilisi, Georgia, October, 21 – 23, 2015), p. 115 – 119.

7. J. P. Dismukes, L. Ekstrom, E. F. Steigmeier, I. Kudman, and D. S. Beers, *J. Appl. Phys*. 35, 2899 (1964).

8. M. Kekua, E. Khutsishvili, Semiconducting Solute Solutions of *Ge-S*i System, Tbilisi, "Metsniereba" 1985, 156.

9. O. Golikova, E. Iordanishvili, and A. Petrov, *Fiz.Tverd.Tela* 8, 500 (1956) [Sov. Phys. Solid State] 8, 397 (1966)].

10. G. Zhu, H. Lee, Y. Lan, X. Wang, G. Joshi, D. Wang, J. Yang, D. Vashace, H. Guilbert, Pillitteri, M. Dresselhaus, G. Chen, and Z. Ren. *PRL*, 102, 196803 (2009).

11. L. I. Anatychuk, L. N. Vikhor, *Functionally Graded Thermoelectric Materials* (Chernivtsi: Bukrek Publ., 2012), 180 p.

Submitted 29.11.2016

D. K. Kadirova, O. V. Yevdulov

Federal State Budget Educational Institution of Higher Professional Education "Dagestan State Technical University", 70, Ave. Imam Shamil, 367015, Makhachkala, Russia

D.K.Kadirova

O.V.Yevdulov

THERMOELECTRIC FLOW-TYPE HEAT TRANSFER INTENSIFIER

The design of a thermoelectric heat transfer intensifier is proposed in which a forced airflow in the respective gaps by means of fan assemblies is used to increase the coefficient of heat transfer between the thermoelement junctions and the media moving in transport zones. The model of the device based on the solution of heat balance equations for media flows in transport zones, thermopile surfaces, the gaps between transport zones and thermopile surfaces for direct flow conditions is considered. Theoretical studies of the heat transfer intensifier according to the developed model have been carried out.

Key words: thermoelectric heat transfer intensifier, thermopile, temperature, model, moving medium, coefficient of heat exchange.

Introduction

At present, the task of studying special technical means for ensuring intensive heat transfer from sources with high thermal loads to heat receivers is becoming topical in order to equalize the temperature levels of the objects. These issues are especially relevant for the utilization of heat generated during the performance of certain technological processes at the production site, removal of heat from the cooling fluids of fuel rods of nuclear reactors, and so on. [1].

One of the promising directions in the development of systems of this type is the use of thermoelectric energy converters that provide the construction of economical, small-sized heat exchangers with wide functionality to maintain a given thermal mode. Thus, in this area we can single out the papers [2 – 4], where the possibilities of using thermoelectric energy converters for intensifying heat exchange between the flows of two liquid or gaseous media. However, despite the availability of theoretical and experimental studies in this field, the question of increasing the intensity of heat exchange between media, optimization of energy and mass-dimensional parameters of devices is still of current interest.

The purpose of the work is theoretical study of a thermoelectric heat transfer intensifier wherein due to the use of a forced air flow along thermoelement junctions a higher coefficient of heat exchange is ensured between the latter and the media moving in transport zones the temperature of which is to be changed.

Design of a thermoelectric heat transfer intensifier

The design of a device for heat transfer intensification between the flows of two media has been developed. Its schematic structure is shown in Fig. 1, and appearance – in Fig. 2. The device consists of a thermopile 1 composed of identical in size and physical properties thermoelements, powered from electric energy source (not shown in fig.), both surfaces of which are at some distance

from walls 2 of transport zones 3 with media 4 moving therein. At the beginning and end of transport zones 3 in the direction perpendicular to motion of media 4 mounted are fan assemblies 5, powered from the same source of electric energy as thermopile 1. Fan assemblies 5 serve to purge the air in the gap between walls 2 of transport zones 3 and the surfaces of thermopile 1, one fan unit working for injection of air flow, and the other – for its exhaust. Thermopile 1, transport zones 3 and fan assemblies 5 form a rigid mechanical construction by means of fixing accessories 6.
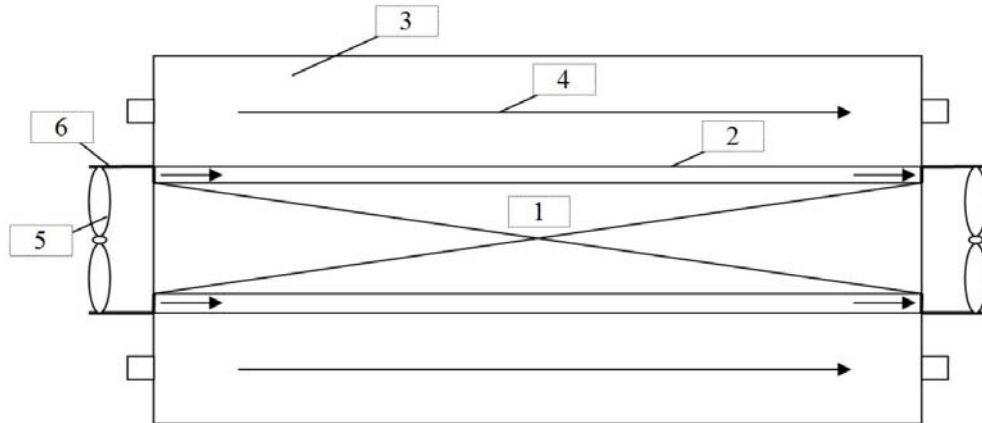

Fig. 1. Schematic structure of thermoelectric
heat transfer intensifier

Fig. 2. Appearance of thermoelectric
heat transfer intensifier

The thermoelectric heat transfer intensifier functions as follows. On passing through thermopile 1 of direct electric current from the source of energy, on some thermoelement junctions the Peltier heat will be absorbed, and on the other – released. If the cold thermoelement junctions are close to wall 2 of transport zone 3 with the hot moving medium 4, and the hot junctions of thermoelements – to the wall of transport zone with the cold moving medium, due to the available temperature difference there will be intensification of thermal energy exchange between the two medium flows. In so doing, purging of air in the gaps between walls 2 of transport zones 3 and the surfaces of thermopile 1 and fan assemblies 5 will allow increasing the coefficient of heat transfer between them due to ensuring the mode of forced convection whereby the value of given coefficient is higher than in the case of conductive mechanism of heat exchange.

Model of thermoelectric heat transfer intensifier

For the considered construction a mathematical model was developed describing electro- and thermophysical processes occurring in the device. The model is based on heat balance equations for medium flows in transport zones, thermopile surfaces, the gaps between transport zones and thermopile surfaces [5]. Condition of a direct flow is considered.

Heat balance equations in the gaps between the walls of transport zones and thermopile junctions for the above schematic are given by:

$$W'\frac{dT_1}{dx} = \alpha'L(T_{1TEM} - T'_1) \tag{1}$$

$$W'\frac{dT_2}{dx} = \alpha'L(T_{2TEM} - T'_2) \tag{2}$$

where $T_{1TEM,2TEM}$ are temperatures of the cold and hot thermopile junctions, respectively, $T_{1,2}$ are the temperatures of air flow in the gaps, W′ is total heat capacity of air medium flowing along thermopile junctions (in the gaps) per unit time (equal to mass flow rate multiplied by medium specific heat), L is the length of transport zones, α′ is coefficient of heat exchange between thermopile junctions and air medium in the gap.

Thermal balance equations for medium flows in transport zones are found from the relationships:

$$W_1\frac{dT_1}{dx} = \alpha_1 L(T'_1 - T_1) \tag{3}$$

$$W_2\frac{dT_2}{dx} = \alpha_2 L(T'_2 - T_2) \tag{4}$$

where $T_{1,2}$ are temperatures of cooled and heated media, W_1 is total heat capacity of the medium flowing along the cold junctions of thermopile per unit time, W_2 is total heat capacity of the medium flowing along the hot junctions of thermopile per unit time, α′ is coefficient of heat exchange between the cooled air medium in the gap and cooled medium in transport zone, α′ is coefficient of heat exchange between the heated air medium in the gap and the heated medium in transport zone.

Heat balance equations on thermopile junctions on the side of thermoelements are given by:

$$\alpha'(T'_1 - T_{1TEM}) = \overline{e}jT_{1TEM} - \frac{1}{2}j^2\rho d - \frac{\lambda}{d}(T_{2TEM} - T_{1TEM}), \tag{5}$$

$$\alpha'(T_{2TEM} - T'_2) = \overline{e}jT_{2TEM} + \frac{1}{2}j^2\rho d - \frac{\lambda}{d}(T_{2TEM} - T_{1TEM}), \tag{6}$$

where $\bar{e}$ is the Seebeck coefficient of thermoelements, j is electric current density, ρ is electric resistivity of thermoelement legs, λ is thermal conductivity of thermoelement legs, is the height of thermoelement legs.

The system of equations (1) – (6) was solved by numerical method of finite elements. The results of calculations are represented in Fig.3. As a medium, water was used. The characteristics of thermoelements were as follows: $\lambda = 1.5$ W/(m·K), $\rho = 10,65 \cdot 10^{-6}$ Ω·m, $\bar{e} = 0,2 \cdot 10^{-3}$ V/K, $d = 0.003$ m. Coefficients of heat exchange: $\alpha_1 = \alpha_2 = 100$ W/(m²·K), the values of $W' = 90$ W/K, $W_1 = W_2 = 120$ W/K.

Dependences of the temperature of the media at the outlet of the heat transfer intensifier on the value of coefficient of heat transfer between thermopile junctions and the air medium in the gap at a fixed value of the thermopile supply current equal to 5 A are shown in Fig.3.
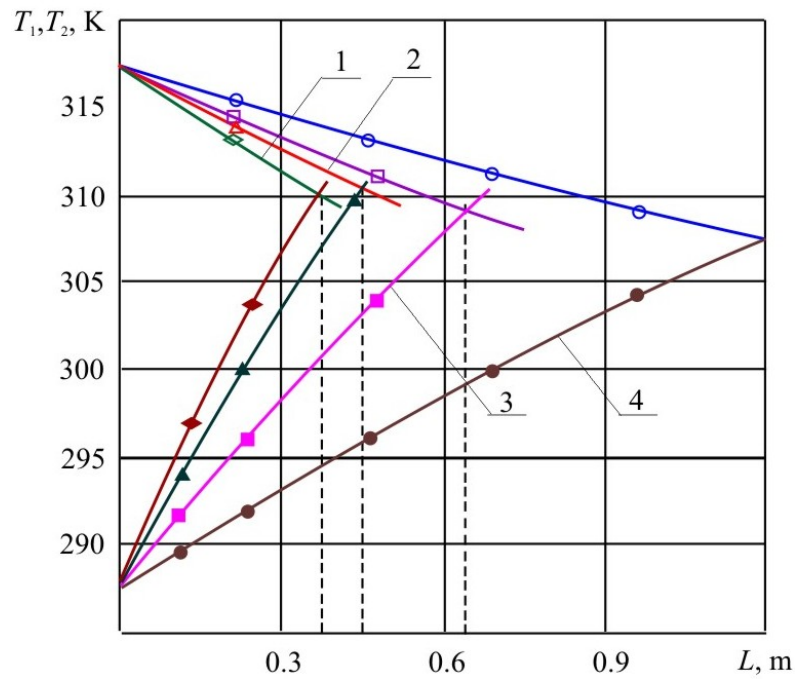
Fig. 3. Change in medium temperatures at the outlet of heat transfer
intensifier versus the length at different values of α' *(1 –* α' *= 90;*
2 – α' *=80; 3 –* α' *= 70; 4 –* α' *= 60 W/(m²·K)*
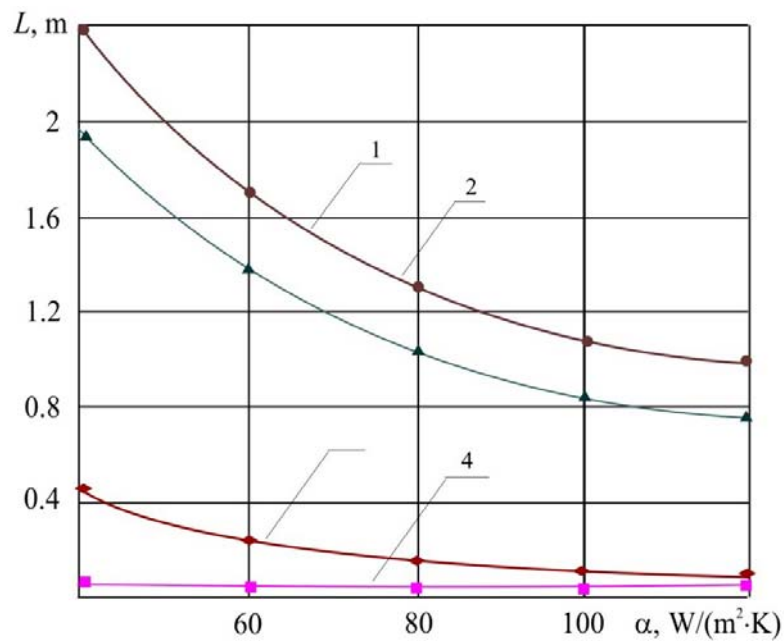

Fig. 4. Limiting lengths of thermopile in the intensification mode versus filling
ratio at different values of temperature difference at the inlet to heat transfer intensifier
(1 – ΔT = 40; 2 – ΔT = 30; 3 – ΔT = 10; 4 – ΔT = 5 K; I = 5A)

According to the data obtained, the increase in the value of α' allows reducing (increasing) their temperature at the outlet of heat exchange unit for its equal length. Thus, a change in α' by 10 W/(m²·K) changes the temperature of cooled medium on the average by 2 K, and heated – by 3 K.

Fig.4 represents the plots of change in the limiting lengths of thermopile depending on the value of α', i.e. for those lengths whereby the temperatures of liquids at the outlet of heat transfer intensifier

are equal to each other. As follows from the presented data, the greater the difference in the temperatures of the coolant at the inlet to the device, the greater the length of the thermopile needed to maintain the intensification mode. The plots are monotonously decreasing depending on the coefficient of heat exchange between the thermopile junctions and the air medium in the gap. The greater the difference in temperatures at the inlet, the more drastically decrease the functions $L = L(\alpha')$ at constant supply current $I = 5$ A.

Conclusions

1. Construction of a thermoelectric heat transfer intensifier is proposed wherein to increase the coefficient of heat exchange between thermoelement junctions and the media moving in transport zones use is made of a forced air flow in the corresponding gaps through use of fan assemblies.

2. The model of a thermoelectric heat transfer intensifier is developed which is based on solving heat balance equations for medium flows in transport zones, thermopile surfaces, the gaps between transport zones and thermopile surfaces for direct flow conditions.

3. It was established that increasing the value of coefficient of heat exchange between thermopile junctions and air medium in the gap makes it possible to reduce (raise) their temperature at the outlet of heat exchange unit with its equal length. In this case, a change in α' by 10 W/(m²·K) on the average changes the temperature of cooled medium by 2 K, and heated – by 3 K4. It is established that increase in the difference in temperatures of media at the inlet contributes to a more drastic decay of the functions of dependence of limiting lengths of thermopile on the coefficient of heat exchange between thermopile junctions and air medium in the gap with constant supply current.

References

1. T. A. Ismailov. *Thermoelectric Semiconductor Devices and Heat Transfer Intensifiers* (St-Petersburg: Politekhnika, 2005), 534 p.

2. L. I. Anatychuk. *Thermoelements and Thermoelectric Devices* (Kyiv: Naukova Dumka, 1979), 768 p.

3. L. P. Bulat. Applied Investigations and Developments in the Field of Thermoelectric Cooling in Russia, *Kholodilnaya Tekhnika* 7, 34 – 37 (2009).

4. B. E.-Sh. Malkovich. Thermoelectric modules Based on Bismuth Telluride Alloys, *Proc. of XI Interstate Workshop "Thermoelectrics and Their Application"* (Saint-Petersburg, 2008, p. 462 – 468).

5. M. A. Kaganov, M. P. Privin. *Thermoelectric Heat Pumps* (Leningrad: Energiya, 1970), 176 p.

Submitted 19.11.2016

L.I. Anatychuk[1,2], A.V. Prybyla[1]

[1]Institute of Thermoelectricity of the NAS and MES
Ukraine, 1 Nauky str., Chernivtsi, 58029, Ukraine;
[2]Yu.Fedkovich Chernivtsi National University,
2 Kotsyubynsky str.,Chernivtsi, 58012, Ukraine

L.I. Anatychuk

AIR CONDITIONER FOR HUMANS WITH A THERMOELECTRIC HEAT FLUX SENSOR

A.V. Prybyla

The paper presents the results of development of air conditioner for humans with a thermoelectric heat flux sensor. Physical, mathematical and computer models of air conditioner have been developed. Its effcieincy for different values of heat release from human body has been determined. The efficiency of using thermoelectric sensor for control of temperature and heat release from human body has been confirmed.

Key words: thermoelectric heat flux meter, computer simulation, air conditioner for humans.

Introduction

General characterization of the problem. The use of personal air conditioners arranged in garment is a promising way of ensuring comfortable conditions for humans [1]. It is particularly important for persons who fulfill their professional duties in unfavourable temperature conditions for a long time (military men, workers in hot shops, sportsmen, doctors, etc.) [2].

In [1], physical models of personal air conditioners are described that are based on different physical methods of cooling and heating, in particular, the use of heat accumulators, blasting with ambient air, substance phase transition, thermoelectric and compression energy conversion. The simplest model is the physical model of air conditioner that employs forced heat removal from human body by ambient air.

Designs of such air conditioners are known [3 – 6]. To ensure heat removal by air flow, they employ low-power fans providing air flow circulation in peculiar channels created by garment. This design has disadvantages caused by low efficiency of heat exchange between human body and air flow due to the presence of additional garment layer. This, in turn, makes worse heat removal by sweating. In this paper, we propose to improve air conditioner for humans increasing considerably its efficiency by using heat exchange directly between human body and air flow. It eliminates the disdvantages of earlier variants of air conditioners (worse heat exchange due to the presence of intermediate layers of fabric on the body), and ensures additional heat exchange by intensification of natural heat exchange process of human body by evaporation of liquid (sweating).

Moreover, an important element of air-conditioner for humans is a device for control of the fans which ensures their necessary operating condition at different heat release levels from human body [7]. For the purpose of control of body temperature and its heat release it was proposed to use special bio heat flux meter [8, 9]. Its specific feature is the presence of channels through which perspiration products are transferred to the free surface of heat flux meter. The latter allows determining heat removal not only due to convective heat exchange, but also due to evaporation from human body surface.

Thus, *the purpose of this work* is to improve the efficiency of air-conditioner for humans with a thermoelectric heat flux sensor.

Physical model of a thermoelectric air-conditioner for garment

Calculations of the air-conditioner were performed with the use of a physical model represented in Fig. 1.
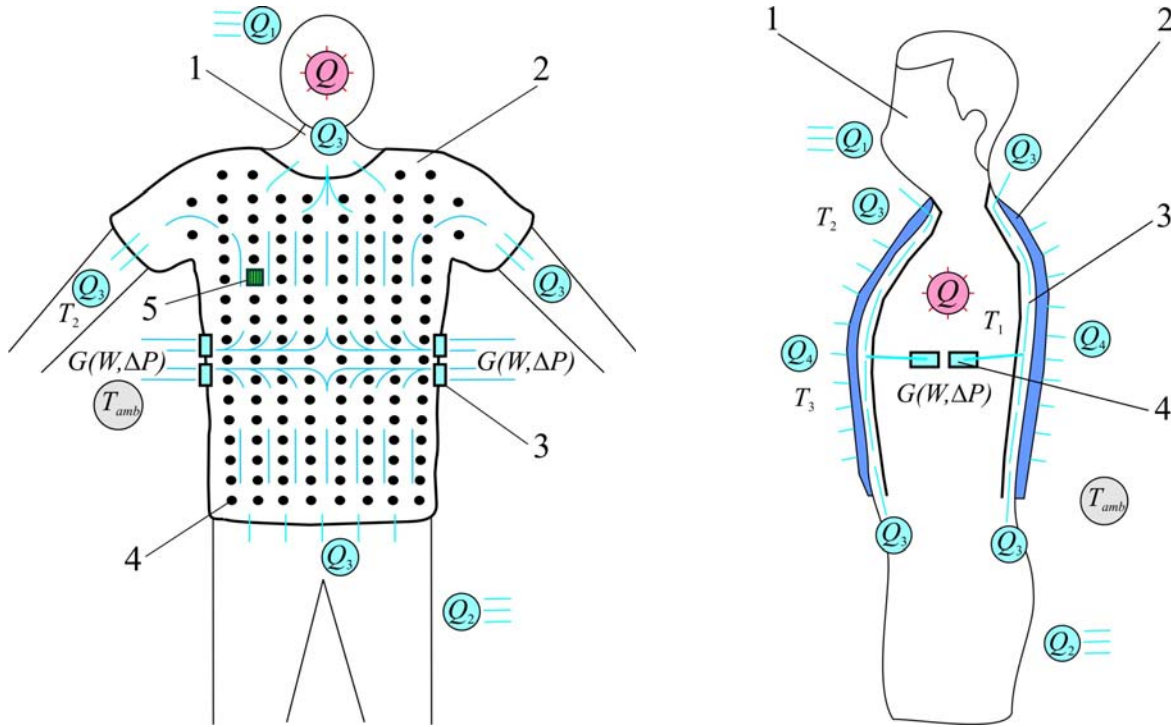

Fig. 1. Physical model of air-conditioner for humans: 1 – human body;
2 – elastic linen; 3 – fans; 4 – spacers on the internal surface of garment
that form air gaps, 5 – thermoelectric temperature and heat flux sensor.

Physical model of air-conditioner for humans is composed of human body 1 which releases heat flux of power Q and has temperature $T_1 = 36.6\,°C$. Elastic linen 2 is put directly on human body 1. On the linen 2 flat fans 3 are fixed which create air flow between the linen and the human body. Air flow created by the fans is transferred through the gaps created by spacers 4 fixed on the internal surface of the linen.

Depending on the body condition (rest, physical loads of various intensity, etc), it releases heat flux of power $Q = 100 - 800$ W [7]. Part of thermal power from human body Q_1 is removed through breathing, part by heat exchange from other body areas not covered with linen 2 with the ambient Q_2, and part through mechanisms of heat exchange from the surface of linen 2 Q_4. Created by fans 3, heat flux with consumption G which depends on power supply to fans W and pressure difference ΔP (created inside the garment by air flow) removes thermal power Q_3. Air flow which is heated in the garment to temperature T_2, is removed to the environment with temperature T_{amb} through the holes in the garment (as shown in Fig. 1).

It is clear that to ensure the necessary heat removal, of vital importance is information on the dimensions and arrangement of spacers on the garment, as well as on the supply power to electric fans.

Mathematical and computer models of air-conditioner for humans

To calculate the energy characteristics of air-conditioner for humans on the basis of a physical model shown in Fig. 1, object-oriented computer simulation in Comsol Multiphysics software was used. Mathematical description of the model is given below.

The processes of heat and mass exchange of heat carrier in the air gaps of the garment created by spacers in the steady-state case are described by Eqs. (1 – 3):

$$-\Delta p - f_D \frac{\rho}{2d_h} v |\vec{v}| + \vec{F} = 0 \tag{1}$$

$$\nabla(A\rho\vec{v}) = 0 \tag{2}$$

$$\rho A C_p \vec{v} \cdot \nabla T_2 = \nabla \cdot A k_2 \nabla T_2 + f_D \frac{\rho A}{d_h} |\vec{v}|^3 + Q_2 + Q_{wall}, \tag{3}$$

where p is pressure, ρ is heat carrier density, A is effective cross-section of the channel where heat carrier is moving, $\vec{F}$ is the sum of all forces, C_p is heat carrier specific heat, T_2 is temperature, $\vec{v}$ is velocity vector, k_2 is heat carrier thermal conductivity, f_D is the Darcy coefficient, $d = 4A \div Z$ is effective diameter, Z is channel wall perimeter, Q_2 is heat released due to viscous friction [W/m] (from the unit length), Q_{wall} is heat flux coming from heat carrier to the walls [W/m].

$$Q_{wall} = h \cdot Z \cdot (T_1 - T_2), \tag{4}$$

where h is heat transfer coefficient found from the equation

$$h = \frac{Nu \cdot k_2}{d}. \tag{5}$$

To determine the Nusselt number, the Gnielinski equation is employed ($3000 < Re < 6\cdot10^6$, $0.5 < Pr < 2000$)

$$Nu = \frac{\left(\frac{f_d}{8}\right)(Re - 1000)Pr}{1 + 12.7\left(\frac{f_d}{8}\right)^{\frac{1}{2}}\left(Pr^{\frac{2}{3}} - 1\right)}, \tag{6}$$

where the Prandtl number $Pr = C_p\mu \div k_2$, μ is dynamic viscosity, $Re = \rho v d \div \mu$ is the Reynolds number.

To determine the Darcy coefficient f_D, we will use Churchill's equation for the entire spectrum of the Reynolds number and all the values of $e \div d$ (e is surface roughness)

$$f_D = 8\left[\frac{8}{Re}^{12} + (A + B)^{-1.5}\right]^{1/12}, \tag{7}$$

where $A = \left[-2.457 \cdot \ln\left(\left(\frac{7}{Re}\right)^{0.9} + 0.27(e/d)\right)\right]^{16}$, $B = \left(\frac{37530}{Re}\right)^{16}$.

Solving Eqs (1) – (3), we obtain the distribution of velocities and pressure for heat carrier.

To determine the electric power of the fans, their real characteristics [11] in the form of polynomials were used.

Thermoelectric temperature and heat flux sensor

Fig. 2 represents a physical model of thermoelectric temperature and heat flux sensor which is composed of human body 1 which releases heat flux Q, thermoelectric sensor comprising chains of thermoelectric materials legs 2 and air gaps 3.
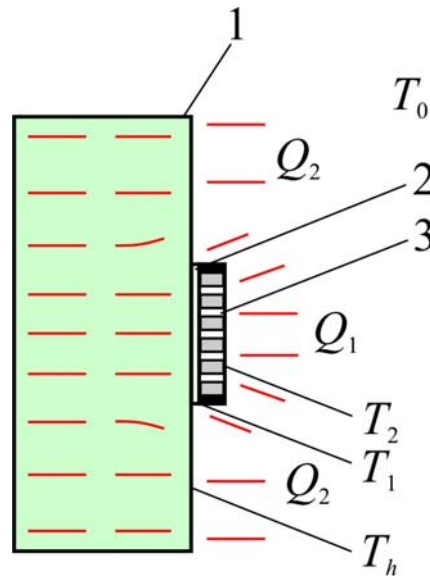

Fig. 2. Physical model of a thermoelectric temperature and heat flux sensor:
1 – human body; 2 – sensor material; 3 – air gaps.

The thermoelectric sensor used in this paper is composed of 50 couples of legs of *n*- and *p*-type material legs interconnected by solder into a series chain, in rows 10 couples each, with air gaps arranged in between. Its appearance is shown in Fig. 3.
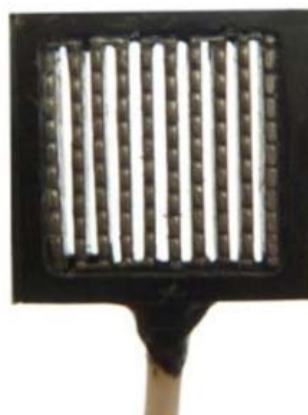

Fig. 3. Appearance of a thermoelectric temperature and heat flux sensor.

The use of such temperature sensor allows precise control of heat release from human body and its temperature with a minimum effect of the sensor itself on the body heat exchange.

Determination of the effect of such sensor on the heat release from human body and its

optimization to achieve the highest precision of temperature and heat flux measurement is the subject of a separate study and was performed in [10].

Simulation results

Thus, the input parameters of the model include: thermal power which is to be removed from the human body via thermoelectric modules and which is a function of ambient temperature and physiological condition of the body; ambient temperature T_1 = 20, 25, 30 °C; the area of the external surface of the vest from which heat exchanbge takes place S = 0.5 m^2; dimensions and arrangement of spacers on the internal surface of the linen – spacer radius r = 5 mm, its height h = 5 mm, the number of spacers n = 136; air fans are located as shown in Fig. 1.

As a result of simulation, heat carrier consumption necessary to ensure constant temperature of human body (T = 36.6 °C) was calculated as a function of ambient temperature and heat release from the body (Fig. 4).
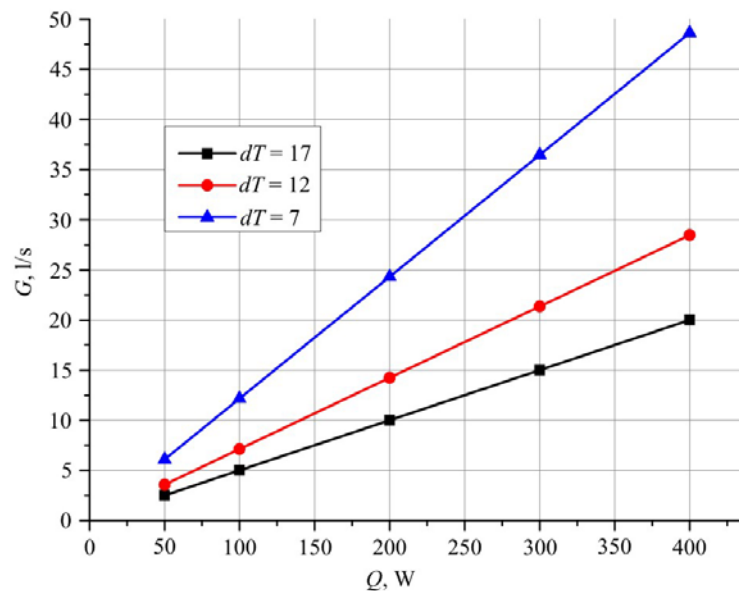

*Fig. 4. Heat carrier consumption necessary to ensure constant temperature
of human body (T = 36.6 °C) versus temperature difference between the
body and the environment and heat release from the body.*

Moreover, to determine electric power supply to the fans that ensured the necessary heat removal from the body at its constant temperature, pressure difference created by air flow from the fans was calculated as a function of air consumption (Fig. 5). Comparison of these results to real characteristics of the fans [11] made it possible to establish the real electric power supply to such air conditioner for humans.

Thus, to ensure heat removal from human body by means of a fan with characteristics described in [11], the required electric power is 5 W (for heat release in a calm state (100 W) and temperature difference between human body and the environment ΔT = 7 K), which corresponds to 4 fans of power W = 1.25 W. For heat release from human body corresponding to strong physical load (800 W), the required electric power grows to 35 W (at temperature difference ΔT = 7 K). Increase in temperature difference between human body and the environment to ΔT = 12 K results in the reduction of electric power necessary for heat removal by a factor of ≈ 1.7, to ΔT = 17 K – by a

factor of ≈ 3.

Thus, the above described design of air conditioner for human body with a thermoelectric heat flux sensor has proved its efficiency at temperatures lower than human body temperature.
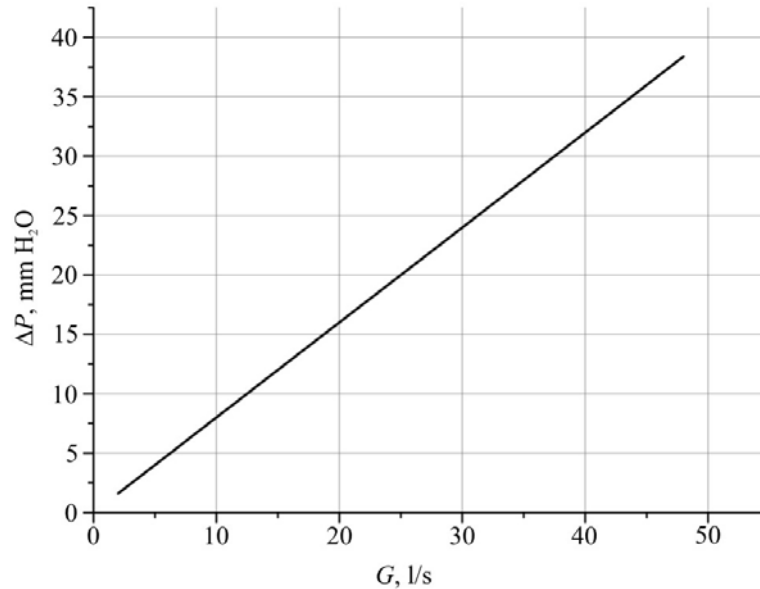

Fig. 5. Pressure difference created by air flow from the
fans versus air consumption.

Conclusions

1. The possibility of creating air-conditioner for humans with a thermoelectric heat flux sensor has been confirmed.
2. It has been calculated that to ensure heat removal from human body by means of fans, the required electric power should be 5 W (for heat release in a calm state (100 W) and temperature difference between human body and the environment ($\Delta T = 7$ K).
3. For heat release from human body corresponding to strong physical load (800 W), the required electric power to ensure heat removal increases to 35 W (at temperature difference $\Delta T = 7$ K).
4. Increase in temperature difference between human body and the environment to to $\Delta T = 12$ K results in the reduction of electric power necessary for heat removal by a factor of ≈ 1.7, to $\Delta T = 17$ K – by a factor of ≈ 3.

References

1. A. V. Prybyla. Physical Models of Personal Air-Conditioners (Part one), *J.Thermoelectricity* 1, 16 – 41 (2016).
2. S. V. Belov, A. V. Ilnitskaya, A. F. Kozyakov. et al., *Life Safety. Textbook for High Schools*, ed. by S.V.Belov (Moscow: Vyshchaya Shkola, 1999), 616 p.
3. *Pat. CN 203633537 U.*– Fan type cooling human body air conditioning clothes / Tian Weiguo.– Pub. Date: June, 11, 2014.
4. *Pat. US 20060191270 A1.*– Air conditioning system for a garment / Ray Warren.– Pub. Date: Aug, 31, 2006.
5. https://www.empa.ch.

6. http://www.kuchofuku-products.com/.

7. N. K. Vitte. *Human Heat Exchange and its Hygienic Significance* (Kyiv: Gosmedizdat, 1956), 148 p.

8. *Pat. 72032 Ukraine*, InCl 2012.01. Thermoelectric Sensor for Temperature and Heat Flux Measurement / L. I. Anatychuk, R. R. Kobylianskyi; Publ. 10.08.12, Bul. № 15.

9. V. S. Gischuk. Electronic Recorder of Signals from Human Heat Flux Sensors, *J. Thermoelectricity* 4, 105 – 108 (2012).

10. L. I. Anatychuk, R. R. Kobylianskyi, Research into the Effect of Thermoelectric Heat Meter on Human Heat Release Measurement, *J. Thermoelectricity* 4, 60 – 66 (2012).

Submitted 20.01.2017

ARTICLE PREPARATION RULES

The article shall conform to the journal profile. The article content shall be legible, concise and have no repetitions.

The article shall be submitted to the editorial board in electronic version.

The text shall be typed in text editor not lower than MS Word 6.0/7.0.

Page setup: "mirror margins"- top margin – 2.5 cm, bottom margin – 2.0 cm, inside – 2.0 cm, outside– 3.0 cm, from the edge to page header – 1.27 cm, page footer – 1.27 cm.

Graphic materials, pictures shall be submitted in color or, as an exception, black and white, in .opj or .cdr formats, .jpg or .tif formats being also permissible. According to author's choice, the tables and partially the text can be also in color.

The article shall be submitted in English on A4 paper sheets; the number of pages shall not exceed 12. By agreement with the editorial board, the number of pages can be increased.

To accelerate publication of the article, please adhere to the following rules:

• the authors' initials and names are arranged in the centre of the first page at the distance of 1 cm from the page header, font Times New Roman, size 12 pt, line spacing 1.2;

• the name of organization, address (street, city, postal code, country) – indent 1 cm below the authors' initials and names, font Times New Roman, size 11 pt, line spacing 1.2, center alignment;

• the title of the article is arranged 1 cm below the name of organization, in capital letters, semi-bold, font New Roman, size 12 pt, line spacing 1.2, center alignment. The title of the article shall be concrete and possibly concise;

• the abstract is arranged 1 cm below the title of the article, font Times New Roman, size 10 pt, in italics, line spacing 1.2 ,center alignment;

• key words are arranged below the abstract, font Times New Roman, size 10 pt, line spacing 1.2, justified alignment. The title "Key words" – font Times New Roman, size 10 pt, semi-bold;

• the main text of the article is arranged 1 cm below the abstract, indent 1 cm, font Times New Roman. size 11 pt, line spacing 1.2, justified alignment;

• formulae are typed in formula editor, fonts Symbol, Times New Roman. Font size is "normal" – 12 pt, "large index" – 7 pt, "small index" – 5 pt, "large symbol" – 18 pt, "small symbol" – 12 pt). The formula is arranged in the text, centre aligned and shall not occupy more than 5/6 of the line width, formulae are numbered in round brackets right;

• dimensions of all quantities used in the article are represented in the International System of Units (SI) with the explication of the symbols employed;

• figures are arranged in the text. The figures and pictures shall be clear and contrast; the plot axes – parallel to sheet edges, thus eliminating possible displacement of angles in scaling;

• tables are arranged in the text. The width of the table shall be 1 cm less than the line width. Above the table its ordinary number is indicated, right alignment. Continuous table numbering throughout the text. The title of the table is arranged below its number, center alignment;

• references should appear at the end of the manuscript. References within the text should be enclosed in square brackets. References should be numbered in order of first appearance in the text. Examples of various reference types are given below.

– L.I. Anatychuk, *Thermoelements and Thermoelectric Devices: Handbook* (Kyiv: Naukova Dumka, 1979), p.766. (Book)
– T.M. Tritt, Thermoelectric Phenomena, Materials, and Applications, *Annual Review of Materials Research* **41**, 433 (2011). (Journal paper)
– U. Ghoshal, *Proceedings of the XXI International Conference on Thermoelectrics* (N.Y., USA, 2002), p. 540. (Proceedings Conference)

The article should be supplemented by:

• letter from the organization where the work was performed or from the authors of the work applying for the publication of the article;

• information on the author (authors): last name and initials; full name and postal address of the institution where the author works; academic degree; position; telephone number; E-mail;

• author's (authors') photo in color or, as an exception, in black and white. With the number of authors more than two their photos are not given;

• author's application to the following effect:

<table>
<tr><td>

We, the undersigned authors, … transfer to the founders and editors of "Journal of Thermoelectricity" the right to publish the article…in Ukrainian, Russian and English. This is to confirm that the present publication does not violate the copyright of other persons or organizations.

Date   Signatures
</td></tr>
</table>